UAV-based remote sensing of fluvial hydrogeomorphology and aquatic habitat dynamics

by

Aaron Tamminga

BSc. (Honors) Queen's University

A THESIS SUBMITTED IN PARTIAL FULFILLMENT
OF THE REQUIREMENTS FOR THE DEGREE OF

Doctor of Philosophy

in

THE FACULTY OF GRADUATE AND POSTDOCTORAL STUDIES
(Geography)

The University of British Columbia
(Vancouver)

September 2016

Abstract

Recent advances in methodological and theoretical approaches in fluvial sciences have given rise to increased interest in riverscape perspectives that embrace environmental variability and spatial relationships. These approaches facilitate interdisciplinary understanding of complex fluvial processes that supports conscientious management of river systems. In this context, this dissertation presents the development and application of novel methods to study fluvial structure and eco-hydrogeomorphic relationships. Specifically, the research addresses three main questions: (1) how can UAV-based remote sensing advance the study of fluvial forms and processes? (2) what are the reach-scale geomorphic effects of an extreme flood and to what extent are these changes predictable? and (3) what are the linkages between flood-induced geomorphic change, reach hydraulics, and aquatic habitat?

Results based on the case of an extreme flood event on Elbow River, Alberta demonstrate the utility of UAVs to efficiently and accurately measure many aspects of fluvial ecosystem form and function. The combination of high resolution imagery and photogrammetrically derived elevation models provides a powerful way to characterize rivers for a wide range of applications, particularly when combined with numerical flow modeling for a seamless representation of fluvial hydrogeomorphology. Pre- and post-flood UAV surveys documented flood effects with unprecedented detail, showing a largely unpredictable fluvial response characterized by complete channel planform reorganization and widespread bank erosion. These geomorphic changes negatively impacted the study reach in terms of hydraulic diversity and habitat suitability for brown trout and constrain future fluvial adjustment during smaller floods. Overall, the dissertation presents a new way to

measure rivers and extract meaningful information and provides an integrative assessment of relationships between geomorphology, hydraulics, and aquatic ecology in a complex, dynamic river system.

Preface

This dissertation presents research conduced by Aaron Tamminga under the supervision of Dr. Brett Eaton. Aaron Tamminga was the primary researcher and was responsible for the main study design, data collection, analysis, interpretation, and writing of the content. Conceptual and analytical support were provided by Dr. Brett Eaton, Dr. Marwan Hassan, Dr. Chris Hugenholtz and Dr. Sarah Gergel. Ventus Geospatial provided technical support for the field surveys and photogrammetry.

A version of Chapter 2 has been published: Tamminga, A., Hugenholtz, C., Eaton, B., and Lapointe, M. (2015a). Hyperspatial remote sensing of channel reach morphology and hydraulic fish habitat using an unmanned aerial vehicle (UAV): A first assessment in the context of river research and management. *River Research and Applications* 31(3) 379-391. DOI:10.1002/rra.2743. Aaron Tamminga wrote the manuscript, which was then reviewed by the co-authors.

Material from Chapter 2 was also published in: Whitehead, K., Hugenholtz, C., Myshak, S., Brown, O., LeClair, A., Tamminga, A., Barchyn, T., Moorman, B, and Eaton, B. (2014) Remote sensing of the environment with small unmanned aircraft systems (UASs), Part 2: Scientific and commercial applications. *Journal of Unmanned Vehicle Systems* 2(3) 86-102. DOI:10.1139/juvs-2014-0007. Aaron Tamminga wrote the relevant section of this review paper.

A version of Chapter 3 has been published: Tamminga, A., Eaton, B., and Hugenholtz, C. (2015b). UAS-based remote sensing of fluvial change following an extreme flood event. *Earth Surface Processes and Landforms* 40(11) 1464-1476. DOI:10.1002/esp.3728. Aaron Tamminga wrote the manuscript, which was then reviewed by the co-authors.

Table of Contents

List of Tables

List of Figures

Acknowledgments

Many people aided in the successful completion of this dissertation, both scientifically and otherwise. First and foremost, I wish to thank my supervisor Brett Eaton. Since I first arrived at UBC, Brett has encouraged (and challenged) me to seek out and pursue my fluvial interests. His optimism, flexibility, mathematical mind, and curiosity have all shaped my scientific experience at UBC and will undoubtedly follow me throughout my career.

Invaluable guidance and support were also provided by Chris Hugenholtz, both in terms of technical UAV applications and his enthusiastic and open approach to science more broadly.

I am also grateful to Sarah Gergel, Marwan Hassan, and Michel Lapointe for their early contributions to my fluvial education and for the perspectives they offered throughout the process.

Thank you to the many people I worked with collecting and analyzing data over the years: Lesley Winterhalt, Dan McParland, Al Davis, Byeong Kim, Ariel Kettle, and Lea Zhecheva especially provided valuable support and friendship during field work no matter how leaky the hip waders were.

Thank you also to friends and family more broadly. My parents Ken and Nancy and sisters Meredith and Mila have been an unwavering source of love, encouragement, and advice through my life that has made me who I am today.

Lastly, thank you Danielle for your love, support, and companionship. I look forward to sharing a post-gradschool future with you.

Chapter 1

Introduction

1.1 Preamble

Riverine ecosystems globally are subject to a wide range of stressors that threaten wildlife populations and ecosystem services. To support successful management and conservation of these environments, a strong cooperative underpinning from a diverse array of scientific disciplines is needed. However, the past century has been characterized by drastic negative impacts to stream ecosystem habitats and organisms [Williams et al., 1993, Warren Jr and Burr, 1994, Taylor et al., 1996]. These declines can be attributed to a suite of cultural, economic, and natural factors [Lackey, 1999], but a fundamental problem has been disparate epistemological approaches to understanding fluvial systems and a lack of appropriate tools to provide information at relevant spatial and temporal scales. This problem is compounded by the logistic realities of studying and conceptualizing rivers; a history of theory-laden field observations and spatially discrete targeted sampling methods has contributed to a recursive focus on smoothly varying trends or average conditions. However, work from a range of backgrounds has led to an increased view of rivers as spatially continuous lateral and longitudinal mosaics with rich heterogeneity resulting from linked physical-biological processes acting at a range of scales [Schlosser, 1991, Ward, 1998, Fausch et al., 2002, Wiens, 2002, Carbonneau et al., 2012]. This riverscape perspective provides a holistic framework that embraces

complexity and facilitates collaboration across scientific disciplines in an applied management context.

The emergence and acceptance of this view has been supported by recent methodological and technological advances. In particular, remote sensing and numerical modeling approaches provide valuable tools to collect data at scales and resolutions that can characterize heterogeneous fluvial environments. Feedbacks between physical and biological processes makes rivers particularly dynamic systems; geomorphology both drives and reflects processes of flow and sediment transport, which in turn form the physical template that mediates ecological structure and function. However, mechanistic understanding of eco-hydrogeomorphic relationships is still limited [Vaughan et al., 2009]. Remote sensing provides an efficient and accurate way to collect data that can be used as empirical support in the development and testing of conceptual models and theories. When combined with numerical and physical modeling, such an approach is a valuable way to understand landscape and ecosystem evolution in an environmental change context. In this thesis, I contribute to this ongoing maturation of river sciences through the development and testing of new methods of fluvial remote sensing using small unmanned aerial vehicles (UAVs) to characterize physical river structure. These tools are then used to address the overall question of how large flood events condition morphology and aquatic habitat dynamics in gravel-bed rivers.

1.2 Thesis organization

This thesis consists of five chapters. This introduction chapter provides an overview of the scope of the research and the context within which it was conducted, as well as a brief review of literature pertinent to the research chapters. Each of the following three body chapters is then structured as a self-contained research paper with its own focused introduction, literature review, description of methods and results, discussion, and conclusion sections. Chapter 2 presents tests of UAV-based remote sensing in a fluvial setting, with a focus on data quality and derived metrics of geomorphic and habitat structure. Chapter 3 applies these methods in a multi-temporal investigation of reach-scale morphodynamics associated with an extreme flood event. Chapter 4 then extends the analysis of physical flood

effects to include subsequent geomorphic readjustment and uses a combined numerical flow modeling and statistical classification method to quantify spatiotemporal hydrodynamics and patterns of habitat suitability for brown trout. A final concluding chapter then summarizes results from and linkages between each research chapter and puts the findings in broader context.

1.3 Literature review

1.3.1 Geomorphic principles

In its simplest form, channel morphology in terms of width, depth, and slope, has long been understood as a function of sediment load and discharge. While early studies in fluvial geomorphology were largely concerned with qualitative descriptions of historical landscape evolution [Baker, 1988], examples exist of attempts to disentangle relationships between interrelated factors and to determine their relative importances. Analysis of stable engineered canals led to the formulation of hydraulic geometry relationships under equilibrium conditions termed regime relations. Lindley [1919] described channels as changing width, depth, and gradient through sediment transport until a stable channel formed and provided empirical relations between channel dimensions and velocity. He also recognized the controlling influence of bed material on channel shape [Lindley, 1919]. Lane [1955] continued with this equilibrium approach in natural systems, introducing the relationship

$$Q_s D \propto QS$$

where Q_s is the quantity of sediment, D is the particle diameter, Q is the discharge, and S is the channel slope. Similarly, Leopold and Maddock [1953] described simple power-law relationships between sediment load, discharge, and channel dimensions, indicating that changes in discharge and sediment load could result in channel adjustments in terms of width, depth, slope, or sediment size.

These hydraulic geometry relations marked an important step in describing river morphology in terms of cross sectional dimensions, but several early studies also examined planform channel patterns. Leopold and Wolman [1957] seminal study of braided, meandering, and straight river patterns described potential con-

trols on planform geometry and put forth the empirical relationship (in its original imperial units)

$$S = 0.06Q^{-0.44}$$

marking the critical slope threshold below which channels were generally meandering and above which channels were generally braided or straight. Schumm and Khan [1972] also analyzed planform geometry using flume experiments relating sediment load and slope, illustrating the potential for changes in sediment load to induce changes in river pattern.

While these early conceptual models of channel morphology performed well in describing empirical patterns, they lacked a solid physical basis. Numerous researchers have since expanded on these concepts, providing interpretations of the physical processes that create channels and give rise to the empirical scaling relations discovered for most natural fluvial systems. Sediment transport and the flow of water can be described by the laws of conservation of mass and Newton's laws of motion [Stevens and Nordin, 1987]. Assumptions of uniform one-dimensional steady flow are usually applied, meaning the downstream gravitational force of the flowing water is balanced by the resistance of the channel bed and banks. This can be described in terms of the shear stress the water exerts on the banks by

$$\tau_0 = \rho g R S$$

where τ_0 is the total basal shear stress, ρ is the fluid density, g is gravitational acceleration, and R is the hydraulic radius. Newton's Second Law can be applied in several manners to relate velocity and channel resistance [Ferguson, 2007]:

$$u = \frac{d^{2/3} S^{1/2}}{n} = C\sqrt{dS} = \sqrt{\frac{8gdS}{f}}$$

where u is the mean velocity, n is the Manning roughness coefficient, d is the mean flow depth, C is the Chezy resistance factor, and f is the Darcy-Weisbach friction factor.

Sediment transport is related to shear stress and can be considered in terms of a dimensionless shear stress termed the Shields number as

$$Q_b/Q = f[\rho g d S/g(\rho_s - \rho)D]$$

where Q_b is bed material load and D is grain size to be moved. The term in brackets represents the Shields number, often denoted τ^* [Church, 2006]. This relationship describes the ability of a stream to move sediment, which occurs when τ^* exceeds the critical value τ_c^*. The Shields number can be rearranged with the constants replaced to yield

$$S = 1.65\tau^* D/d$$

which indicates that slope, scale, and sediment characteristics determine sediment transport in a channel [Church, 2006]. Rivers can therefore adjust slope, roughness, or channel dimensions to accommodate changes in conditions. The principle of continuity can also be applied to conceptualize changes in sediment transport through a channel section and bedload sediment transport can be related to sediment supply (Q_s) through

$$Q_s - Q_b = \Delta S_s$$

where ΔS_s is the change in sediment storage in a given area. This relationship states that if the sediment supply to a reach is greater than sediment transport capacity, sediment will be stored in the reach [Montgomery and Buffington, 2004].

The above physical determinants relating sediment transport, discharge, and channel morphology provide a better understanding of how and why channels may respond to perturbations than empirical relationships do. While the interrelationships are complex, they provide the necessary basis with which to explain channel forms. For example, Church [2006] described alluvial river channels in terms of physical sediment transport processes, relating stream competence (quantified by the Shields number) and sediment budgets to channel morphology and stability. The concept of river regime has also benefited from a physical explanation; Eaton et al. [2004] developed a rational regime model based on work done by Millar and

Quick [1993] and Millar [2005] to relate physical river processes such as flow resistance, sediment transport and bank stability to predictions of hydraulic geometry. This regime model approach has also been extended to a physically based reevaluation of planform morphology. Eaton et al. [2010] reviewed Leopold and Wolman [1957] data in a regime model context and proposed more refined slope-discharge relationships differentiating channel types. However, such regime analyses are most applicable to rivers that have sufficiently adjusted to their conditions to be considered in equilibrium and may not apply to very short or very long timescales over which most landscapes can be considered to be in transient conditions [Lane, 1955]. The stochastic nature of sediment transport in rivers also complicates simple relationships between sediment transport and channel form, particularly in mountainous regions where mass wasting events dominate sediment transport processes [Einstein, 1950, Engelund and Fredsøe, 1976, Benda, 2003, Church, 2010].

1.3.2 Physical aquatic habitat

Physical habitat is strongly controlled by stream hydrogeomorphology. Habitat can be described in terms of many features and at many scales; watershed habitat characteristics can be considered nested hierarchies of geomorphic features ranging from microhabitats such as individual cover features and mesohabitats at the scale of riffles and pools, to the overall catchment scale determined by factors such as surficial geology and bioclimatic control [Gregory et al., 1991]. Factors commonly considered to be important to physical habitat include water depth and velocity [Hogan and Church, 1989], riparian vegetation cover [Roy et al., 2005], sediment size and availability [Kondolf, 2000], water temperature [Hari et al., 2006], and in-stream large wood [Abbe and Montgomery, 1996]. Many of these factors have reciprocal relationships with hydrogeomorphology. For example, feedbacks between riparian vegetation and physical processes shape both in-stream and floodplain ecosystems through complex relationships between sediment stabilization, physical disturbance patterns, and vegetation succession [Stallins, 2006]. Understanding these recursive relationships is necessary for informed management of riverine habitat. Although the direct influence of physical habitat on population-level ecological changes can be difficult to demonstrate and is dependent on the

species and organism being studied, many studies have found effects of some aspects of physical habitat on species composition. Litvan et al. [2008] found that rip-rap grade control structures led to increases in macroinvertebrate biomass, density, and diversity, and Rowe et al. [2009] found that 18 different physical habitat variables were significant predictors of fish assemblages. Smokorowski and Pratt [2007] also found strong links between habitat alterations and fish biomass in a meta-analysis of direct habitat manipulation experiments.

Given the importance of physical habitat for overall aquatic ecosystem health, many methods have been developed to quantify habitat. Fish habitat is the major focus of most methods, as fish can be easily captured and measured, are responsive indicators of potential stressors, and are 'charismatic' and economically important organisms [Davis, 1995]. One widely used method is the Physical Habitat Simulation System (PHABSIM, [Bovee, 1982]) which relates in-stream hydraulics to fish habitat using empirical habitat preference curves for different species. PHABSIM is commonly used to inform stream habitat analysis using the in-stream flow incremental methodology [Bovee et al., 1998] and can give weighted usable area (WUA) curves describing available habitat as a summation of physical microhabitat quantity and quality. Although common, these types of methods that rely on empirical abundance-environment relations have been criticized for ignoring biological interactions such as density-dependent competition and for unfounded interpretations of cause-and-effect when other causal mechanisms may be at play [Van Horne, 1983, Lancaster and Downes, 2010]. They are also difficult to modify for broader scale controls on fish populations such as lateral and longitudinal connectivity and metapopulation dynamics. However, regardless of individual method applicability, available physical habitat is a primary control driving many key biological processes.

In practical terms, one of the most relevant scales for the assessment of river ecosystem structure is the mesoscale [Frissell et al., 1986, Fausch et al., 2002]. Working at this spatial scale allows for efficient characterization of in-stream habitats while still providing relevant measures that are directly relatable to smaller scale controls on fish populations. At this scale, physical habitat patches can be explicitly identified in terms of geomorphic units (pools, glides, runs, and riffles) with distinct depth, velocity, and sediment patterns [Rosenfeld et al., 2011] and there-

fore different quality as habitat. Because of the general correspondence between the size of fluvial geomorphic features and the time scale at which they change [Ward, 1998], working at this scale facilitates understanding of linkages between reach-scale geomorphic processes such as lateral channel migration or changes in sediment supply and habitat changes relevant to fish populations. It also allows for the identification of other factors of importance such as floodplain and hyporrheic connectivity, backchannel characteristics, riparian vegetation patterns, and large wood features. Although in-stream habitat unit classification based on geomorphic features has been criticized as being subjective and often improperly used in monitoring and management applications [Poole et al., 1997], mesoscale physical habitat is a vital component of aquatic ecosystems and may provide a useful eco-geomorphological framework for interdisciplinary studies [Thoms and Parsons, 2002]. This is particularly true over longer time scales where more detailed measures of physical habitat are impossible to assess. However, as with any scale-dependent measure, it is important to complement measures of mesohabitat with perspectives from other scales, such as the stream segment scale where more general morphologic controls may be evident, and the microhabitat scale where unique combinations of velocities, depths, and sediment sizes may provide more detailed quantitative measures of actual fish habitat distributions.

1.3.3 Characterizing river structure

This thesis focuses on remote sensing of river structure in terms of topography and bathymetry. Fluvial remote sensing has expanded rapidly since the mid-1990s, fueled both by the proliferation of new sensors and platforms and commensurate advances in computing power and geographic information systems (GIS) [Fitzpatrick, 2001]. The most common methods include aerial photography, satellite imagery, RADAR and LiDAR [e.g., Fryer, 1983, Leclerc and Hickin, 1997, Lorang et al., 2005, Williams et al., 2011, Hugue et al., 2016], each of which comes with trade-offs in data quality, ease of acquisition, resolution (temporal and spatial), extent, and cost. As the broader perspective of discontinuities and spatial complexity has gained traction in geomorphology, more focus has been placed on the accurate determination of river morphology in three dimensions to quantify

morphological adjustments over multiple scales, to visualize vertical in addition to planform channel adjustments, and as input to two or three dimensional numerical models of channel processes [Lane, 2000]. In particular, digital photogrammetry (or structure-from-motion) techniques have emerged as an efficient and accurate way to quantify river channel topography, making use of multiple images overlapping covering features of interest from different angles to reconstruct three dimensional structure [Lane, 2000, Fonstad et al., 2013, Javernick et al., 2014, Woodget et al., 2014, Javernick et al., 2015]. Because these methods can be applied with consumer-grade imagery and without rigorous estimation of camera parameters or position [e.g., Micheletti et al., 2015], digital photogrammetry can provide an accessible, accurate, and efficient way to measure channel elevations. However, some logistical challenges exist depending on site and setting; issues such as turbid or deep water, high relative vertical relief, and vegetation obstructions can all limit the applicability of digital photogrammetry in fluvial environments.

In order to generate a seamless characterization of river structure in three dimensions, measures of submerged bathymetry are often required to correct or mosaic with elevation data measured for exposed areas. Passive optical remote sensing such as that used for photogrammetry measures incoming reflected solar radiation. When light passes through water it is absorbed exponentially according to Beer-Lambert's law, causing deeper areas to look darker. Empirical models [e.g., Lyzenga, 1981] take advantage of this fact to generate a regression between field-measured depths and radiance values measured at the sensor. Because different frequencies of light are absorbed at different rates in the water column, a band ratio is often used. The band frequencies that are most applicable vary based on condition and environment, but red and green bands (longer wavelenths, absorbed more quickly) from optical imagery vary more strongly in shallow water than blue (shorter wavelength, absorbed less quickly), so many applications rely on a ratio of red and green bands to relate to water depth [e.g., Winterbottom and Gilvear, 1997, Legleiter et al., 2004, Carbonneau et al., 2006]. Although this empirical calibration procedure is site specific (as opposed to physically based radiative transfer models that should be broadly applicable) and requires ground-measured data (which is counterproductive to the basic advantage of remote sensing), it implicitly accounts for factors such as changing stream bottom conditions and atmospheric influences

on radiative transfer. Also, field data are usually collected regardless to assess accuracy in targeted remote sensing applications, so ground truthing and collection of calibration data can often go hand in hand [Flener, 2015].

1.4 Thesis objectives

The strong interrelationships between channel morphodynamics and ecosystem function mean that lotic ecosystems are sensitive to perturbations and changes in governing conditions. It is therefore essential to understand the process-form linkages that drive both geomorphic change and aquatic habitat dynamics. This is best achieved by interdisciplinary study through a combination of empirical observations, conceptual, physical, and numerical modeling, and long-term monitoring. While these factors have long been a foundation of fluvial study and management in some form, recent methodological and conceptual advances have led to an increased call for multi-scale investigations that embrace spatiotemporal variability. In particular, remote sensing and numerical modeling approaches have recently emerged as efficient and accurate ways to measure and model dynamic river systems. However, the body of research applying and interpreting such analyses is still underdeveloped, and more studies of eco-hydrogeomorphic variability are needed, particularly in an environmental change or disturbance context. With this broad motivation in mind, the overall research objective of this dissertation is to determine how large flood events shape channel morphology and what the implications are for aquatic habitats. Given the rarity of large flood events, their relative contribution to geomorphic processes is difficult to determine; smaller competent floods may contribute more overall geomorphic work due to their frequency, but large events can leave lasting legacies that condition future geomorphic responses and shape ecosystems for decades to come [Wolman and Miller, 1960]. To address this research objective, the dissertation focuses on three primary questions:

1. How can remote sensing using UAVs advance the methodological underpinnings of data collection and information extraction in spatially complex fluvial environments?

2. What are the detailed reach-scale geomorphic effects of an extreme flood event, and can fluvial adjustments be explained by pre- and post-flood conditions?

3. What is the relationship between flood-induced geomorphic change, hydromorphic diversity, and aquatic habitat structure?

Chapter 2

Hyperspatial remote sensing of channel reach morphology and hydraulic fish habitat using an unmanned aerial vehicle (UAV)

2.1 Introduction

Recent advances in digital image collection and processing techniques have led to the increased use of remote sensing and photogrammetry for river research and management. Applications range from broad scale analyses of change from conventional aerial photography [e.g., Lapointe et al., 1998] and satellite-based assessments of stream temperature [e.g., Cherkauer et al., 2005], to close range photogrammetry of small streams under vegetation cover [e.g., Bird et al., 2010], or of gravel structures in flume experiments [e.g., Butler et al., 2002]. Such studies have demonstrated the utility of remotely sensed data at many scales and supported the call for spatially continuous perspectives of fluvial systems that embrace heterogeneity of physical processes and aquatic habitat [Fausch et al., 2002, Carbonneau et al., 2012].

Central to any remote sensing application is the need to balance data type, quality, and ease of acquisition at appropriate spatial and temporal scales. Although satellite imagery and conventional aerial photography are widely available and can provide sub-meter spatial resolutions with a wealth of historic data, they can be costly and are not suited to tailored, site-specific studies at fine scales. Both approaches also offer limited utility for determination of topography, which is becoming increasingly necessary in studies focusing on three-dimensional river features [Lane, 2000]. While elevation data have traditionally been collected through ground-based surveys, this approach is time consuming and does not benefit from the complete spatial coverage offered by remote sensing. Airborne LiDAR surveys can also provide high quality topographic data [Biron et al., 2013], but typically require a substantial financial investment, thus potentially limiting the adoption of airborne LiDAR as a monitoring tool. To address such issues, a focus on photogrammetric production of DEMs has emerged, and the accuracy and limitations of these techniques in fluvial systems are well documented [e.g. Pyle et al., 1997, Westaway et al., 2001, Carbonneau et al., 2003, Fonstad et al., 2013].

Using photogrammetry to efficiently produce high quality DEMs from remotely sensed data provides an ideal method with which to address questions of dynamic linkages between geomorphic processes and aquatic habitat in three dimensions. In particular, a focus at intermediate spatial scales (i.e. 10^1 - 10^3 m) is needed to bridge existing gaps between research and conservation at scales relevant to fish populations and communities [Fausch et al., 2002, Wheaton et al., 2010a]. At such scales, fish habitat is often estimated in terms of flow depth and velocity distributions [e.g. Rosenfeld et al., 2011], or mesohabitat characteristics [e.g. Hauer et al., 2009]. However, difficulties exist in efficiently collecting the necessary topographic data, and important qualitative aspects of habitat such as cover are often neglected [Ayllón et al., 2012, Boavida et al., 2012]. Similarly, channel morphology is often treated as a constant factor, due largely to the difficulties associated with coupling morphologic change with habitat analyses. To gain a better understanding of intermediate-scale morphology-habitat relationships, tailored data collection with high spatial and temporal resolution is required. These data should be able to be easily integrated with other spatial data in a GIS framework to facilitate cross-scale applications [e.g. Hardy and Addley, 2001] and repeated

frequently in monitoring and adaptive management contexts [Downs and Kondolf, 2002].

Many remote sensing platforms aimed at intermediate or reach scales have been developed and tested. Tethered balloons [Church et al., 1998] and kite aerial photography [Smith et al., 2009] have been applied to feature mapping and DEM generation, and Vericat et al. [2008] and Fonstad et al. [2013] demonstrated the potential of lighter-than-air helikites to determine topography and map reach scale fluvial features such as wetted channel outlines. However, these systems are easily affected by weather conditions and may lack the stability needed to produce high quality DEMs. Appropriate imagery can also be acquired from helicopters or small aircraft [e.g. Booth et al., 2007], but these can be limited by flying height restrictions and do not offer the operational flexibility needed to capture many scales of environmental change. One emerging method for the collection of suitable scale and quality imagery is the use of unmanned/uninhabited aerial vehicles (UAVs). UAV technology has diversified rapidly in the past decades as miniaturized components (autopilots, inertial measurement units, GPS receivers, and telemetry) and platforms have advanced, and UAV-based sensors have been applied to a range of civil and research applications [e.g. Hugenholtz et al., 2012, Watts et al., 2012, Hugenholtz et al., 2013].

In fluvial settings, Lejot et al. [2007] tested imagery from a fixed-wing Pixy drone in a variety of contexts, mapping bathymetry of a 5 km length of river and an oxbow lake, and using photogrammetry to create DEMs of two small exposed gravel bars. They were able to produce high quality bathymetric maps over a range of bed substrates and 5 cm pixel resolution DEMs, with average vertical errors between 0.157 and 1.069 m. However, they noted drawbacks associated with platform instability during image acquisition, and their photogrammetry was limited by poorly defined external image parameters due to the fact that the drone could not support an inertial navigation system or differential GPS [Lejot et al., 2007]. With the technological advances that have occurred in even the past five years, continued investigation of the usefulness of UAVs to river research is warranted. In this paper, we address the applicability of UAVs to fluvial systems. Specifically, we test the accuracy of an orthomosaic and DEM generated from images captured by a fully autonomous quadcopter and evaluate the ability to measure key metrics of reach-

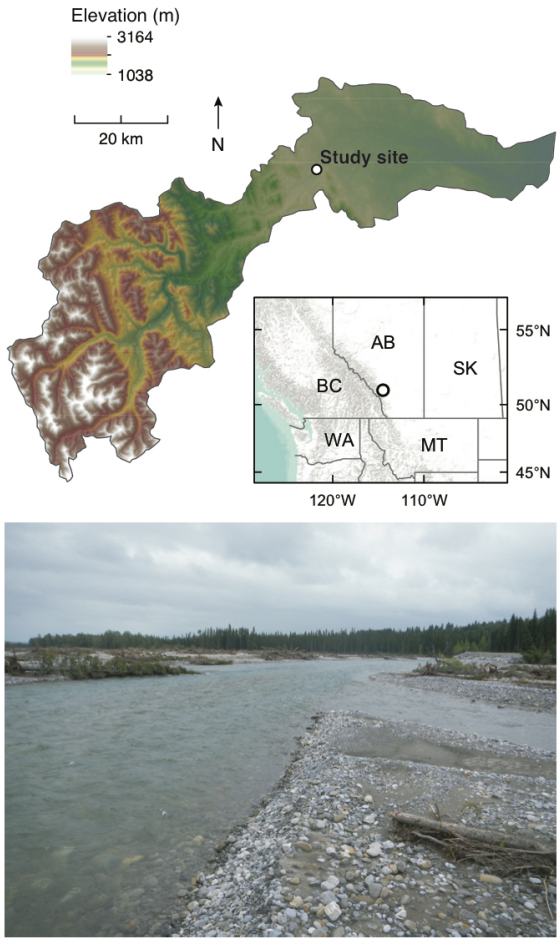

Figure 2.1: Location of the study reach within the Elbow River watershed and example ground-level image

scale morphology. We then assess the utility of the data in producing estimates of available hydraulic habitat through the initialization of a 2D hydrodynamic model and mapping of important aquatic habitat features.

2.2 Methods

2.2.1 Study site

Elbow River is a gravel bed river in southern Alberta, Canada that flows east out of the Rocky Mountains (Figure 2.1. At the study site near the town of Redwood Meadows (50.988°N, 114.509°W), the river flows through a 200 m wide active channel with extensive gravel bars and is split into 2-4 anabranches. The drainage area is 791 km^2 at the Water Survey of Canada gauging site directly upstream at Bragg Creek, and elevation at the site is 1,250 m. The study reach was 1 km long and the survey extended across the active channel and into floodplain forest for a width of approximately 350 m. All survey work was performed on September 25, 2012 when water levels were low at a discharge of 5.9 m^3/s.

2.2.2 UAV survey and photogrammetry

The UAV used to acquire the imagery for the orthomosaic and DEM generation was an Aeryon Scout (Aeryon Labs Inc.) with a Photo 3S high-resolution (non-metric) camera (Figure 2.2). The Scout is a small quadcopter that can be pre-programmed to fly set waypoints using a small tablet PC. These waypoints correspond to image center coordinates calculated from the specified flying height, image overlap and camera parameters. At each waypoint, the 3-axis stabilized camera with an 8.4mm lens and a field of view of 37° x 29° captures true-color images with embedded geo-tags and metadata. To ensure correct camera positioning for each image, onboard servos automatically adjust the platform position and camera orientation throughout the flight.

For the aerial survey, we positioned 45 highly visible ground control points (GCPs) throughout the study reach to assist with the photogrammetric processing. We measured the position of each GCP on the ground with a real-time kinematic (RTK) GPS, as well as 297 geolocated check points for testing of the generated DEM. The UAV survey itself was performed in eight flight lines running parallel with the river for a total of 192 separate images, with the quadcopter flying at a speed of 5 m/s and a height of 100 m above the ground surface. Although the Scout can fly up to 3 km from the base station, regulations dictate that the aircraft

Figure 2.2: Aeryon Scout quadcopter

must be within line of sight during flight (∼800 m). At the study reach, the wide, straight channel allowed for easy sightlines and all images were captured in a single flight that took about 30 minutes.

The autopilot log and geotagged images were then processed with the Enso-MOSAIC UAV package (MosaicMill Ltd., Finland). This software was used for all photogrammetry steps, including calculation of internal orientation of the Photo 3Sł camera to create a calibration file for subsequent processing. The photogrammetry sequence involved the automatic identification of image keypoints and bundle block adjustment (BBA) and automatic aerial triangulation (AAT). BBA was used to calculate the location and rotation of the camera for each image and solve the AAT based on a combination of manual and automatic tie points (including GCPs). After each iteration the adjustment error was assessed, tie points with largest residuals were removed, and the process was repeated until the final BBA converged. This continued until the largest residuals were deleted and the accuracy of the mosaic was optimized. Following this step, the final DEM was generated by the software and used to orthorectify the image mosaic. Although processing time varies based on computer memory, number of images, and experience of the operator, the data for this study were processed completely in approximately a day.

2.2.3 Submerged DEM correction

One of the most commonly cited challenges of photogrammetric analyses of rivers is the lack of reliable through-water photogrammetry, limiting the accurate determination of submerged topography [e.g. Lane, 2000, Westaway et al., 2000, Bird et al., 2010]. Although the shallow, clear water at Elbow River study reach allowed for an apparent submerged topography to be calculated in the initial DEM generation based on homologous points, refraction at the air-water interface, water surface waves, and white-water areas in riffles can complicate automated photogrammetry [e.g. Fryer, 1983, Fryer and Kniest, 1985], often resulting in an underestimation of actual water depths and therefore erroneously high bed elevations. To account for this, we tested two methods of DEM correction: a simple first-order correction for the refractive index for water [Westaway et al., 2000], and an empirically calibrated depth estimate based on pixel color values in the orthomosaic. As both methods require a water surface from which to subtract depths, we extracted elevations at points spaced 1 m apart along the waters edge, removed unreliable points (e.g. under overhanging vegetation), and then interpolated a water surface profile using ordinary kriging [Westaway et al., 2001, Legleiter, 2012, Williams et al., 2013b].

For the refractive index correction method, we subtracted the uncorrected DEM from the water surface elevations, yielding a map of apparent water depth. We then multiplied apparent water depths by a constant refractive index for water (1.34) to determine actual depths, which were subsequently subtracted from the water surface elevations to give the corrected DEM. For the second correction method, we produced a map of water depths based on an empirically calibrated relation between measured water depth at GPS check points and orthomosaic pixel color values [e.g. Winterbottom and Gilvear, 1997, Legleiter et al., 2004, 2009, Flener et al., 2013]. After testing all available RGB band combinations, we found that a ratio of log-transformed red/green values within a moving filter of 1 m^2 to account for substrate and water surface irregularities yielded the strongest relationship (R^2 = 0.77). These water depths were then subtracted off of the water surface elevations to produce the corrected DEM.

2.2.4 Fluvial morphology metrics and habitat mapping

To assess the ability to extract key metrics of reach-scale morphology and available aquatic habitat, we combined a depth-averaged hydrodynamic model with features mapped from the orthomosaic. We determined sediment sizes on exposed bars using techniques similar to Carbonneau [2004], taking 30 close range, geolocated vertical photos of 1 m^2 bar surface patches with visually consistent sediment size distributions. We then determined the median grain size (D_{50}) of each image using a manual photosieving graphical user interface programmed in MATLAB (Mathworks, 2008) to measure the b-axis of 50 clasts spaced on a 5x10 grid in each photo. These D_{50} values at each close range image location were then related to image texture calculated as standard deviation within a 1 m^2 moving window in the UAV aerial orthomosaic (Figure 2.3). Image texture, defined as a the variation between the spectral properties of a pixel and its neighboring pixels, was calculated with the Spatial Analyst ArcGIS extension's neighborhood statistics tool. Although Carbonneau [2004] compared the use of local image texture to two-dimensional semivariance and chose semivariance because it is less sensitive to illumination changes associated with daylight or camera exposure times, we found image texture to produce a high quality empirical relationship (R^2 = 0.82) and had no issues with lighting given the consistent sunlight during the 20 minute acquisition flight. To produce a final map of grain sizes throughout the reach, we extracted exposed gravel areas using a supervised classification and applied the texture/(D_{50}) relationship.

With the 5 cm resolution of the orthomosaic, large wood (LW) pieces and jams were clearly distinguishable and were manually digitized. Jams were defined as groups of LW with three or more pieces and were digitized as polygons, while each individual piece of LW was digitized as intersecting lines representing the diameter at breast height and the length. In addition to LW, we digitized features that could provide cover to fish, with a focus on brown trout (*Salmo trutta*). Although preferences may vary based on factors such as geographical region, fish life stage, time of year, and changing flow conditions [e.g. Ayllón et al., 2009], brown trout are heavily dependent on cover throughout their life cycle [Armstrong et al., 2003]. We digitized important cover features that included overhead vegetation, undercut

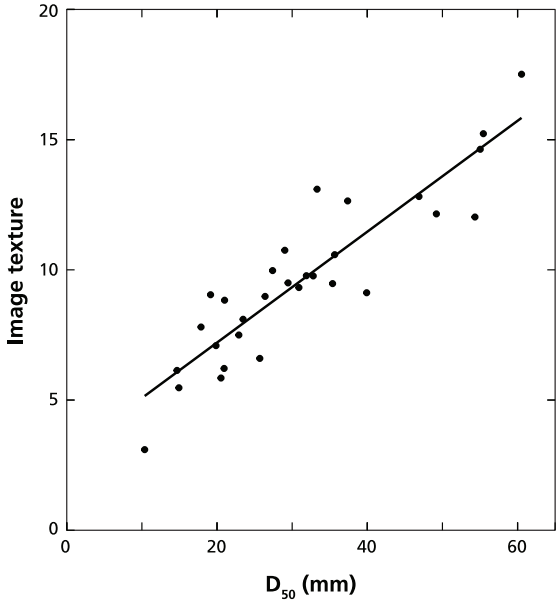

Figure 2.3: Relationship between D_{50} determined through photosieving and orthomosaic image texture within a 1-m^2 window

banks, pools, and water surface turbulence. All of these features can provide visual overhead cover, and, in addition to in-stream and overhanging LW, constitute the main sources of cover use [Courtney et al., 1998].

We then used the two-dimensional depth averaged hydrodynamic model River2D to model flows at the 5.9 m^3/s discharge during the time of image acquisition. River2D is a finite element model that is based on a conservative Petrov-Galerkin upwinding formulation and solves the Saint-Venant equations for conservation of mass and momentum. The model was developed for use in natural streams and has been tested in a wide range of systems [e.g. Katopodis, 2003, Lacey and Millar, 2004, Waddle, 2009]. River2D also includes a component to evaluate fish habitat that facilitates the incorporation of habitat preference curves and calculation of suitabilities and overall weighted usable area (WUA) throughout the modeled reach based on depths, velocities and a channel index describing physical features such as substrate or cover. The model takes an input topography file and creates a finite element mesh of triangular polygons used to solve for flow

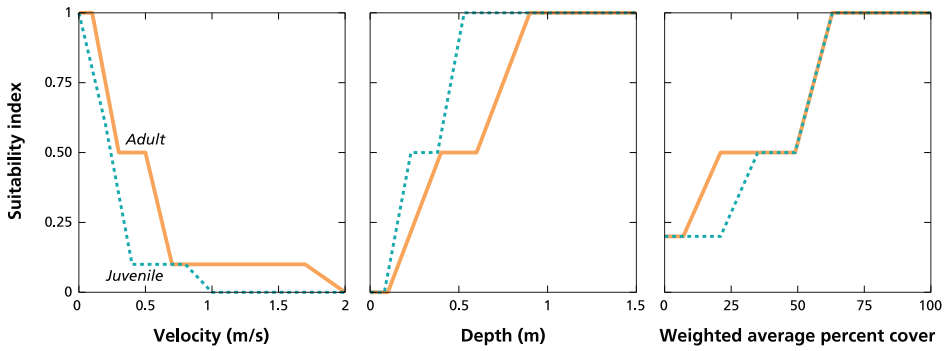

Figure 2.4: Brown trout habitat suitability curves for depth, velocity, and weighted average percent cover

depths and velocities. Other necessary inputs include equivalent roughness height (k_s), initial flow conditions, and boundaries to define the model extent.

To model flows in the Elbow River study reach, we selected a 640 m long subsection downstream of a point where all flow was contained in a single channel to ensure inflow discharge at the upstream boundary was accounted for correctly. We extracted elevations from the corrected DEM at points spaced 1 m apart and created a bed topography file supplemented with breaklines and boundaries that were digitized directly from the orthomosaic. Breaklines were placed to aid in correct interpolation along linear features such as steep cutbanks. We then used a uniform fill with a 1 m spacing to develop the computational mesh, resulting in 105,525 nodes and 209,353 elements throughout the modeled area. We calibrated the model by varying k_s until the water surface elevations of the steady-state solution matched observed water surface elevations from the orthomosaic and DEM. Although a wide range of estimates for equivalent roughness height have been used, the final value we used was 0.12 m, which is equivalent to $\sim 2 * D_{84}$ and lies within commonly cited ranges [Millar, 1999]. The model was run to steady state convergence based on the inflow discharge of 5.9 m^3/s measured at the Water Survey of Canada gauge upstream and an outflow water surface elevation of 1239.5 m measured directly from the DEM.

Available hydraulic habitat was calculated as WUA based on the modeled depths and velocities and digitized cover features as in the commonly used physical

habitat simulation system (PHABSIM). Because of the strong impact that regional differences can have on fish preference, we used habitat preference curves developed for juvenile and adult brown trout in the Kananaskis River, AB [Courtney et al., 1998]. These curves describe the suitability of different depth, velocity, and cover values as a habitat suitability index (HSI) from 0 to 1 and were based on field data of fish habitat selection and supplemented by data from a telemetry study by Bunt et al. [1999]. The preference curves are shown in Figure 2.4. To create a channel index file representing cover availability, we used our digitized cover features to determine percent cover, assuming 100% cover directly under features and 50% cover within a buffer of 1 m. Courtney et al. [1998] developed a weighting system based on relative value of cover types, so we grouped our cover features into instream objects (*instream*, provided by instream LW), instream overhead (*overhead*, provided by pools, water surface turbulence, and cutbanks), and offstream overhead ($offstream$, provided by overhanging LW or live vegetation). We then used the equation:

$$cover = (10 * instream + 10 * overhead + 2 * offstream)/22 \tag{2.1}$$

to calculate weighted average percent cover as in Courtney et al. [1998]. This format matched their determined cover preference curves, but we also modified the channel index curve to have a suitability of 0.2 at 0% cover, effectively assigning areas with no cover the suitability determined for gravel substrates [e.g. Ayllón et al., 2012]. A composite suitability index (CSI) was calculated for each model node as the product of the HSI values for depth, velocity, and channel index, and multiplied by the area associated with each node for a local WUA. The sum of all local WUAs gave the total WUA for the study reach.

2.3 Results

2.3.1 Accuracy assessment

The orthorectified image mosaic and DEM of the study reach are shown in Figure 2.5. Visually, the high resolution orthomosaic and DEM clearly display the form and distribution of fluvial features of interest, with no visible artifacts from the pho-

Table 2.1: Error statistics equations. DEM elevations are termed z_{mod}, measured check point elevations are termed z_{obs}

Error metric	Equation
Mean error (ME)	$ME = \frac{\sum_i^n (z_{mod} - z_{obs})}{n}$
Root-mean-square error (RMSE)	$RMSE = \sqrt{\frac{\sum_i^n (z_{mod} - z_{obs})^2}{n}}$
Standard deviation of error (SDE)	$SDE = \sqrt{\frac{\sum_i^n ((z_{mod} - z_{obs}) - ME)^2}{n-1}}$
Maximum error (E_{max})	$E_{max} = max\|z_{mod} - z_{obs}\|$

togrammetry process. To assess the vertical accuracy of the DEM, we compared the modeled (DEM) elevations with the 297 independent GPS check points, stratified by subaerial exposed points and subaqueous submerged points. We calculated four accuracy parameters (Table 2.1) for exposed and submerged points: the mean error (ME), the root mean square error (RMSE), the standard deviation of the error (SDE), and the maximum absolute error. ME is a measure of the accuracy of the data that indicates any positive or negative systematic error, RMSE is a measure of dispersion of the frequency distribution of residuals that is sensitive to large errors, SDE provides information about precision and the distribution of residuals about the mean, and maximum absolute error describes the largest residual present for an understanding of the limits of the data quality [e.g. Li, 1992, Lane, 2000]. Residuals were calculated as field-measured GPS elevations subtracted from modeled DEM elevations; positive values indicate an overprediction of elevations in the DEM, negative values indicate an underprediction of elevations in the DEM. For submerged areas, we compared the error statistics for the uncorrected DEM, the DEM corrected using the red-green optical empirical method, and the DEM corrected using the simple refraction index method as described by Westaway et al. [2000]. Values for exposed and submerged points are shown in Table 2.2. Density plots for the exposed and the three submerged residual distributions were also created, as well as a scatterplot of elevation residuals against measured water depth for the three submerged DEMs (Figure 2.6).

Overall, exposed points were more accurate and precise than submerged points, with an RMSE of 8.8 cm and SDE of 0.68 cm. For submerged points, both cor-

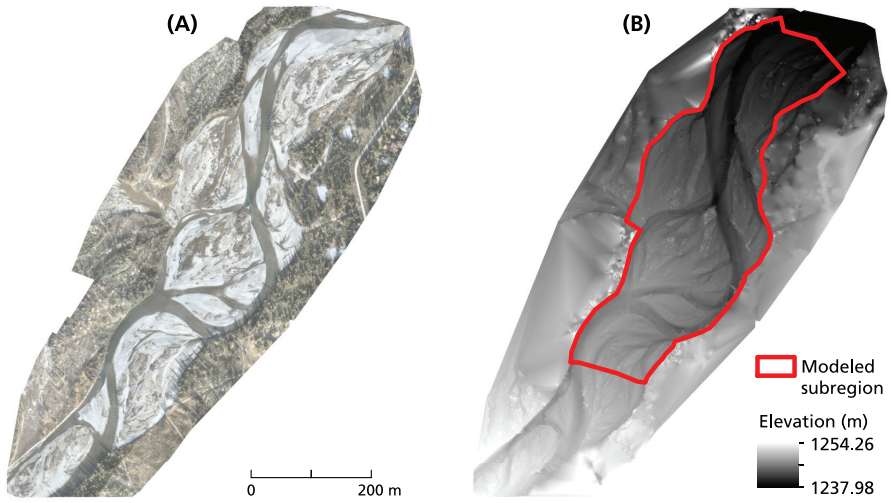

Figure 2.5: (a) Photogrammetry generated orthomosaic and (b) DEM, showing the extent of the subregion modelled with River2D

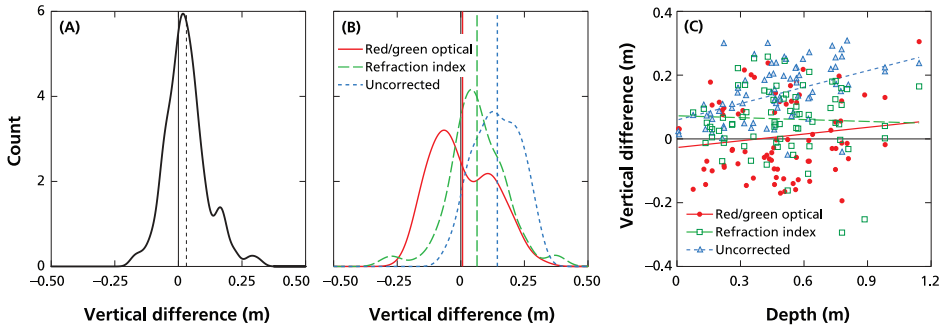

Figure 2.6: Density plots of vertical DEM elevations compared with RTK GPS check points for (a) exposed points, (b) uncorrected submerged points and the two depth correction methods, and (c) scatter plot of vertical errors versus depth for uncorrected submerged points and the two depth correction methods. Vertical lines on the density plots represent the mean error of each data set; elevation differences were calculated as DEM elevations minus RTK GPS elevations

Table 2.2: Error statistics comparing GPS checkpoint elevations with DEM elevations

	n	ME (m)	RMSE (m)	SDE (m)	E_{max} (m)
Exposed	221	0.032	0.088	0.007	0.320
Uncorrected submerged points	76	0.144	0.169	0.008	0.306
Red-green empirical correction	76	0.007	0.119	0.016	0.305
Refraction correction	76	0.064	0.130	0.003	0.387

rection methods improved the ME and RMSE compared to the uncorrected DEM, which consistently over-predicted bed elevations due to the effect of refraction on apparent water depths. Although the red-green empirical correction had a lower RMSE and ME than the refraction index method, it introduced substantial scatter to the residuals and had a high SDE. It also showed a slight increase in vertical error with water depth, while the refraction index did not. As both methods had strengths and weaknesses and overall similar errors, the choice of corrected surface to use was based on a visual comparison of the integrity of fluvial forms in the context of the desired application of hydrodynamic modeling. Although it was affected by shadows in certain areas, the topography generated by the red-green optical correction was chosen to be the most reliable, particularly along steep cutbanks where the refraction index method could not adequately correct the oversimplification generated in the original photogrammetry. For the River2D applications, we were able to remove unreliable shaded areas and interpolate between them, ensuring a submerged topography that captured the meaningful features in terms of bathymetry and instream habitat.

2.3.2 Feature detection and hydraulic habitat

The digitized cover features and calculated D_{50} values for exposed sediment are shown for the modeled subregion in Figure 2.7. The distribution and orientation of LW pieces and jams are evident; mid-channel braid bars contain large amounts of LW, and several large key log jams exist at channel confluences and adjacent to deep pools. This spatial complementarity of cover features is particularly ev-

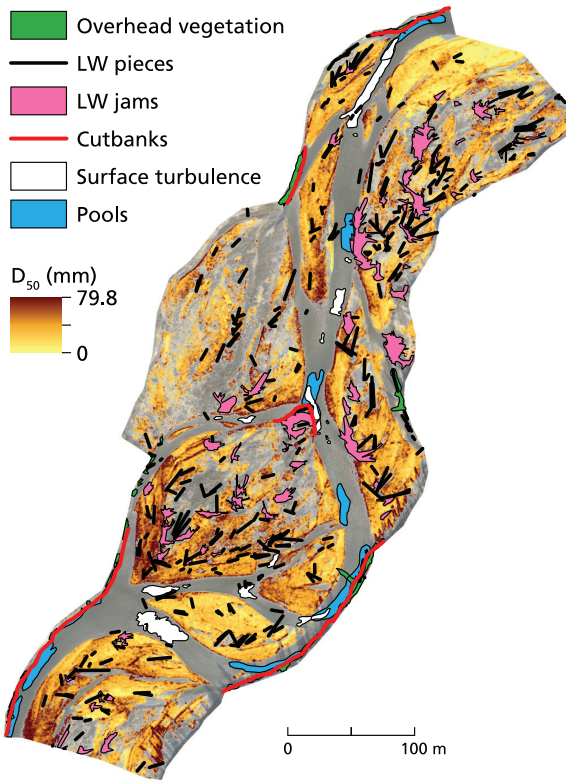

Figure 2.7: Digitized cover features and bar surface D_{50} values for the modelled subregion

ident at the outer banks of bend apices, where scour pools are frequently found in association with cutbanks, overhanging vegetation, LW accumulations on the banks, and broken water surfaces associated with turbulent water coming off of steep upstream riffles. D_{50} values also conform to expected trends, showing coarse sediment at bar heads and downstream fining. However, fine-scale patterns are affected by local shadows associated with topographic breaks and vegetation, which cause unrealistically high image texture values and therefore erroneously high D_{50} values.

The hydrodynamic model results from River2D are shown in Figure 2.8, with depths and velocities overlain on the orthomosaic. The modeling accurately captured complex flow patterns along the braided reach, following all major channels

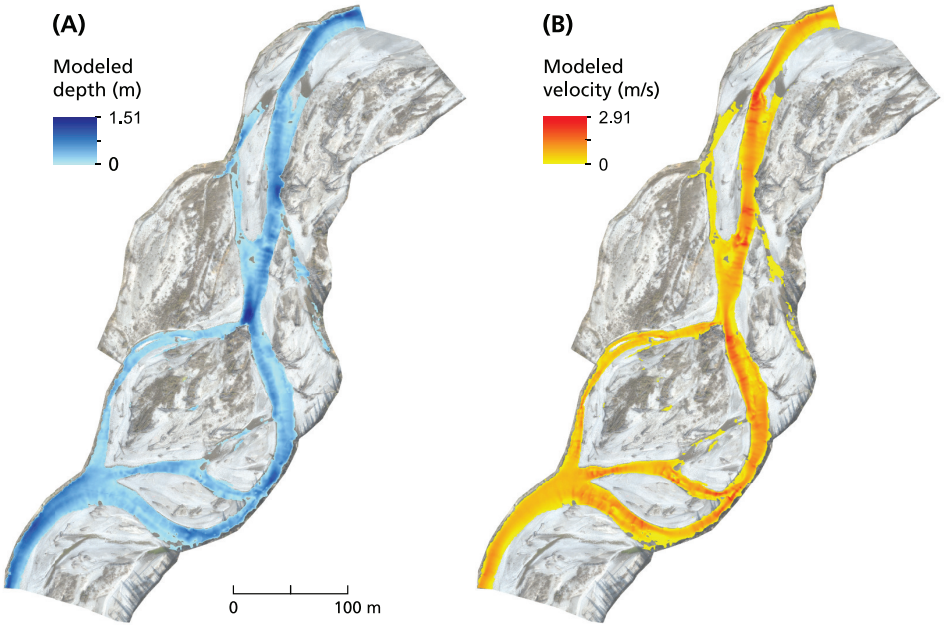

Figure 2.8: Results of River2D modeling showing (a) depths and (b) velocities

and replicating longitudinal pool-riffle sequences. Some sections of small channels with shallow flow were predicted to be dry by the model; depths in these sections are estimated to be less than 10 cm and the misrepresentation could be attributed to vertical errors in the DEM or limitations associated with the use of a uniform roughness length or threshold for groundwater flow across the study area. The effect of using an interpolated water surface during the DEM correction procedure is also evident in some areas, where unnatural transverse ridges show undulations in depth and velocity. These changes are on the scale of 1 m horizontally, which reflects the 1 m-spaced waters edge points used for water surface elevation interpolation. Although flow modeling can be sensitive to topographic uncertainty [Legleiter et al., 2011], these fine scale errors do not detract substantially from the reproduction of aspects of flow that are important to reach-scale hydraulic habitat distributions such depth and velocity distributions in relation to longitudinal pool-riffle morphology, transverse cross section shape and thalweg position.

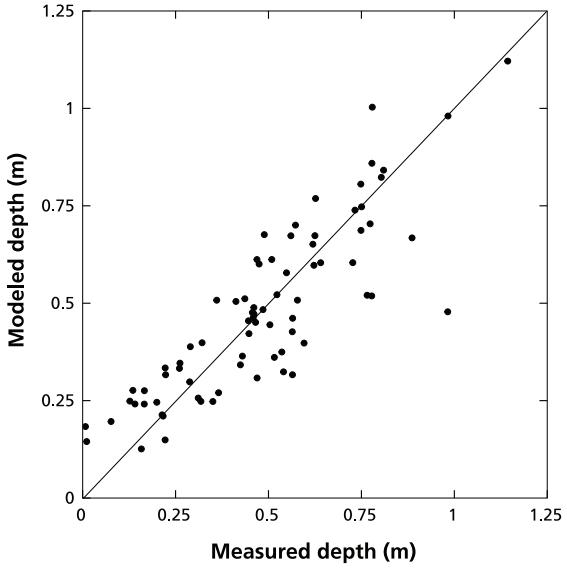

Figure 2.9: Comparison of River2D modelled depths with measured depths, with 1:1 line for reference

Accuracy of the hydrodynamic modeling was assessed with measured depths at 76 geolocated points. A comparison is shown in Figure 2.9. Overall, the points follow a 1:1 line, indicating correspondence between measured and modeled depths (R^2 = 0.73). Residuals are generally largest for deeper water; the largest absolute error was 0.50 m at a measured depth of 0.98 m. The RMSE for the depths was 12.5 cm, ME was -0.37 cm, and SDE was 12.5 cm. These errors likely reflect the propagation of errors from the submerged DEM correction or the effect of comparing GPS point measurements with depth values interpolated from the 1 m node spacing used in the modeling process [e.g. Bailly et al., 2010]. However, these depth errors are of similar magnitude to other reach-scale hydrodynamic models of braided channels (e.g. RMSE = 9 - 13 cm, [Williams et al., 2013a]), and allow for a reliable assessment of available hydraulic habitat throughout the reach.

With the combination of the flow patterns from River2D and the map of cover features from the orthomosaic, we were able to develop continuous maps for available habitat suitability throughout the reach for adult and juvenile brown trout. Patterns of CSI (reflecting combined preferences for depth, velocity, and cover)

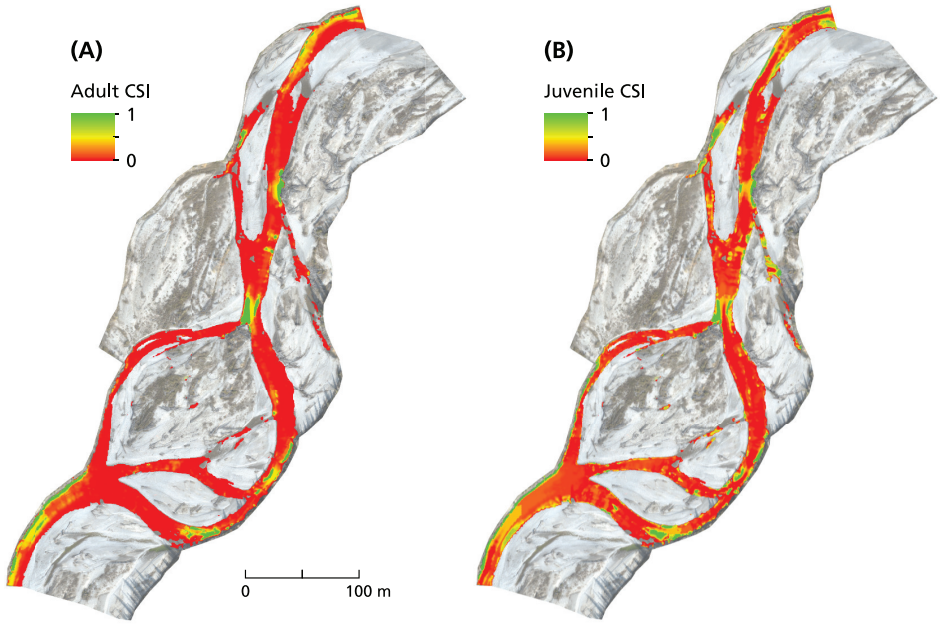

Figure 2.10: Spatial patterns of composite suitability index for (a) adult and (b) juvenile brown trout

are shown in Figure 2.10. High quality potential habitat for adult brown trout is found in pools and along cutbanks where adequate cover sources are present. Shallow riffle areas generally have low CSI values, reflecting their lack of multiple sources of cover and their high water velocities and low depths. High quality juvenile brown trout habitat is found in the same general areas, but CSI values are lower in high velocity thalweg areas or in areas of flow convergence and higher in shallower areas (e.g. pool exit/run areas, shallow side channels). Overall WUA is 338.5 m^2 for adult brown trout and 581.1 m^2 for juveniles. Because of the wide, anabranching nature of the study reach and lack of access to cover in most areas, the WUA values are substantially smaller than similar calculations based on depth and velocity suitability alone would be (due to the multiplication by another factor less than one representing cover). While this may preclude direct comparisons with studies that focus only on depth and velocity, it serves to highlight the importance of cover as a strong determinant of spatial patterns of habitat availability.

2.4 Discussion

This study demonstrated the utility of a small UAV to efficiently and accurately characterize reach-scale morphology and hydraulic habitat. We were able to generate a 5 cm orthomosaic and a DEM with vertical RMSE of 8.8 cm in dry areas and 11.9 cm in submerged areas, sufficient to initialize and run a 2D hydrodynamic model. Important channel features such as grain size on exposed bars, LW, and overhead cover elements were also easily identified from the high resolution orthomosaic and used to inform analyses of available habitat.

The accuracy of the topographic data generated represents an improvement over many other common survey methods. Vertical RMSE values for subaerial portions of airborne LiDAR surveys in similar settings are generally larger: Bowen and Waltermire [2002] found a value of 43 cm along the Green River floodplain in Utah, Legleiter [2012] reported 21 cm for exposed portions of the Soda Butte Creek in Wyoming, and Notebaert et al. [2009] found values of 15, 13, and 50 cm for tests of different LiDAR datasets in Belgian river valleys. However, terrestrial laser scanning can provide slightly better accuracy, with RMSE values in the range of 4 cm [Williams et al., 2013b] to 6 cm [Schürch et al., 2011]. Accuracies of photogrammetry generated surfaces at similar scales vary widely, from 4.5 cm RMSE with terrestrial oblique digital imagery [Chandler et al., 2002] to mean errors up to 1.07 m from aerial photogrammetry [Lejot et al., 2007], but are generally of decimetric scale [Lane, 2000]. The DEM from this study is also an improvement over the UAV-generated DEM of Hugenholtz et al. [2013], who found a vertical RMSE of 29 cm. These improvements over previous UAV photogrammetry could be attributed to platform stability; both Lejot et al. [2007] and Hugenholtz et al. [2013] used fixed-wing aircraft that may not be as stable as the quadcopter we used, and the use of detailed image parameters from the inertial measurement unit and onboard differential GPS clearly aided in DEM construction compared to Lejot et al. [2007].

Because UAVs allow for frequent surveys that could be used for monitoring and geomorphic change detection, it is important to consider the limitations imposed by the errors in the topographic data. If we assume that a repeat flight of the same Elbow River reach would have the same vertical error of 8.8 cm, we can calculate

a simple limit of topographic change (T) that can be reliably distinguished from error:

$$T = \pm 3\sqrt{(RMSE_1)^2 + (RMSE_2)^2} \tag{2.2}$$

where RMSE1 and RMSE2 represent the vertical errors from the first and second survey, and the multiplier 3 represents the extreme tails of a normal probability distribution, corresponding to a 99.7% confidence interval. This gives a threshold value of 37.3 cm, which, in the context of hydrogeomorphic change in a dynamic gravel bed river like the Elbow, would allow for identification of processes such as bar migration, chute cutoff, and bank retreat. Although some diffuse erosion and deposition processes may fall below the limit of topographic change [e.g. Brasington et al., 2003, Wheaton et al., 2010a, Perignon et al., 2013], the main changes on the river associated with competent floods would be detectable. If more detailed measures were required, a ground-based method such as total station surveying or terrestrial laser scanning may offer better results, however, such methods are much less efficient and do not offer the valuable vertical vantage point and high resolution imagery associated with UAV-based photogrammetry.

In terms of habitat analyses, the primary advantage of UAVs is that they can be used to collect a combination of topographic information and aerial imagery at the reach scale, with an appropriate resolution for many applications. Our calculation of habitat availability in terms of WUA demonstrates how new technology can be used to refine long-standing methods; although WUA has been criticized as overly simplistic and easily misinterpreted, coupling a 2D flow model with detailed measures of cover availability in a GIS context allows for intuitive visualization of habitat suitability throughout a reach in addition to a single WUA total. Despite its importance for many fish species, cover is frequently neglected in WUA calculations due to difficulties in characterizing it properly [Boavida et al., 2012]. UAV surveys ameliorate this problem while also providing the necessary topographic information to calculate depth and velocity distributions. The combination of cover features throughout the active channel and a continuous DEM also allows for flexibility in terms of modeling and scenario testing. For example, different flow scenarios could be run to determine how habitat and access to cover change with flow

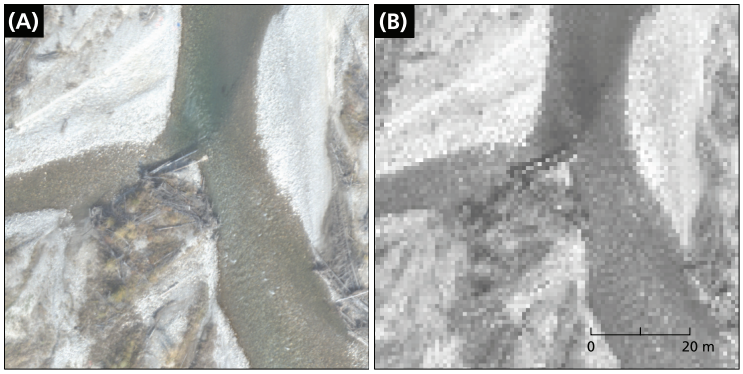

Figure 2.11: Detailed view of UAV orthomosaic with (a) the original 5-cm resolution and (b) resampled 80-cm resolution and grayscale to approximate IKONOS panchromatic imagery

level without the need for further intensive field surveys. Such detailed analyses of habitat features in relation to hydraulics could not be achieved with most other remote sensing sources. For example, Figure 2.11 shows a 70 m by 70 m section of the Elbow River orthomosiac with the original 5 cm resolution and the same area resampled to 80 cm resolution and converted to grayscale to approximate the panchromatic imagery offered by the IKONOS satellite. The loss of visual detail is striking: individual pieces of large wood and exposed grain sizes are indistinguishable, water depth patterns are masked, and cover features such as water surface turbulence are difficult to identify. Panchromatic imagery also precludes the use of band ratios to estimate water depths, and multispectral satellite imagery is of even lower spatial resolution ($\sim$4 m). Similarly, although DEMs can be generated with high resolution satellite imagery, vertical errors are typically on the scale of 5-10 m [Toutin, 2004], which is inadequate for reach-scale analyses of river structure.

Despite the potential benefits of UAVs for study of channel morphology and habitat, some restrictions and drawbacks exist. In terms of practical issues, UAVs are best suited to rivers with a wide active channel where trees do not obscure much of the aerial perspective. Vegetation can also affect the generation of DEMs, as photogrammetry does not allow for the determination of a bare earth DEM with vegetation removed in the way that airborne LiDAR does. In the Elbow River study reach, vegetation effects were minimal given the wide channel belt and prevalence

of unvegetated gravel bars, but floodplain trees adjacent to the wetted channel in some areas did cause problems with unreliable elevations and shading. Similarly, water turbidity and depth are limiting factors in the applicability of any photogrammetry in river settings [Legleiter et al., 2009], but Elbow River presented an ideal case for these as well, with depths less than 1.5 m and clear water allowing for determination of submerged topography.

The regulatory framework associated with UAVs can also limit potential applications in many cases. Because of the rapid expansion of UAV technology and use in recent years, the regulatory landscape in many countries remains relatively immature and restrictive [Rango and Laliberte, 2010]. In Canada, the line of sight restriction of 800 m yields a maximum surveyable area of approximately 2 km^2. While this can be overcome by moving the operator and base station to cover new areas, the potential for beyond line of sight flights would greatly increase efficiency and applicability. Wait times to receive certification to operate and use UAVs can also take up to 6 months, limiting the ability to quickly respond to environmental change. In the United States, the recent Federal Aviation Administration Modernization and Reform Act of 2012 (FAARMA) is set to begin the standardization of regulations relevant to UAV use [Hugenholtz et al., 2012], which will provide an opportunity for further development and testing of UAV applications and legislation. However, with the need to balance safety and applicability across a wide range of uses in a rapidly evolving field, it is unclear whether regulations will become more or less stringent in the future, and continued input from the research community will be necessary throughout the process.

Overall, the ability to rapidly and accurately assess reach-scale habitat and morphology with relatively low costs and training requirements makes UAVs a useful platform to effectively fill a longstanding gap in fluvial remote sensing in terms of spatial and temporal scales. The Elbow River case study provides an example of how the combination of operational flexibility and data quality could tangibly benefit river management. The river experienced unprecedented flooding in late June 2013, extensively damaging infrastructure and causing drastic geomorphic changes. For comparison with the pre-flood (September 2012) imagery used in this study, we were able to mobilize quickly to redo the UAV survey at the study reach to explore questions of geomorphic change detection and aquatic habitat ef-

fects in the context of flood disturbance, potentially aiding restoration efforts or future preventative measures. The continued expansion of such relatively low cost, tailored UAV surveys will support an increased availability of high quality spatial data that can inform effective river management.

2.5 Conclusion

This study assessed the quality of UAV-collected data in a fluvial setting and demonstrated how such information can be used to identify key reach scale metrics of fluvial morphology and characterize important aspects of aquatic habitat. In particular, the combination of high resolution aerial photos and topographic data allows for detailed examinations of habitat-morphology linkages that can be repeated at temporal resolutions that are difficult to achieve with other remote sensing methods. The aerial perspective also allows for intuitive visualization of river structure that can facilitate effective communication, teaching, and outreach. As the technology advances and becomes more widespread, UAVs have the potential to fill a diverse range of data collection niches relevant to river scientists and managers.

Chapter 3

UAV-based remote sensing of fluvial change following an extreme flood event

3.1 Introduction

Understanding the physical processes that dictate channel form and function is a central theme of fluvial geomorphology, with important implications for predictive capacity and management. In Chapter 2, UAVs were shown to be an efficient and accurate way to measure spatial patterns of fluvial features of interest. While this static snapshot of ecosystem conditions provides a wealth of information, a primary benefit of the operational flexibility of UAV-based remote sensing is the ability to easily repeat surveys and measure dynamic environmental systems to capture changes over time. In a fluvial geomorphology context, such methods potentially allow for detailed investigations of process-form relationships and the inference of the underlying mechanisms that drive geomorphic change. In gravel-bed rivers, controls on morphodynamics include flow magnitude and duration, sediment caliber and supply, vegetation, and channel pattern. Many models aimed at untangling the influence of these factors exist, based on a rich history of theoretical, empirical, and conceptual evaluations [e.g. Lane, 1957, Leopold and Wolman, 1957, Wolman

and Miller, 1960, Millar, 2005, Gurnell et al., 2012]. The insights provided by such methods allow for reliable determination of process interactions in a wide range of systems and conditions.

One of the major limitations of the majority of these studies, however, is that the focus is on equilibrium or near-threshold changes; the understanding of morphodynamics related to large flood events is less well developed. Due to the inherent rarity and unpredictability of high magnitude events, reliable data covering pre- and post-flood conditions are generally lacking, inhibiting the development of theory and predictive models that can be applied in hazard assessments, stream ecosystem management, and restoration applications. Many early examples that do exist are based on historical air photo analysis [e.g. Desloges and Church, 1992] and limited topographic survey data [e.g. Miller, 1990], allowing for the assessment of channel planform and, to some extent, vertical change. These studies illustrate the potential variability of responses to large floods: depending on geomorphic setting, channels can experience dramatic restructuring [e.g. Pitlick, 1993], and persistent changes in river regime and geometry [e.g. Newson, 1980, Desloges and Church, 1992], or more minor changes with limited lasting impacts [e.g. Costa, 1974, Gupta and Fox, 1974, Gardner, 1977]. A common theme documented in these studies is channel widening [e.g. Warburton, 1994, Krapesch et al., 2011], but the degree of change is conditioned by variable factors such as vegetation, valley constraints, and stream power patterns [e.g. Miller, 1990, Magilligan, 1992, Lapointe et al., 1998].

More detailed studies supported by recent methodological advances have allowed for the investigation of other aspects of channel adjustment to large floods. In particular, spatially continuous topographic data collected with methods such as light detection and ranging (LiDAR), Structure-from-Motion (SfM) photogrammetry, and terrestrial laser scanning (TLS) facilitate the identification of the three-dimensional river structure and changes due to processes such as scour and fill and bank erosion [e.g. Brasington et al., 2000, Lane, 2000, Charlton et al., 2003, Lane et al., 2003, Wheaton et al., 2010a, Harrison et al., 2011, Williams et al., 2011, Fonstad et al., 2013, Wheaton et al., 2013, Micheletti et al., 2015, Javernick et al., 2014]. For example, Grove et al. [2013], Croke et al. [2013], and Thompson et al. [2013] quantified bank erosion over a large scale due to a catastrophic flood

using LiDAR, highlighting the contribution of mass failures in addition to fluvial entrainment on erosion processes and sediment supply. Perignon et al. [2013] incorporated vegetation analysis into a LiDAR-based study of a large flood on the Rio Puerco, New Mexico, finding spatially variable patterns of sediment erosion and deposition that depended on devegetated sediment source areas and valley wall erosion. Topographic analyses are also complemented by computational methods such as numerical flow modeling, which can be used to simulate fluid forces associated with floods [e.g. Duan, 2001, Horritt and Bates, 2002, Williams et al., 2013a].

Despite advances provided by case study availability and data quality, predicting large flood effects in a management context remains difficult. Piegay et al. [2005] outline a framework for assessing bank erosion risk, promoting a nested approach to address different spatial scales of control. This concept is also emphasized by Krapesch et al. [2011], who studied hydraulic parameter thresholds for major morphologic adjustment and found that while specific stream power is a strong predictor at broad scales, more detailed parameters must be addressed at finer scales. Nardi and Rinaldi [2014], however, found that spatial patterns of morphologic changes due to a large flood on the Magra River were unrelated to a variety of potential controlling factors over 34 km of the river. At the reach scale, thresholds for significant change are still unclear; Eaton and Lapointe [2001] used pre- and post-flood DEMs to assess the adjustment and estimate sediment transport rates associated with two floods on the Sainte Margeurite River and found overall morphologic stability and similar modes of adjustment for both a 7- and 275-year flood. Legleiter [2014b] documented a homogenization of morphology on the Round Prairie reach of Soda Butte Creek, likely associated with a wave of sediment deposition, emphasizing the importance of sediment supply.

Understanding the potential for scour, fill, and bank erosion must also account for differing degrees of bed mobility during flood events. As flood flows increase, gravel-bed rivers typically shift from partial to full mobility as surface grains in a given size class become increasingly entrained [Wilcock and McArdell, 1993, 1997]. The relationship between surface grain size and boundary shear stress is therefore a key factor; full mobility is typically reached when the ratio of shear stress to critical shear stress for incipient motion is approximately two

[Wilcock and McArdell, 1993]. Using numerical flow modeling, Lisle et al. [2000] found that sediment-rich channels have greater areas of full mobility compared to sediment-poor channels at bankfull discharge, but that significant areas of immobility persisted. May et al. [2009] also used flow modeling to predict bed mobilization, and found that mobility thresholds can predict spatial patterns of scour. However, these concepts are best applied to near-threshold conditions, and their applicability to more drastic floods and channel adjustment is not well understood.

In this contribution, we use remote sensing imagery collected with small unmanned aerial vehicles (UAVs) to address the controls on channel adjustment associated with a major flood. Small UAVs have recently been applied to a wide range of environmental science applications, supported by advances in computational power and image processing software [e.g. Hugenholtz et al., 2012, Watts et al., 2012, Hugenholtz et al., 2013, Whitehead and Hugenholtz, 2014, Whitehead et al., 2014]. In fluvial settings, UAV-based remote sensing has proven to be an efficient, flexible, and reliable method of collecting high resolution topographic data and imagery [Lejot et al., 2007, Flener et al., 2013, Woodget et al., 2014], with vertical elevation errors of less than 10 cm and image resolution on the scale of 5 cm/pixel [James and Robson, 2014]. Such continuous high quality data facilitate investigation of aspects of earth surface processes that were previously difficult or impossible to measure [Fonstad and Marcus, 2010, Passalacqua et al., 2014]. By combining UAV surveys bracketing a flood event with hydrodynamic models, we aim to address three related questions: (1) What are the reach-scale geomorphic effects of a large flood event? (2) Can potential high flow conditions be constrained using pre- and post-flood data without knowledge of bed topography during the event? and (3) Are simulated high flow conditions related to patterns of geomorphic change?

3.2 Methods

3.2.1 Study site

Elbow River is a gravel-bed river located in Alberta, Canada, that flows east out of the Rocky Mountains (Figure 2.1). At the 1 km long study site located near

the town of Redwood Meadows (50.999°N, 114.509°W), the channel has a weakly anabranching/wandering pattern typical of the unconfined section of the river between the foothills and the city of Calgary, an elevation of 1250 m, and a drainage area of 791 km^2. At the nearby Water Survey of Canada gauging site at Bragg Creek, the mean annual flood is 87.2 m^3/s and the largest flow on record since 1950 is 377 m^3/s. Before the flood effects, the bed surface D_{50} was 34.72 mm and the bed slope was 0.64%. Active channel width was approximately 150-200 m with extensive gravel bars exhibiting sparse low shrub vegetation. The study reach was chosen prior to flooding as a test site for UAV remote sensing of fluvial structure and aquatic habitat; details can be found in Chapter 2.

3.2.2 2013 flood event

Between June 19-23, 2013, Southwestern Alberta experienced unprecedented flooding leading to widespread social, ecological, and physical infrastructure impacts. The Insurance Bureau of Canada estimated the insured losses exceeded $ 1.7 billion, making it the most expensive natural disaster in Canadian history at the time of writing. A combination of factors led to record flows in the Elbow, Bow, and High River basins: high rainfall caused by unique meteorological conditions, wet antecedent conditions, and remaining snowpack and frozen ground in the mountainous regions where peak rainfall occurred. Precipitation totals exceeded 300 mm during the event, and flashy runoff response caused rapid flooding. On Elbow River, recorded reservoir inflows at Glenmore Dam (30 km downstream of the Redwood Meadows study site) peaked on June 20 at 1,240 m^3/s, corresponding to an approximately 500 year return period. Although peak flow discharges were not available at the Bragg Creek gauging site near the study reach, maximum discharge was estimated at 850 m^3/s with a rating curve relating recorded stage to discharge. Throughout the region, mountain tributaries contributed large sediment loads to higher order streams and bank erosion was widespread, causing substantial geomorphic change to fluvial systems.

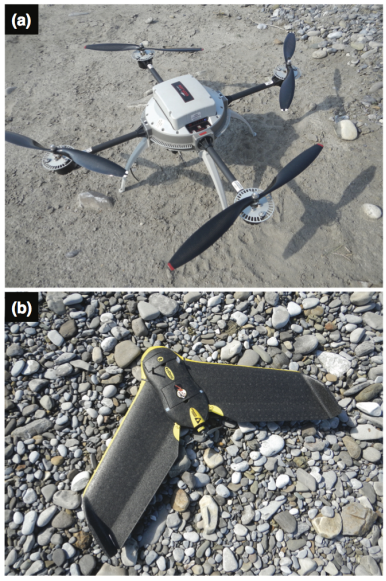

Figure 3.1: (a) Aeyron Scout quadcoptor used in 2012 survey and (b) eBee fixed-wing UAV used in 2013 survey.

3.2.3 UAV surveys

To study the effects of the flooding on the Elbow River study reach, we used UAV surveys bracketing the event. The pre-flood survey was conducted in late September 2012 using an Aeryon Scout quadcoptor (Aeryon Labs, Inc.) that acquired imagery for subsequent photogrammetry (Figure 3.1). The Scout was pre-programed to cover set waypoints; at each waypoint, true-color images were acquired with a three-axis stabilized Photo 3S camera with an 8.4-mm lens and a field of view of 37° x 29°. Eight flight lines running parallel to the river covered the 800 m long study reach, and 192 geotagged images were collected. The flying speed of the quadcoptor was 5 m/s, with a height of 100 m above the ground surface. The survey was supported by 45 visible ground control points (GCPs) which were measured to a vertical precision of 2 cm with a real-time kinematic (RTK) GPS.

The post-flood survey was performed in late September 2013. No geomophically effective floods occurred in the two months between flood event and UAV survey; field visits in July and August 2013 confirmed that the morphology of the river did not change significantly. The UAV used for this survey was an eBee

(senseFly, Ltd.), a fixed-wing platform with a 96 cm wingspan (Figure 3.1). The geographic extent of the 2012 survey was used to guide the setup of 10 flight lines covering the study reach. Flying height was 100 m and speed was 10 m/s, and 310 geotagged RGB images were collected with a 16.1 megapixel Canon IXUS 127 HS camera. Forward image overlap was approximately 80% along the flight path with 70% sidelap across the flight paths. We also laid out 35 GCPs for georegistering, spaced throughout the survey area. Both the 2012 and 2013 UAV surveys and associated ground measurements were completed in less than a day each.

Photogrammetric processing was carried out in a similar overall manner for both surveys. The 2012 images were processed with the EnsoMOSAIC UAV package (MosaicMill, Ltd., Finland), while the 2013 images were processed with Pix4D software (Pix4D SA, Switzerland). Both software suites calculate internal camera orientations and calibration parameters for subsequent steps. The Pix4D software automates traditional photogrammetric steps and incorporates novel algorithms (like the scale invariant feature transform, SIFT, Lowe [2004]) to determine camera positions and match keypoints between images. The process then involves automatic aerial triangulation (AAT) to calculate ground coordinates with reference to the measured GCPs, and bundle block adjustment (BBA) in an iterative manner to optimize mosaic accuracy. Once BBA error is minimized, a digital elevation model (DEM) is generated and used to orthorectify the image mosaic. The resulting orthomosaics and DEMs had spatial resolutions of 5 cm/pixel and 4 cm/pixel for the 2012 and 2013 surveys, respectively.

3.2.4 DEM correction and accuracy assessment

Before the photogrammetry generated DEMs could be used in subsequent analysis, several correction and quality assessment steps were performed. A ubiquitous problem in photogrammetric analyses of fluvial systems is the refractive effects of water, which lead to overpredictions of elevations in submerged areas [e.g. Lane, 2000, Westaway et al., 2000, 2001, 2003, Bird et al., 2010]. Although our UAV surveys were performed during low-flow conditions, both DEMs required correction for this problem. Following tests discussed in Chapter 2, we used an optical/empirical bathymetric correction process similar to that used by Legleiter [2012] and

Table 3.1: Error statistics comparing modeled (DEM) elevations with measured GPS check point elevations

	n	ME (m)	RMSE (m)	SDE (m)	E_{max} (m)
2012					
Exposed	221	0.032	0.088	0.007	0.320
Uncorrected submerged	76	0.144	0.169	0.008	0.386
Corrected submerged	76	0.0001	0.098	0.009	0.354
2013					
Exposed	213	0.007	0.047	0.002	0.191
Uncorrected submerged	82	0.154	0.218	0.009	1.002
Corrected submerged	82	0.0007	0.095	0.023	0.318

Williams et al. [2013b]. This process involved regression of field-measured water depths at geolocated points against natural log-transformed red and green intensity pixel value ratios from the orthomosaics to take advantage of the linear relationship between transformed water color and water depth [Lyzenga, 1981, Legleiter et al., 2009]. We developed a map of water depth by applying this empirical relation to the rest of the wet pixels in the orthomosaic, which we then subtracted off a water surface elevation raster produced by interpolation through water's edge elevation points using kriging. This corrected bed surface was then mosaicked with the dry areas to produce a seamless corrected DEM.

To assess the accuracy of the topographic data generated from the UAV imagery, we used elevations from field-measured checkpoints. These points were independent of DEM generation or image mosaicking and were measured with the RTK GPS. By stratifying points into submerged and exposed dry areas and comparing modeled (DEM) elevations with measured (GPS) values, we were able to calculate error statistics for both surveys, averaged over wet or dry areas. Equations for these metrics are shown in Table 2.1; values for both UAV surveys are shown in Table 3.1. Similarly, density plots of elevation residuals for both years are shown in Figure 3.2. For all calculations, errors were calculated as field-measured elevations subtracted from modeled elevations; positive values indicate overprediction of elevations in the DEM and negative values indicate underprediction of elevations in the DEM.

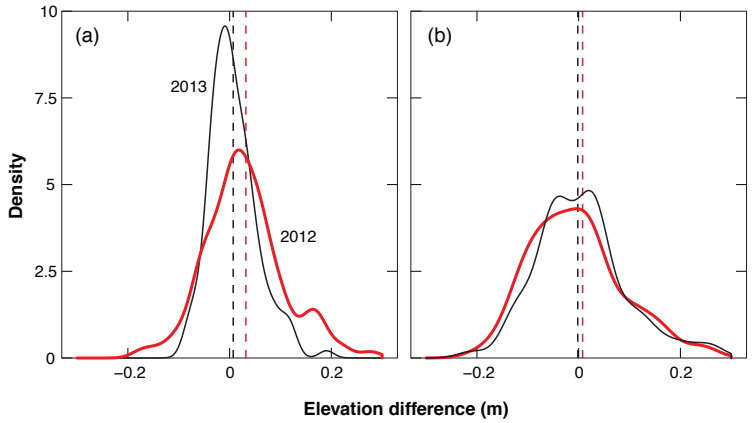

Figure 3.2: Density plots comparing modeled (DEM) elevations with measured GPS check point elevations for (a) exposed and (b) corrected submerged points. Vertical dashed lines indicate the mean error for each dataset; elevation differences were calculated as modeled minus measured

Overall, vertical accuracy in the DEMs was high for both survey years, with a maximum RMSE of 0.098 m in submerged areas of 2012 following DEM correction. For context, this is in the same range as the D_{84} of 0.068 m in the study reach. Correction of submerged areas improved the RMSE by 0.07 - 0.11 m and reduced maximum errors as well. In general the 2013 survey had lower errors than the 2012 survey, which could be attributed to different UAVs, photogrammetry software, or flight conditions between the two years. The errors of these topographic surfaces were deemed appropriate for the DEM differencing and flow modeling performed for this reach-scale investigation.

3.2.5 DEM differencing and change detection

Geomorphic change associated with the flood event was assessed using DEM differencing between the two surveys. We used the Geomorphic Change Detection 5.0 (GCD) software (http://gcd.joewheaton.org) to determine elevation changes and account for DEM uncertainty propagated through the calculation [Wheaton et al., 2010b]. This involved creation of error surfaces based on RMSE values calculated in Table 3.1. Errors were stratified based on submerged or exposed ar-

eas for both years. Because the channel widened significantly between 2012 and 2013, the 2013 DEM had areas where limited elevation data were available for 2012. To account for this mismatch, we added interpolated floodplain surfaces to the 2012 DEM based on field observations of pre-flood bank heights and point measurements of elevation. These interpolated areas were assigned a conservative 0.5 m error value and allowed us to estimate volumes of sediment associated with bank erosion. Patterns of elevation change with changes below the minimum levels of detection (LoD) thresholded out were then mapped throughout the reach, and areas and volumes of erosion and deposition were calculated from the DEM of difference (DoD). A 99.7% confidence interval was chosen for the error propagation from successive surveys, resulting in a stringent assessment of topographic change, particularly when compared to the magnitude of elevation changes observed throughout most of the reach.

As a second method of characterizing reach-scale morphology and change between the two surveys, we used geostatistical models of channel structure [Chappell et al., 2003, Legleiter and Kyriakidis, 2008, Legleiter, 2014a,b]. To do so, we calculated variograms to assess dissimilarity of elevations as a function of distance between observation pairs. In fluvial settings, variogram analysis can be applied to topographic data to determine characteristic horizontal and vertical length scales and variance of elevations. The models are flexible and can account for varying channel complexity and anisotropy in different directions. They can also be applied to detrended and scaled data to provide dimensionless characterization of channel structure and facilitate comparison between different systems and at different times.

We calculated sample variograms in streamwise (along-stream) and normal (across-stream) directions for the pre- and post-flood topographies. Dissolving the analysis into two direction vectors accounted for the inherent anisotropy in river channels, which are typically more variable across the channel than along it. We were therefore able to fit isotropic models to sample variograms computed in each direction. Although coordinate transformation from a Cartesian to channel-centered system is often applied to allow for a consistent frame of reference related to in-stream distances [Legleiter, 2014b], the wide channel belt and irregular braided morphology of the Elbow River study reach made this impractical.

Instead, we rotated the DEMs so that valley slope was oriented north-south and the across-stream direction was east-west [Chappell et al., 2003]. We then detrended the DEMs based on average valley slope and calculated residuals from the mean detrended elevation. To remove scale effects associated with channel size, we normalized elevations by estimated bankfull depth and normalized horizontal distances by average channel width [Legleiter, 2014b]. We then calculated sample variograms $\hat{\gamma}(h)$ for given lag vectors (h), which show the dissimilarity between sample pairs different distances apart. Because of the density of our elevation data, we used small values of directional tolerance ($\Delta\phi$) and band width (b_m) to ensure correct resolution of calculations into streamwise and normal components. With sample variograms calculated, we then fit exponential model variograms to the data, allowing for determination of summary parameters.

3.2.6 Flow modeling

To simulate high flow conditions and investigate their relationship to the quantified geomorphic change, we used the 2D hydrodynamic model Nays2DH implemented within the International River Interface Cooperative (iRIC) framework (http://i-ric.org/en/). This was a change of model from Chapter 2 where River2D was used; this choice was made to capitalize on application stability and computational efficiency in model performance. Nays2DH is a depth-averaged model that solves the Saint-Venant equations of free surface flow with finite differencing based on a general curvilinear coordinate system. Inputs to the model are discharge, topography, and roughness in the form of Manning's roughness parameter. The model approach is based on assumptions of steady hydrostatic flow and accounts for turbulence through an isotropic eddy viscosity.

We first ran simulations of the flows through the pre- and post-flood topographies for the low-flow conditions at the time of each UAV survey. This allowed us to tune the model parameters with accurately measured values of water surface elevations and depths for discharges of 5.9 m^3/s (2012) and 6.1 m^3/s (2013). To account for roughness, we created continuous maps of sediment size (D_{50} and D_{84}) throughout the study reach by relating measured grain sizes with measures of image texture in the orthomosaics [e.g. Carbonneau, 2004]. This involved tak-

ing close-range geolocated vertical photos of 1 m^2 sediment patches on exposed bars during field sampling, determining D_{50} and D_{84} with a photosieving GUI programed in MATLAB that facilitates measurement of particle b-axes, and then relating sediment size for each location to image texture in the orthomosaic calculated as standard deviation within a 1 m^2 window (Figure 3.3). This relationship was then applied to the rest of the exposed areas to map out sediment sizes. For wetted areas, where sediment was not visible, we assigned constant sizes for D_{50} and D_{84} drawn from coarse sediment on exposed bar heads, with the assumption that these deposits are representative of submerged sediments transported at high flows. Using these coarse values provided a conservative estimate of submerged grain sizes. D_{84} distributions were then used as model inputs in Nays2DH to determine Manning's roughness parameter.

Following model calibration to low flow conditions, we performed steady simulations of the peak discharge for the June 2013 flood of 850 m^3/s run through both the 2012 and 2013 DEMs. Although bed conditions during the flood event are unknown and were undoubtedly different than pre- and post-flood configurations, this procedure allowed us bracket potential distributions of flow parameters during the flood peak and investigate channel adjustment to such high flows. Similarly, the flood pulse had a very rapid rising limb, meaning a topographic condition similar to the pre-flood DEM was likely subject to the majority of fluid forces at peak flow. By making the assumption that the pre-flood topography experienced the bulk of the flood flow before substantial adjustment could occur, we were able to examine the extent to which geomorphic change for a flood of a given magnitude can be predicted through hydrodynamic modeling based on pre-flood conditions alone.

Model topography was extracted directly from the DEMs. Computational grid spacing for both simulations was set to 2 m x 2 m. To restrict flood flows to the active channel for the simulations, we created artificial 10 m tall channel banks bounding the areas of interest. Although overbank flooding occurred during the event, water in the floodplain is much less active than that of the channel and does not contribute to geomorphic change. Adding these bank restrictions to the DEMs also allowed us to measure water surface elevations associated with modeled flows. This provided a method with which to assess the model performance relative to high water marks (visible from mud stains, rafted debris, etc.) sur-

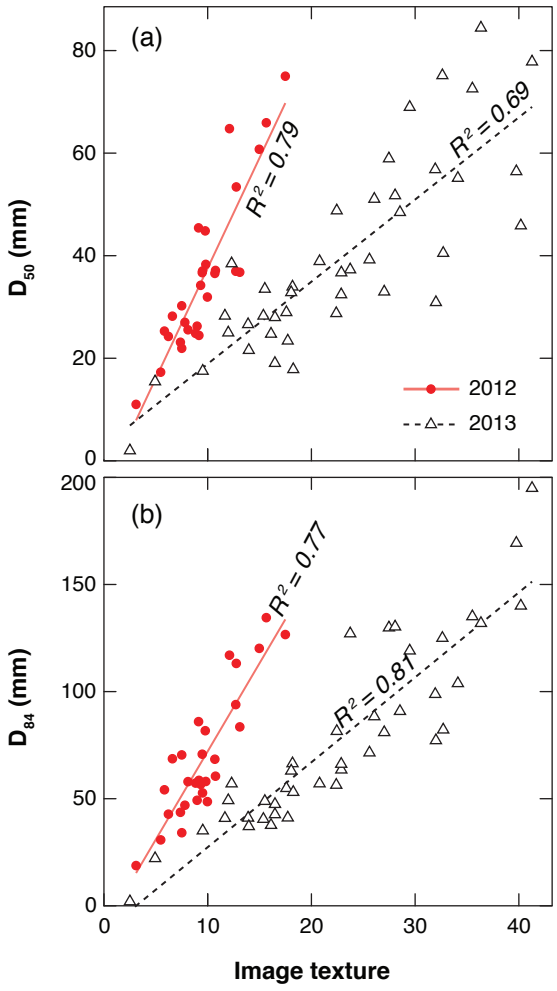

Figure 3.3: Empirical relationships between field-measured surface grain size and image texture in the orthomosaics for (a) the D_{50} and (b) the D_{84}

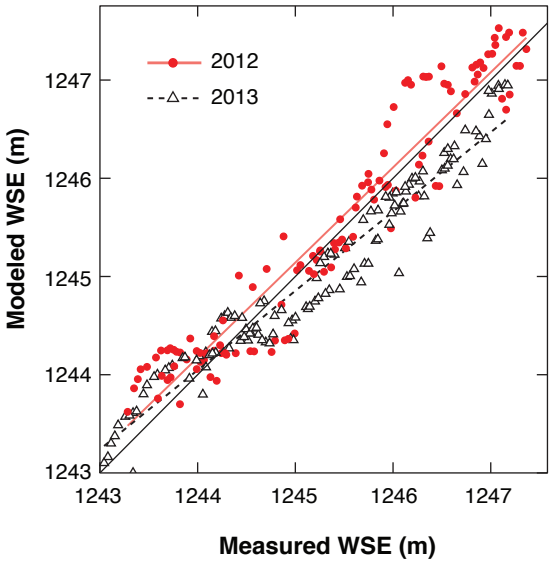

Figure 3.4: Comparison of field-measured evidence of peak flow water surface elevations and modeled water surface elevations for pre- and post-flood simulations.

veyed in July 2013 following the flood [e.g. Baker, 1987]. These measured high water marks were also used as starting downstream water surface elevations required in the Nays2DH model parameterization. While not a perfect measure of true water surface elevations due to splashing and run-up around obstacles, the comparison between modeled and measured water surface elevation showed that the model predictions were in the right range (Figure 3.4) considering the potential degree of variability associated with such large flood events. The 2012 simulation closely followed a 1:1 line ($y = 0.96x + 47.8, R^2 = 0.96$) indicating correspondence between measured and modeled values and supporting the assumption that the pre-flood topography was subject to the majority of peak flows. Modeled water surface elevations were slightly underpredicted in upstream portions of the reach and overpredicted in downstream portions of the reach for the 2013 simulation ($y = 0.83x + 209.3, R^2 = 0.94$); this effect could be attributed to the changes in channel width that occurred through the flood.

With the combination of continuous grain size maps and model-output hydraulic parameters, we determined distributions of shear stress associated with high flows for both the 2012 and 2013 simulations. Because shear stress was not a direct output from Nays2DH, it was calculated as:

$$\tau_o = \rho \left(\frac{V}{(8/f)^{1/2}} \right)^2 \tag{3.1}$$

where τ_o is shear stress, ρ is the density of water, V is velocity, and f is the Darcy-Weisbach friction factor [Ferguson, 2007]. The term $(8/f)^{1/2}$ was calculated from grain size as proposed by Parker [1991]:

$$(8/f)^{1/2} = 8.1(d/2D_{84})^{1/6} \tag{3.2}$$

where d is water depth. Shear stress was therefore determined for each point output from the model in a manner consistent with the Manning's n approach to flow resistance used in Nays2DH.

The calculated shear stresses were then related to the spatially continuous maps of surface grain size to investigate patterns and distributions of potential for sediment transport. We assumed a critical Shields stress value of 0.045 for entrainment of the D_{50} in unstructured gravel mixtures [e.g. Komar, 1987, Church, 2006], allowing calculation of the critical shear stress for the D_{50} at each model point:

$$\tau_{c50} = 0.045(\rho_s - \rho)gD_{50} \tag{3.3}$$

where ρ_s is the sediment density (assumed to be 2,650 kg/m^3) and g is the acceleration due to gravity. We also calculated critical shear stress for the D_{84} as in Wilcock and Crowe [2003]:

$$\tau_{c84} = \left(\frac{D_{84}}{D_{50}} \right)^{0.67} \tag{3.4}$$

We then normalized calculated shear stresses by critical shear stresses for ease of interpretation in the context of proposed thresholds for partial and full mobility, where a normalized shear stress greater than one indicates potential partial mobility

for the size fraction and greater than two indicates potential full mobility for that size fraction.

3.3 Results

Orthomosaics developed for both survey years are shown in Figure 3.5. Qualitatively, the geomorphic change is striking: the channel widened substantially and pre-flood features were erased completely. Reach average width, measured as active channel area divided by length, increased from 149.15 m to 192.03 m. Vegetation and accumulations of large wood were stripped from bar top locations; new wood jams formed throughout the channel, particularly along outer bank bends. Low flow patterns were also rearranged. Whereas the pre-flood low flow channel split into 2-3 main anabranches around mid-channel bars, the post-flood configuration is much more concentrated in a single thread pattern interrupted occasionally by smaller-size bars. This new low flow channel also appears to have a long meander wavelength (on the scale of 800 m) within the active channel, approximately twice that of the dominant thread in 2012.

Observable flood effects from the orthomosaics can be examined in more detail with the use of the DEMs and the change detection analyses applied. Pre- and post-flood DEMs and the DoD are shown in Figure 3.6. The planform changes evident in the orthomosaics are supported by the topographic data, with low flow channels clearly demarcated in detrended DEMs. Bar features appear to have a larger, more elongated characteristic scale following the flood and are less dissected. The DoD shows variable changes in elevation, with overall reliable change detection due to the high magnitude elevation changes relative to the minimum threshold. Of the 183,447 m^2 study area, 89% of vertical change was above the detection threshold. Spatial variations in the DoD reflect infilling of pre-flood low flow channels and carving of new channels, along with significant bank erosion.

Summaries of areal and volumetric erosion and deposition are shown in Table 3.2; distributions for each measure are shown in Figure 3.7 For these analyses, areal changes reflect the total surface area within a given vertical change bin, and volumetric changes are calculated as areal distributions multiplied by the depth of elevation change for each area. Overall, the study reach experienced a net vol-

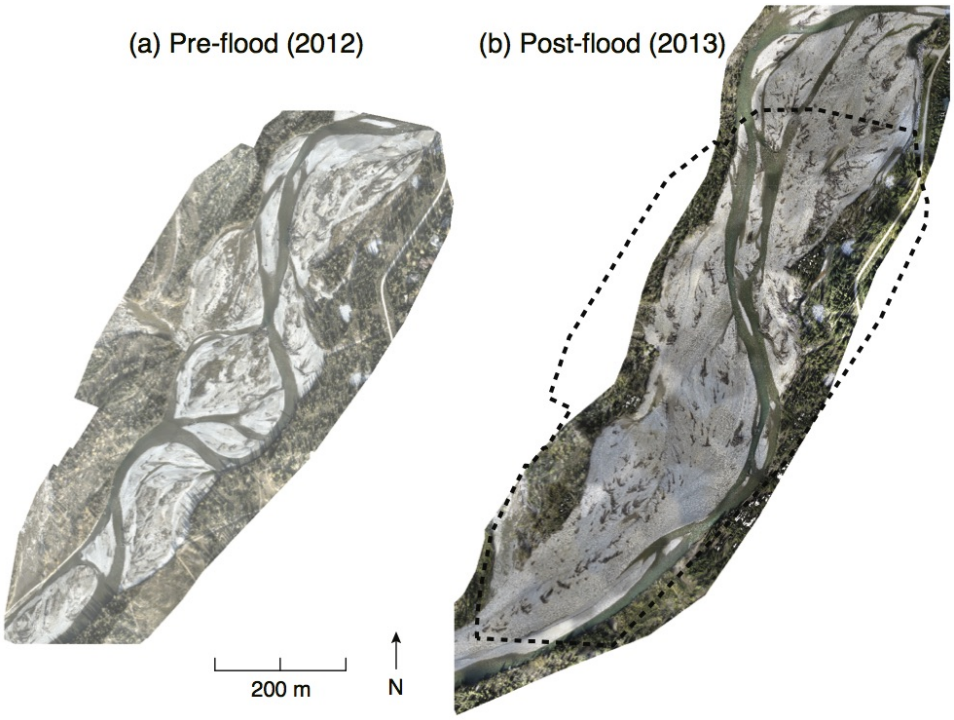

Figure 3.5: Orthomosaics for (a) pre- and (b) post-flood UAV surveys. The black dashed outline on the post-flood image corresponds to the extent of the 2012 survey, for reference

Table 3.2: Topographic change determined through DEM differencing

	Area (m^2)	Volumetric change (m^3)	Mean elevation change (m)
Including bank erosion			
Aggradation	77,122	50,306 $\pm$ 8,528	0.65 $\pm$ 0.11
Degradation	86,582	-89,294 $\pm$ 22,284	-1.03 $\pm$ 0.26
Net change		-38,988 $\pm$ 23,860	-0.24 $\pm$ 0.15
Excluding bank erosion			
Aggradation	64,371	43,580 $\pm$ 3,314	0.68 $\pm$ 0.06
Degradation	58,561	28,805 $\pm$ 4,841	-0.64 $\pm$ 0.07
Net change		14,775 $\pm$ 4,277	0.13 $\pm$ 0.04

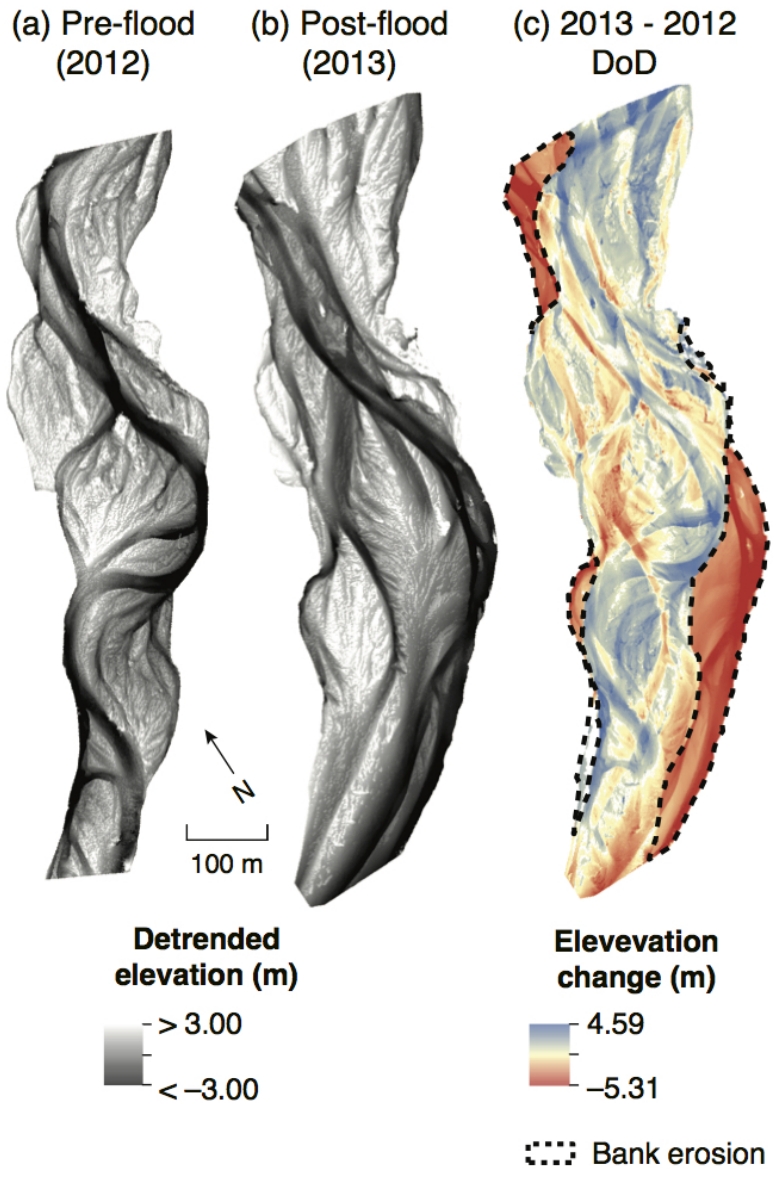

Figure 3.6: Detrended pre- and post-flood DEMs and DEM differencing. Detrended elevations reflect the removal of valley slope and normalization relative to mean reach elevation; positive values are above mean elevation, negative values are below mean elevation

umetric change of -38,988 $\pm$ 23,860 m^3, much of which is attributable to bank erosion. The conservative error values for interpolated bank areas explain the high uncertainty in this estimate. This net volumetric change corresponds to a net elevation change of -0.24 $\pm$ 0.15 m averaged over the study reach. However, scour and fill were both significant throughout the reach, as 36% of volumetric change was depositional and 64% was erosional. If the areas of bank erosion are excluded from the change detection to focus on the active channel bed, the net volumetric change is 14,775 $\pm$ 4,277 m^3. Given the accuracy of elevation data for the active channel, uncertainty is substantially reduced, showing a net depositional budget in the channel bed itself.

To further investigate patterns of erosion and deposition, we stratified elevation changes based on geomorphic unit classification of the pre-flood reach. Areas were classified as either low flow channels, bar edges/chutes, or bar tops to relate to general elevation distributions of features. This allowed for an investigation of whether elevation changes due to flooding depend on pre-flood geomorphic configuration. Plotting elevation change against detrended relative pre-flood elevation (Figure 3.8) shows that the classified features generally have characteristic elevations as expected, with low flow channel points at low elevations, bar edges/chutes at intermediate elevations, and bar tops at higher elevations. In terms of elevation change due to flooding, low flow channel and bar edge/chute areas experienced similar, generally positive elevation changes, whereas bar tops experienced changes closer to zero or negative. While differences in elevation change between low flow channel and bar edges/chute areas were not statistically significant, bar tops experienced significantly more scour than both other classes (ANOVA p <0.001, post hoc Tukey HSD p <0.001). These results suggest an evening out of pre-flood topography: higher elevation bar top areas were generally scoured whereas lower elevation bar edges, chutes, and low flow channel areas were generally infilled.

Analysis of the geomorphic changes and their relation to pre-flood topographic condition can be further supported by the variograms applied to pre- and post-flood configurations. Dimensionless sample variograms and fitted models are shown in Figure 3.9 for both years. In the streamwise direction, the sill increased substantially from 2012 to 2013, with a slightly larger range. This suggests an increase in topographic heterogeneity and a longer characteristic streamwise length scale

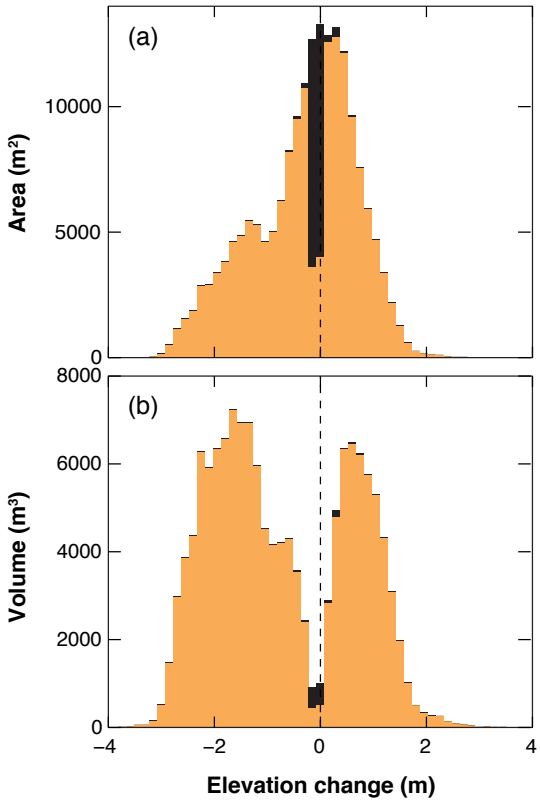

Figure 3.7: Distributions of (a) areal and (b) volumetric elevation changes determined through DEM differencing. Changes were calculated as 2013 elevation minus 2012 elevation; positive values represent deposition and negative values represent erosion. Dark grey portions of histograms are data that were below LoD thresholds.

of bar features. However, a distinct along-stream pattern in variability is shown in 2013 beyond the initial sill, with peak in dissimilarity at lags of 2 and 4 channel widths, and a minimum at 3. This effect is likely attributable to the increasingly single-thread, sinuous nature of the main channel that developed as a result of the flood; this underlying pattern was not removed through the analysis because we centered the coordinate system along the entire active channel rather than this newly developed thalweg. The across-stream variograms also reflect an increase in heterogeneity resulting from the flood. For both 2012 and 2013, the normal sill

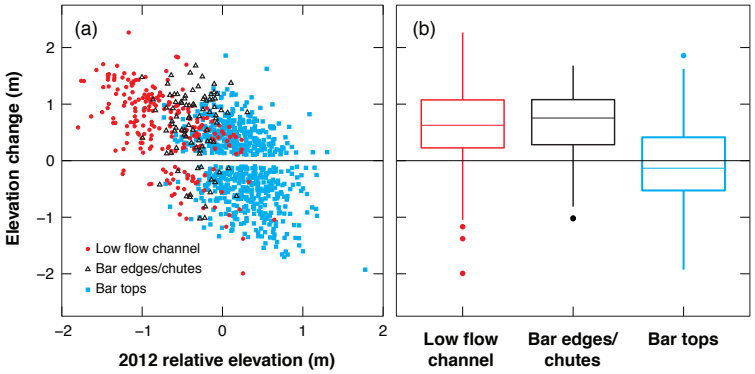

Figure 3.8: (a) Scatterplot showing flood-induced elevation change in relation to pre-flood detrended relative elevation for different geomorphic units and (b) distributions of elevation change associated with each unit type

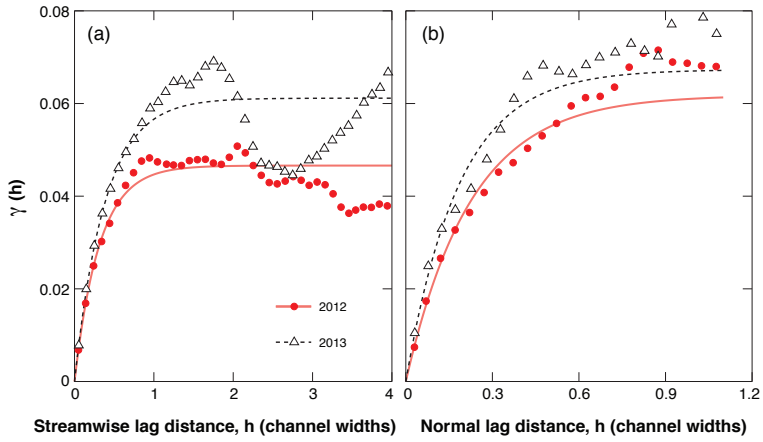

Figure 3.9: Sample and model variograms in (a) streamwise and (b) normal directions for pre- and post-flood DEMs

is greater than the streamwise sill, suggesting the characteristic anisotropy of river channels remains. However, the difference between streamwise and normal sill is much less for 2013, caused by the increase in streamwise variability.

Results of the flow modeling provide insight into the relationship between the flood magnitude, forces applied to the channel bed, surface sediment sizes, and channel morphodynamics. Density plots and cumulative distributions comparing

simulations of 2012 (pre-flood topography) and 2013 (post-flood topography) flood forces are shown in Figure 3.10. These distributions reflect the variation in modeled shear stress and mapped sediment size for pre- and post-flood simulations. For both 2012 and 2013, a large proportion of normalized shear stresses far exceeded thresholds of entrainment, partial mobility, and full mobility. In general, normalized shear stresses for both the D_{50} and D_{84} were much higher in the 2012 model: 66.6% of bed area had a value over two for D_{50} in the pre-flood configuration compared to 49.7% in the post-flood configuration. For the D_{84}, 50.3% of bed area exceeded a normalized shear stress of two for the pre-flood topography whereas 26.3% did for the post-flood. Despite the high shear stresses for both years, calculated distributions of normalized shear stress predicted some of the bed to remain immobile ($\tau_o/\tau_{ci} < 1$), particularly in the post-flood configuration where 40.0% of bed area was below thresholds for entrainment of the D_{84}. In the simulation using the pre-flood topography, only 26.6% of bed area was below this threshold. These results suggest a topographic or grain size adjustment due to the flood, resulting in differing distributions of local boundary shear stresses in relation to surface grain size.

Because thresholds for sediment transport have been shown in previous studies to relate to the proportion of bed surface area experiencing geomorphic adjustment and to the magnitude of elevation change, we examined the relationship between our modeled normalized shear stresses for the pre-flood simulation and the erosion and deposition determined through DEM differencing. If elevation changes are dependent on modeled shear stress values from pre-flood conditions, this relationship could be used predictively to assess potential distributions of geomorphic changes for future flood events. Scatterplots for both the D_{50} and D_{84} normalized shear stresses are shown in Figure 3.11, and mapped patterns of normalized shear stresses in comparison to pre-flood topography and observed elevation changes are shown in Figure 3.12. If τ_o/τ_{ci} were a direct control on elevation change, more scour would be expected for higher τ_o/τ_{ci} values. However, our results show no detectable relationship. A wide range of scatter exists in the data; some areas with small τ_o/τ_{ci} values experienced elevation changes representing up to 2m of scour or 2m of aggradation, whereas some areas with τ_o exceeding 10-20x thresholds for entrainment showed minimal elevation changes. In fact, the largest elevation

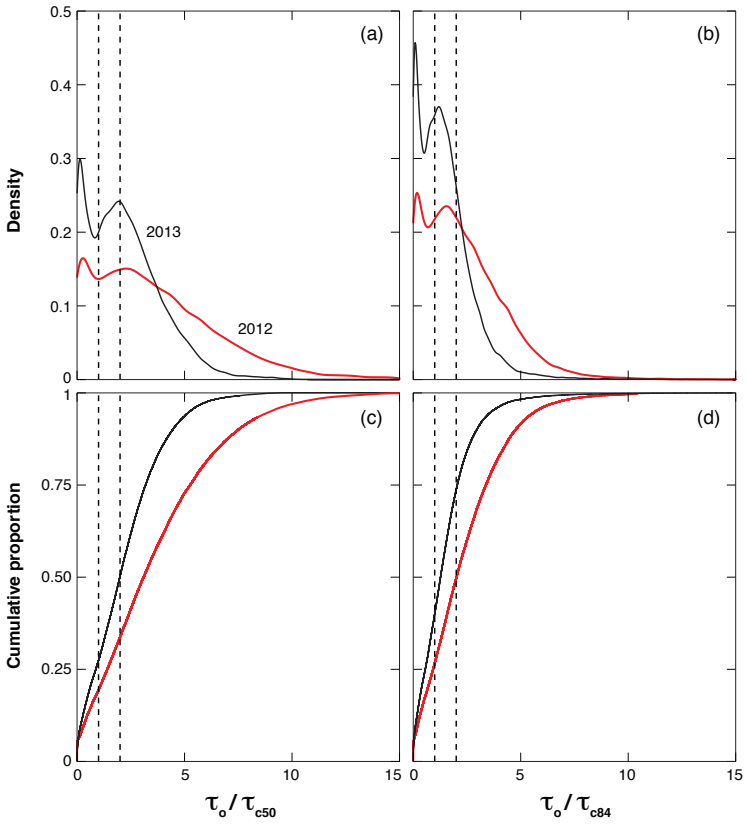

Figure 3.10: Distributions of modeled normalized shear stress for pre- and post-flood simulations. Vertical dashed lines represent thresholds for partial and full mobility

changes appear to correspond to values of τ_o/τ_{ci} in the 5-10 range. While such values are still far above thresholds for full mobility and likely correspond to zones of intensive sediment transport, this analysis shows that the signal of sediment entrainment thresholds is masked by confounding factors such as changing patterns of scour and fill through the flood event related to sediment supply and complete reworking of bed morphology.

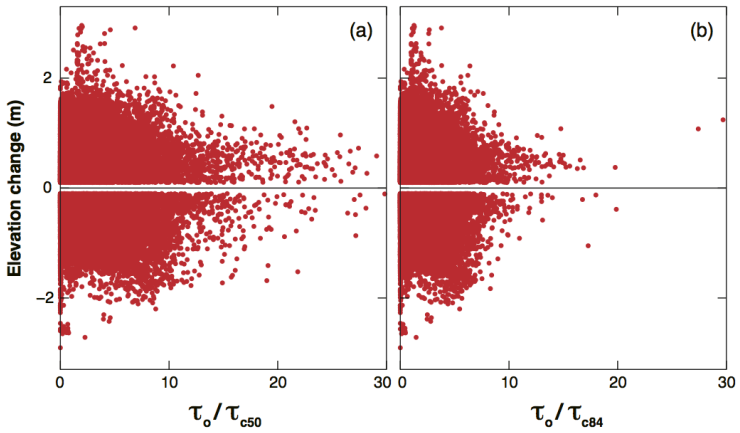

Figure 3.11: Relationships between elevation changes and modeled normalized shear stress for (a) the D_{50} and (b) the D_{84}

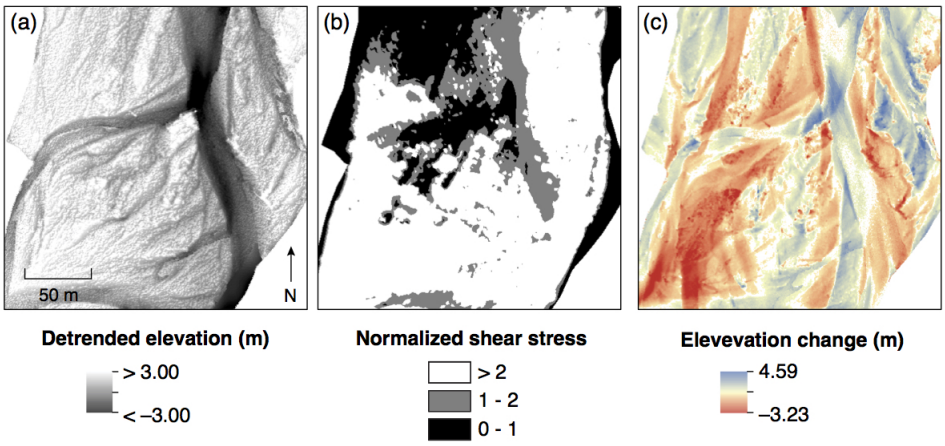

Figure 3.12: Comparison of patterns of (a) pre-flood elevations, (b) modeled normalized shear stresses for the D_{84}, and (c) elevation changes in a subsection of the study reach

3.4 Discussion

The June 2013 flooding on Elbow River caused substantial geomorphic change. By combining UAV-based remote sensing, photogrammetry, and flow modeling, we characterized three-dimensional topographic changes and placed them in the context of simulations bracketing potential high flow conditions. Overall, the flood event was degradational with large elevation changes throughout the study reach. Bank erosion was prominent and contributed to major morphologic changes including widening, increased elevation variability, and a restructuring of channel pattern. These patterns of change were largely unrelated to initial conditions and resulted in a morphologic adjustment towards bed surface stability.

The observed topographic change of the reach suggests that the flooding resulted in a catastrophic change in the sense that the channel morphology is now adjusted to a new regime associated with a larger formative discharge [e.g. Desloges and Church, 1992]. To put this event in the general context of other studies of flood changes, unit stream power ω was calculated as $\omega = \gamma QS/w$, where γ is the specific weight of water, Q is the peak discharge, S is the gradient, and w is the channel width. Based on the pre-flood topography, the reach experienced a peak unit stream power of 4,816 W m^{-2}. This is far above proposed thresholds for major morphologic adjustment and floodplain stripping (e.g. 300 W m^{-2}, Magilligan [1992]), and fits into ranges measured by Krapesch et al. [2011] for reaches that widened substantially due to flood events. Given the degree of bank erosion and vertical change associated with the June 2013 flood, this is not surprising, and suggests that unit stream power could be a useful predictor of general flood effects (widening, entrainment of most sediment sizes) on Elbow River if pre-flood topography and a modeled discharge were used predictively.

While reach-average factors such as unit stream power can be used as general screening tools, a primary goal of our study was to assess the possibility of using more detailed parameters to address local interactions between flow patterns and morphologic changes. This approach was facilitated by the imagery and elevation data provided by UAV-based remote sensing, which allowed for accurate assessments of elevation changes at a hyperspatial resolution. Combining these elevation changes with hydrodynamic modeling at a similar scale provides a powerful tech-

nique with which to investigate a wide range of geomorphic questions that would be difficult or impossible to address in such a spatially continuous manner with more traditional approaches such as manual surveying.

In terms of potential controls on bed adjustments, we found that there was no relationship between patterns of modeled shear stress and topographic change. Although classified geomorphic unit types stratified elevation changes to some extent (Figure 9), with bartops generally experiencing erosion, these patterns could not be explained by modeled shear stresses relative to surface grain sizes in the pre-flood configuration. This result contrasts with studies that took similar approaches to fluvial adjustments associated with smaller floods. For example, May et al. [2009] found that although the relationship between scour depth and modeled Shields parameter was highly variable, there were distinct probability distributions of scour for given ranges of Shields stress. Similarly, Lisle et al. [2000] suggested that mobile areas of river channels with high boundary shear stress and fine bed surface material are prone to rapid morphologic change. In the case of Elbow River, the magnitude of the flood was such that significant areas of the reach experienced conditions far above thresholds for mobility (Figure 11). Complex patterns of compensating scour and fill occurred, related to large volumes of sediment supplied from upstream areas and local bank erosion. The spatially variable topographic adjustments are largely unpredictable, suggesting a nonlinear relationship between initial conditions, flow forces, and morphologic change. This finding supports the concept that sediment transport is controlled by entrainment in near-threshold conditions, but shifts to depend on the rate at which momentum is transferred from the fluid to the boundary materials (related to stream power) at higher magnitude flows [e.g. Bagnold, 1966, 1980, Laronne and Carson, 1976, Eaton and Church, 2010]. Morphologic adjustment in this case is therefore more dependent on sediment flux than entrainment, meaning relationships between shear stress and sediment sizes like the ones we tested are inadequate predictors of elevation changes. Determining potential scour hazards for large flood events in streams like Elbow River is therefore difficult as the system transitions to a largely chaotic regime where spatial changes cannot be accurately predicted from initial conditions.

The geomorphic restructuring of the reach appears to have led to an adjustment towards future stability in the face of large flows. Analysis of the thresholds for

partial and full mobility (Figure 11) shows that if the pre-flood topography were subject to the entire peak flow, at least 50% of the bed surface D_{84} would be fully mobile. If the same flood discharge were run through the post-flood morphology, only 25% of the bed surface would be fully mobile, leaving 75% of the reach either partially mobile or below thresholds for entrainment. Since coarse grains control much of bed stability, larger flows will be required to produce major restructuring in the post-flood reach. This contrast in normalized shear stresses between pre- and post-flood conditions could be caused by a combination of bed surface coarsening related to large sizes in sediment supply and armoring during waning flows [e.g. Parker and Klingeman, 1982, Dietrich et al., 1989] and the widening associated with bank erosion leading to a conveyance of flood flows with lower shear stresses. These findings support the notion that the channel adjustments associated with large floods may remain as a long-term control on geomorphic processes [e.g. Hickin and Sichingabula, 1988, Desloges and Church, 1992, Gardner, 1977]. Future monitoring of morphodynamics associated with more common, smaller floods on Elbow River will provide further insight into the persistence of these effects and the potential of channel readjustment through sinuosity changes, revegetation, and bed sediment sorting.

Overall, this study demonstrates how recent advances in data collection and analysis methods can be applied to novel questions about Earth surface processes. In fluvial settings, changes that occur at intermediate spatial and temporal scales are of critical importance for both the physical geomorphic template and ecological processes [Fausch et al., 2002]. Similarly, the importance of spatial heterogeneity has increasingly been recognized as fluvial science and remote sensing technologies have developed [Carbonneau et al., 2012]. UAV-based remote sensing provides a flexible, efficient, and accurate tool for geomorphic studies in this context. As shown in this work, detailed spatial relationships between pre-existing topography and fluvial change are easily identified, both qualitatively through comparison of high resolution orthoimagery and quantitatively through DEM differencing and geostatistics. This scale of analysis also meshes easily with numerical flow modeling, particularly two and three-dimensional approaches that can be applied to geomorphically complex reaches and extended to ecological applications. When high-resolution elevation models are combined with meter-scale hydraulics, ques-

tions of controls on geomorphic change can be addressed in ways that were previously not possible. With the operational flexibility associated with UAV surveys and the rapid proliferation of the technology, multi-temporal datasets capturing geomorphic processes in three dimensions will become more common [e.g. Passalacqua et al., 2014, Tarolli, 2014]. The case study of Elbow River shows potential strengths and limitations of how such datasets and modeling can contribute to the wider understanding of fluvial processes at intermediate scales. Future work extending these techniques to flood events in other systems and incorporating aspects of habitat quality and complexity will allow for identification of thresholds for physical and ecological changes and inform sustainable management of fluvial systems.

3.5 Conclusion

The inherent rarity of large flood events means that studying and predicting their effects is difficult. Reliable pre-flood data are often lacking, prohibiting detailed analyses of geomorphic change. In this study, we used high resolution pre- and post-flood topographic data and imagery collected with UAVs to document detailed morphologic adjustment resulting from a major flood on Elbow River. The flood resulted in large ($>$2 m) elevation changes, widespread bank erosion, and a complete reorganization of channel pattern. These effects seem likely to persist in the future as the reach morphology is now stabilized and adjusted to larger flows. Because such datasets can now be collected reliably and efficiently with current methods and technology, it is also important to know whether predictive capacity can be enhanced as more examples of large flood effects are obtained. We found that simulations of peak flows can be used to constrain ranges of flood forces in relation to bed surface sediment sizes and are related to reach-scale adjustments, but that local patterns of erosion and deposition are unrelated to initial conditions in such a high magnitude event. Continued collection of such detailed examples of fluvial change will support the development of more advanced predictive and theoretical understanding of the geomorphic effects of large floods.

Chapter 4

Impacts of geomorphic change on reach scale flow structure and aquatic habitat

4.1 Introduction

As shown in Chapter 3, the geomorphic effects of a high magnitude flood event on Elbow River were major, resulting in complex adjustments to vertical and planform geomorphic structure. Simulations of peak flood forces showed that the majority of the active channel of the reach experienced bed shear stresses far in excess of sediment entrainment thresholds; significant erosion and deposition resulted in a complete rearrangement of channel morphology and substantial bank retreat. Given the evidence of similar geomorphic response along the length of the river, the 2013 flood event potentially impacted aquatic ecosystems throughout the region, both through immediate acute flood impacts to aquatic organisms [e.g. Jensen and Johnsen, 1999, Korman et al., 2011] and more lasting effects on physical habitat. However, relationships between overall geomorphic adjustments and ecologically relevant changes that may directly influence aquatic species are complicated. This chapter therefore focuses on expanding previous interpretations of geomorphic impacts in an ecohydraulics context, addressing the way that changes to the physical

structure of Elbow River alter reach-scale hydraulics at the sub-bankfull flows that most frequently define aquatic habitat.

Flow velocity and depth patterns are fundamental controls on stream ecosystem structure and function. Hydraulic attributes determine habitat availability and quality for aquatic organisms ranging from macrophytes and benthic invertebrates to fish communities [Hughes and Dill, 1990, Madsen et al., 1993, Silva et al., 2014], with important implications for linked aquatic and terrestrial ecosystems [Nakano and Murakami, 2001, Gende et al., 2002]. Flow patterns also control physical processes such as sediment flux in alluvial channels that can reshape morphology and consequently restructure local hydraulics. These relationships between hydrogeomorphology and ecology create dynamic fluvial environments that are sensitive to changing external pressures and controls.

A rich history of research linking flow conditions with species preference and use exists [e.g. Chapman, 1966, Statzner et al., 1988, Leclerc, 2005, Clifford et al., 2008]. In particular, a focus on lotic fish habitat based largely on correlative habitat/use studies has shown that specific physical conditions are required for the spawning, rearing, and feeding of different fish species and life stages [Morantz et al., 1987, Heggenes and Saltveit, 1990, Armstrong et al., 2003]. Although extension of these microhabitat preferences to broader-scale community and population dynamics is difficult and the distribution of individuals is strongly mediated by other factors such as predation and competition [Van Horne, 1983], the 'fundamental niche' of habitat preference [cf. Hutchinson, 1957] remains a strong foundation upon which to relate species' ecology to physical stream conditions [Rosenfeld, 2003], and physical habitat has been shown to be a key control on patterns of fish distribution and abundance [Milner et al., 2003].

The importance of physical habitat is recognized in river management and restoration applications. As rivers globally have been increasingly subject to regulation, impoundment, flood control measures, and other modifications, collaboration between physical and biological sciences at the ecohydraulics/geomorphology interface has blossomed [Wassen and Grootjans, 1996, Clarke et al., 2003, Parsons et al., 2003, Noffke, 2005, Vaughan et al., 2009]. Disruption of the hydrological cycle is also commonly predicted as an impact of climate change, which will further stress freshwater ecosystems and the services they provide [Jackson

et al., 2001, Wilby et al., 2010]. To properly address potential effects of such changes, a thorough understanding of the underlying mechanisms that drive fluvial adjustments is needed, along with investigation of how these processes shape distributions of ecologically relevant patterns. However, the importance of a dynamic physical template is often neglected in correlative empirical studies. Building a robust and practically applicable eco-hydromorphic science requires explanation of static patterns through experimentation and longer-term monitoring of environmental change [Gaston and Blackburn, 1999, Vaughan et al., 2009].

Recent advances in data collection and analysis methods provide ideal tools to address issues of fluvial change. In particular, remote sensing allows for efficient and accurate characterization of riverine environments that facilitates high resolution, spatially-continuous perspectives and investigation [Fausch et al., 2002, Mertes, 2002, Carbonneau et al., 2012]. Remote sensing has been widely used for stream structure and habitat classification and mapping at scales ranging from individual sediment grains to entire watersheds [Winterbottom and Gilvear, 1997, Legleiter et al., 2002, Marcus et al., 2003, Westaway et al., 2003, Legleiter et al., 2004, Dugdale et al., 2010, Williams et al., 2013b, Javernick et al., 2015, Hugue et al., 2016]. This view has contributed to increased interest in discontinuities and variations rather than gradually varying or smooth conceptualizations of river systems; heterogeneity results from a diversity of linked physical and ecological processes, giving rise to a riverscape characterized by multi-scale complexity. In this context, approaches from landscape ecology provide valuable tools, such as concepts of patch dynamics, connectivity, spatial arrangements, and threshold changes in relation to disturbance regimes [Wiens, 2002, Brierley et al., 2006, Wohl, 2013].

In an eco-hydromorphic context, focusing on spatio-temporal variability provides a valuable way to link process and structure. Geomorphic literature is replete with examples of landform mapping and analysis, especially at the reach scale where river sections are often seen as mosaics of morphological units such as pools and riffles [Richards, 1978, Lisle, 1982, Halwas and Church, 2002]. Such channel units result from specific interactions between hydraulic and sedimentological factors [Richards, 1976, Lisle et al., 2000, MacWilliams et al., 2006, Hassan et al., 2008]. Stratifying river systems at this scale allows for investigation of geomorphic mechanisms and provides a bottom-up framework for spatial ecological ap-

plications [Buffington and Montgomery, 2013, Wheaton et al., 2015]. Because geomorphic processes result in non-random assemblages of flow properties and sediment sizes throughout a river reach [Wyrick and Pasternack, 2014], ecologically significant patches also arise at this scale, with differing quality in terms of habitat for various organisms. As a result, many examples of habitat analyses for target species are based on meso-scale (1-10 channel widths) discretization of stream environments [Newson and Newson, 2000, Parasiewicz, 2001, Dunbar et al., 2011, Silva et al., 2014], with similar approaches forming a core physical-biological link in management activities [Crowder and Diplas, 2002, Hauer et al., 2012]. In these applications, high spatial heterogeneity is usually viewed as desirable, providing a range of unique ecological conditions and habitat niches [Maddock, 1999, Thoms, 2006].

Despite the recognized importance of fluvial complexity, the understanding of relationships between geomorphic change and spatio-temporal dynamics of stream habitats is limited. In particular, information about process rates and magnitudes in response to external change is needed to support conscientious management in the face of long-term challenges. One key aspect of this is the role of disturbance; quickly acting pulse events such as large floods can completely restructure fluvial systems. Due to their inherent rarity and unpredictability, the effects of large infrequent disturbances are poorly understood [Turner and Dale, 1998]. Flood impacts are highly variable and affect components of the ecosystem in different ways that may leave lasting legacies that condition future processes [Church, 1980, Turner et al., 1998]. For example, Parsons et al. [2006] highlighted the importance of pre-flood reach morphology in determining different biotic response to a large flood event, and many examples focusing on geomorphic changes have demonstrated lasting shifts in channel form relative to sediment transport or bank erosion thresholds [Gupta and Fox, 1974, Desloges and Church, 1992, Magilligan, 1992, Grove et al., 2013, Thompson and Croke, 2013]. In this context, long-term investigation is necessary to address potential issues of non-linearities at play; rivers can exhibit multiple stable states based on thresholds in internal or external physical forcing or bio-geomorphic feedback mechanisms [Lane and Richards, 1997, Dent et al., 2002, Stallins, 2006]. Similarly, rivers are controlled by processes interacting across a hierarchy of scales, and short time-scale and small space-scale processes

can influence broader-scale behavior [Lane and Richards, 1997]. Making sense of the interactions between environmental change and eco-hydromorphology therefore requires detailed field measurement at a range of nested scales supported by numerical and physical modeling to build and test conceptual models of ecosystem evolution.

In this paper, we focus on the relationship between geomorphic change due to a large flood event and spatio-temporal hydraulic variation. Reach-scale channel form strongly controls depth and velocity distributions; Stewardson and McMahon [2002] showed that the degree of lateral versus longitudinal structural variation is important, with simple channels that lack pronounced pool-riffle morphology displaying a positive correlation between depth and velocity. In such systems, flow patterns are mainly related to thalweg position, with deep, fast water at the thalweg grading to slower, shallower water towards the banks. In channels with stronger longitudinal structure, a more negative correlation between depth and velocity generally develops, with faster water in shallow riffles and slower flows in deeper pools [Stewardson and McMahon, 2002, Schweizer et al., 2007]. This relationship is also highly discharge dependent; geomorphic structure influences flow variation most strongly at low flows, whereas higher discharges lead to convergence in flow conditions throughout a reach [Keller, 1971, Wallis et al., 2010]. However, these general conceptualizations may not apply in all systems or morphologies, and a more thorough mechanistic examination of how channel structure controls flow distributions is needed [Rosenfeld et al., 2011].

To investigate how geomorphic change influences flow patterns, we take a combined remote sensing and hydrodynamic modeling approach. Numerical flow modeling has proven to be a valuable tool for ecohydraulic analysis, allowing for detailed characterization of flow patterns at varying discharges [Pasternack et al., 2006, Clifford et al., 2009, Benjankar et al., 2014]. When combined with multitemporal elevation datasets that capture changes in geomorphic structure, such an approach allows for extraction of information at scales and resolutions that are ideal to investigate ecohydromorphic questions. To this end, we examine changes in flow structure at three discharges (10, 30, 50 m^3/s) for three distinct reach-scale morphologies (surveyed in Sept. 2012, Sept. 2013, and Sept. 2014) bracketing an extreme flood event that occurred in June 2013 on a section of Elbow River,

Alberta. To address spatial patterns of unique hydromorphic conditions, we apply statistical clustering techniques [Legleiter and Goodchild, 2005] to modeled flow distributions and then interpret the results in terms of habitat variability, configuration, and suitability for brown trout.

4.2 Methods

4.2.1 Study site

Elbow River is a gravel bed river draining the eastern slopes of the Canadian Rocky Mountains in Southwestern Alberta. Part of the South Saskatchewan River basin, it originates in sub-alpine areas of the mountains, flowing through foothills into prairie and farmland before joining with Bow River in Calgary. Although fish assemblages vary geographically throughout the watershed, the river supports native bull trout (*Salvelinus confluentus*), westslope cutthroat trout (*Oncorhynchus clarkii lewisi*) and mountain whitefish (*Prosopium williamsoni*) populations, as well as non-native brook trout (*S. fontinalis*), rainbow trout (*Oncorhynchus mykiss*) and brown trout (*Salmo trutta*) [Nelson and Paetz, 1992]. Bull trout and cutthroat trout populations have declined over the past century due to inter-species competition, exploitation, and habitat degradation [Post and Johnston, 2002]. All of the local salmonids are valued as sport fish, so understanding their contrasting and/or competing ecological requirements and geographical distributions is important to sustainable fisheries management.

Our study reach was a 1 km section of Elbow River near Bragg Creek, AB (Figure 2.1. At this point, the river has exited the mountains and exhibits an anabranching/braided morphology flowing through a wide (200-300 m) sediment-rich gravel/cobble active channel. The reach was chosen initially as a test site for fluvial remote sensing methods using unmanned aircraft systems (UAVs) and was surveyed in detail in September 2012 (Chapter 2). The following summer (June 19-22, 2013) the region experienced extreme flooding caused by a large sustained rainfall event and rapid melting of a lingering snowpack in the mountains; water levels were the highest in 60 years and the estimated damages of CAD$6 billion make the event the costliest natural disaster in Canadian history at the time of writ-

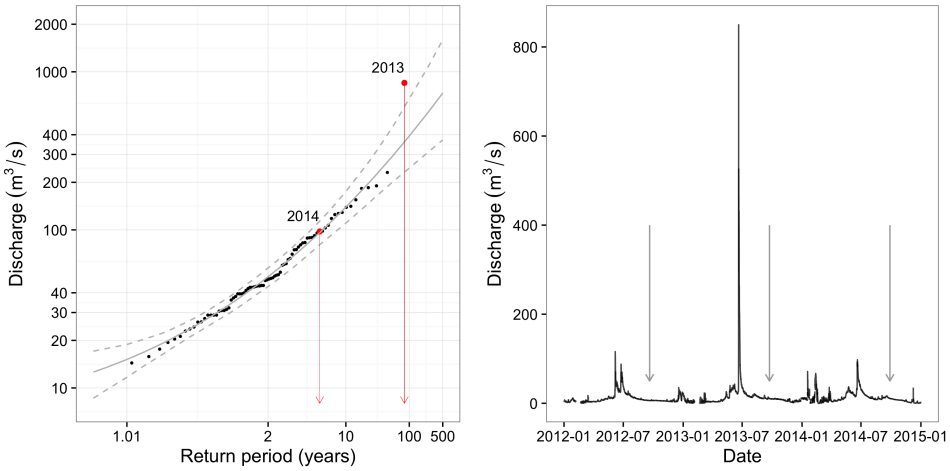

Figure 4.1: (a) Flood frequency analysis for Elbow River at Bragg Creek, 1935-2014. Grey dashed boundaries indicate 90% confidence intervals, the two flood years covered in this study are annotated by red points (b) 2012-2015 hydrograph showing flow conditions relative to timing of UAV surveys (denoted by vertical grey arrows).

ing [Pomeroy, 2015]. At the Elbow study reach, peak discharge was estimated at greater than 800 m^3/s. Although the short record of stream gauge data and difficulty in applying statistical analysis to events generated by different mechanisms (snowmelt vs. rainfall vs. rain-on-snow) make flood frequency analysis for the event highly uncertain, annual peak discharges for the Bragg Creek Water Survey of Canada gauging station (05BJ004) for 1935-2014 are shown for context with a Log Pearson Type III distribution in Figure 4.1. In this analysis the previous largest flow was 231 m^3/s in 2005, which corresponds to a return period of approximately 40 years. The 2014 freshet had a return period of about 5 years. The 2013 flood is a large outlier from the data; the return period as shown is just under 100 years but extending the fitted distribution would predict a return period of over 500 years for this magnitude of event. A longer time period including other large events would help reduce this uncertainty. Regardless of exact return periods, the 2013 flood was very uncommon, a fact that is reflected in the high magnitude geomorphic adjustments documented along Elbow River.

4.2.2 UAV surveys and DEM analysis

In this study, we make use of three datasets collected through UAV-based remote sensing. For this scale of analysis, UAVs provide an ideal platform to provide high resolution optical imagery covering the study reach; 200-300 individual geo-referenced images taken from approximately 100 m flying height with 60-80% overlap were collected each year. These photos were processed with photogrammetry software (EnsoMOSAIC, Pix4D) to generate ortho-rectified image mosaics (4-5 cm/pixel resolution) and digital elevation models (DEMs). After areas with submerged topography were corrected using an optical/empirical depth estimation procedure, DEM vertical root mean square errors were 5-10 cm. Further details of photogrammetry and DEM accuracy assessment can be found in Chapter 2 and Chapter 3. Timings of the surveys relative to the hydrograph for the period 2012-2015 are shown in Figure 4.1; each survey was conducted in late September at low flow conditions (6-10 m^3/s). The September 2012 survey captured pre-flood conditions, the September 2013 survey shows the reach structure following the June 2013 flood event (no geomorphically effective floods occurred between the flood and the data collection), and the September 2014 survey shows how the reach adjusted following a more common (yet still significant) spring freshet.

To assess geomorphic change between each year, we created DEMs of difference (DoDs) by subtracting successive DEMs. Subtracting the earlier DEM from the later one (i.e. 2013-2012, 2014-2013) gives elevation change values throughout the reach, where negative changes indicate degradation and positive values indicate aggradation. To account for uncertainty, we thresholded the DoDs using vertical error values surveyed for each year, stratified by whether areas were exposed or submerged because errors are generally larger in submerged cells. After propagating errors from each DEM to determine a minimum level of detection, we discarded elevation changes below this level that could not reliably be distinguished from noise [Brasington et al., 2003, Lane et al., 2003, Wheaton et al., 2010b]. The resulting thresholded DoDs were used evaluate spatial patterns of erosion and deposition that resulted from the 2013 flood event and subsequent reworking and to quantify the specific morphodynamic adjustments that condition reach-scale flow patterns.

4.2.3 Hydrodynamic modeling

The photogrammetry generated DEMs were also used as topographic input to Nays2DH, a depth-averaged hydrodynamic model implemented within the International River Interface Cooperative (iRIC). Nays2DH solves the shallow water equations using a general curvilinear grid for numerical discretization; grid spacing for our models was set to 1 m by 1 m based on estimates of the Peclet number [e.g., Papanicolaou et al., 2010] to minimize numerical diffusion while maintaining computational efficiency and the ability to resolve the small-scale geomorphic forms such unit bars and pool/riffle-associated breaks in slope that control flow patterns over a sufficiently long study reach. Other model inputs included downstream water surface elevation, discharge, and roughness in the form of Manning's n. For each year, we initially calibrated steady flow models at the discharge captured during the UAV surveys (6 m^3/s in 2013, 10 m^3/s in 2013 and 2014). This allowed for comparison of modeled and measured water surface elevations (extracted directly from the DEMs along the water's edge in the orthomosaic) and fine tuning of the flow resistance parameter. Flow resistance was treated as spatially uniform and starting values were estimated from D_{84} values using the Manning-Strickler approach, and lateral eddy viscosity was estimated as $LEV = 0.01 * Y * U$, where Y is reach average depth and U is reach average velocity [Nelson and McDonald, 1996]. We also compared field-measured depths with modeled depths to further check these low-flow model results (Table 4.1). Relative to the size of sediment throughout the reach (D_{84} = 0.068 m), which introduces inherent uncertainty in point-measured elevations and fluctuations in water surface, model performance following calibration was good and adequately captured the scale of hydraulic variation that we were interested in.

We then ran steady flow simulations based on the calibrated model parameters for three specified discharges for each year: 10, 30, and 50 m^3/s. These values range from the base flow typical of the late summer or fall (10 m^3/s) to an approximately two-year flood (50 m^3/s) and therefore reflect the hydraulic conditions fish in Elbow River would be subject to throughout a normal year. Although extending low-flow resistance values to higher discharges is an uncertain process [Ferguson, 2010], the high resolution model topography meant that form roughness was

Table 4.1: Calibration summary of modeled versus measured depth and water surface elevations for Nays2DH hydrodynamic simulations

Year	Q (m^3/s)	WSE R^2	WSE RMSE (m)	Depth R^2	Depth RMSE (m)
2012	6.1	0.99	0.12	0.72	0.11
2013	10.3	0.97	0.18	0.80	0.09
2014	10.1	0.98	0.17	0.75	0.08

largely captured in our calibration procedure, enabling more reliable extension to higher flows [Williams et al., 2013a]. Similar scale modeling studies have also reported few meaningful differences in indicators of boundary roughness at low and high flows [Hauer and Habersack, 2009, Krapesch et al., 2011, Wyrick and Pasternack, 2014].

These nine simulations were used to examine flow structure in terms of reach-average parameters and depth-velocity distributions. According to the simple conceptual model of Stewardson and McMahon [2002], two end-member bivariate depth-velocity distributions can be considered: one with a positive association between depth and velocity resulting mainly from bank effects and minimal longitudinal structure, and one with a negative association due to strong pool-riffle effects. They suggest most reaches can be described by some mixture of these two general forms. Schweizer et al. [2007] explained this concept by using mixed bivariate normal and bivariate lognormal distributions and a mixture parameter (s_{mix}) describing the relative contribution of each end-member distribution (a higher s_{mix} reflects a shift away from mostly normal to more skewed lognormal). They found that an increase in reach Froude number corresponds to a more symmetrical/normal distribution shape (lower s_{mix}), and that streams with larger roughness elements produce more spatial variation in depth and velocity, resulting in a shift to a more skewed lognormal shape (higher s_{mix}). Although these concepts were developed primarily in single-thread rivers, they provide a useful framework to examine the relationship between geomorphic form and flow distributions. As an analogous measure of the normally distributed, positive association between depth and velocity, we predicted a simple flow resistance-based set of velocities for the range of reach depths using

the reach average slope. Deviations of each depth-velocity distribution from this curve (calculated as R^2) therefore reflect local changes in bed topography that produce spatial flow variability and hydraulic diversity. To put the hydraulic parameters in geographic context, spatial flow patterns were also examined by generating maps of specific discharge (q, $m^3/s/m$) calculated as modeled depth multiplied by modeled velocity.

4.2.4 Cluster analysis

To interpret flow patterns in terms of ecologically relevant units, we used fuzzy set theory to classify modeled flow distributions into cohesive groups. Classification is fundamental to the understanding of the geospatial organization of fluvial environments, but the subjectivity and reliance on expert knowledge associated with many conventional habitat classification methods compromises their transferability and reliability [Poole et al., 1997]. Similarly, rigid Boolean classification schemes tend to obscure uncertainty, transitions between classes, and within-class variability [Fisher, 1998]. For this reason, we applied fuzzy logic to classify the aquatic variability in Elbow River, as proposed by Legleiter and Goodchild [2005]. This approach allows individual data points to exhibit partial membership in multiple classes, retaining a measure of uncertainty in the creation of fuzzy sets. With an unsupervised fuzzy c-means algorithm [Bezdek et al., 1984], data points (in this case, 1 m^2 pixels of Nays2DH model outputs) are grouped into a number of sets based on Euclidian distance from the cluster center and have membership values ranging from 0 (completely unlike the set) to 1 (perfect example of the set) in each set. If desired, rigid classes can then be formalized by choosing a threshold membership value [Cheng et al., 2001].

We applied the clustering algorithm (implemented in the R package 'e1071') to the modeled 10 m^3/s discharge in the pre-flood (2012) morphology. We chose to use low flow data to define the clusters because it reflects the common conditions that fish experience throughout most of the year while performing their daily actions such as feeding, resting, and rearing. Periods of low flow are also when geomorphic structure exerts the strongest control on hydraulic patterns. Classifying based on low flow data in the pre-flood morphology therefore stratifies the

river reach into hydraulic units that have strong associations with underlying landforms, providing a baseline to compare with different geomorphic configurations and discharges.

For the clustering, we chose three variables that strongly reflect hydraulic variability: flow depth, depth-averaged velocity, and Froude number. Including Froude number provides an explicit weighting to the relationship between depth and velocity; stream habitat structure and use are often associated with distinct combinations of depth and velocity as opposed to either variable independently [Statzner et al., 1988, Kemp et al., 1999]. We scaled each of these factors and then applied the clustering algorithm, varying the number of clusters and degree of fuzziness (m) until we settled on four distinct clusters and $m = 2$ as a way of balancing detail and interpretability while minimizing the within-group sum of squares to ensure separate and internally compact clusters. We then extended the analysis to the 2012 higher flows (30, 50 m^3/s) and all flows for 2013 and 2014 by calculating partial memberships for each flow model point to each of the four cluster centers determined through the 2012 10 m^3/s classification. To facilitate interpretation of spatial patterns, we then also assigned each point to the cluster to which it belonged most strongly, creating rigid hydraulic units with discrete boundaries while still being able to access the original partial membership values that describe the uncertainty in the classification. Cluster patterns were then mapped as hydraulic patches displaying particular flow conditions and landscape metrics describing geospatial organization were calculated with the FRAGSTATS-based ClassStat tool in the 'SDMTools' R package.

4.2.5 Brown trout habitat

Although the hydraulic units developed with the clustering approach objectively divided reach-scale flow patterns into ecologically relevant patches, they were created without a target species in mind. This was done intentionally to focus on the relationship between morphodynamics and spatial flow structure. However, it is also useful to interpret the cluster results and general fluvial adjustments through a fish habitat lens. For this reason, we also used the modeled depths and velocities to calculate measures of habitat suitability for brown trout. We chose brown

trout because it is a common salmonid in the region with well-documented habitat preferences. Using preference curves generated for the nearby Kananaskis River [Courtney et al., 1998], we calculated habitat suitability indices reflecting preferences for depth (D_{HS}) and velocity (V_{HS}) for juvenile and adult brown trout. The values for each factor range from 0 (completely unsuitable) to 1 (ideal habitat). Overall adult and juvenile composite suitability values ($Adult_{HS}$, Juv_{HS}) were then calculated as $HS = (D_{HS})^{1/2}(V_{HS})^{1/2}$. Calculating habitat suitability based on depth and velocity alone is useful because it isolates the role of hydraulic changes, but an equally important aspect of salmonid habitat is access to overhead cover. In Elbow River, cover is primarily provided by large wood (LW) or steep undercut banks. We used the high resolution orthomosaics and topographic information from the DEMs to digitize these features and then calculated cover suitability C_{HS} as an exponential decay with distance from cover within the wetted area for each modeled flow. Composite suitability values including cover ($Adult_{HSC}$, Juv_{HSC}) were then calculated as $HSC = (D_{HS})^{1/3}(V_{HS})^{1/3}(C_{HS})^{1/3}$ in a manner similar to suitability calculations that include a channel index or substrate factor [Leclerc et al., 1995, Pasternack et al., 2004].

4.3 Results

4.3.1 Morphodynamics

The general geomorphic changes for the study period are shown in Figure 4.2. Overall, pre-flood reach morphology was characterized by a sinuous primary low-flow thread with several major anabranches associated with bar dissection and chute cutoff. The 2013 flood event resulted in substantial bank erosion (10s of meters of bank retreat) on both sides of the 2012 channel as width adjusted to the large discharges, along with a complete reworking of sediment and morphology within the active channel. The bulk of the low-flow discharge in 2013 appears to be mainly confined into one or two wide, shallow anabranches with a long meander wavelength reflecting the path cut by the waning flood flows. The 2014 morphology reflects more subtle changes that occurred during the 2014 freshet including bank erosion at bend apices and associated bar deposition, along with infilling of

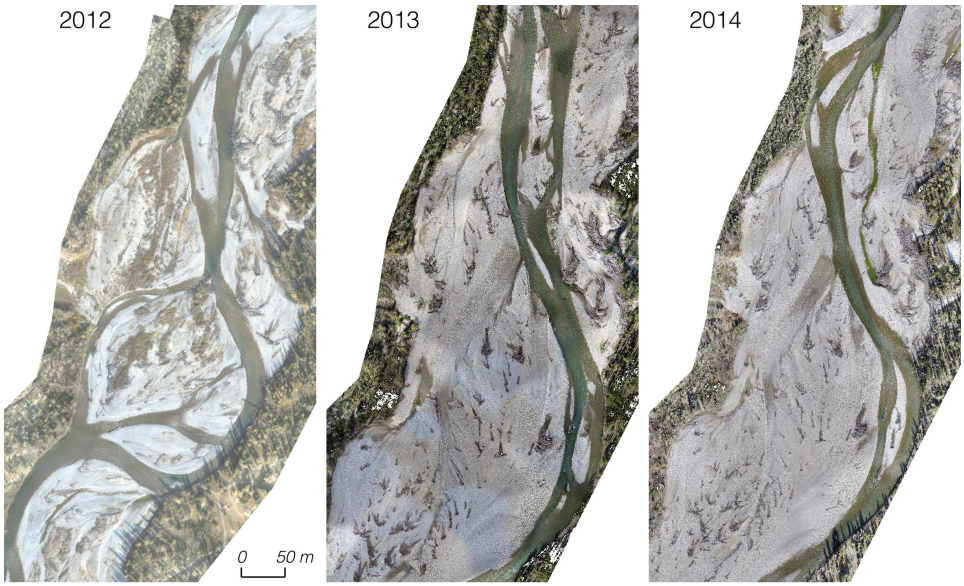

Figure 4.2: UAV orthomosaics for each survey year. Flow direction is from bottom to top

smaller high elevation secondary channels produced by the 2013 flood but likely not accessed during the 2014 freshet. These general channel pattern changes are also reflected in Table 4.2, where a braiding parameter (B) and a sinuosity parameter (P) are calculated for low flow wetted channels as: $B = L_{ctot}/L_{cmax}$ and $P = L_{cmax}/L_R$ where L_{ctot} is the sum of the lengths of all channels in the reach, L_{cmax} is the length of the widest channel through the reach, and L_R is the straight-line length of the channel belt [Friend and Sinha, 1993]. The flood event caused a reduction in sinuosity (P) from 2012 to 2013 along with an increase in braiding (B) due to the presence of two to three linear medial bars splitting the main low-flow anabranch. In 2014, an increase in P reflects cutbank retreat and bar deposition, and the concentration of flows into one main channel results in a large decrease in B.

DEM differencing (Figure 4.3, Figure 4.4) supports and quantifies the observed morphodynamics. Summaries of elevation adjustments are shown in Table 4.3. Geomorphic turnover from the 2013 flood was extensive; 88% of the reach area experienced detectable elevation changes in the 2013-2012 time period, but it is likely

Table 4.2: Channel pattern parameters. Values were calculated for wetted two-way connected anabranches at low flow. B is the braiding parameter, P is the sinuosity parameter

Year	B	P
2012	2.02	1.28
2013	2.31	1.08
2014	1.69	1.10

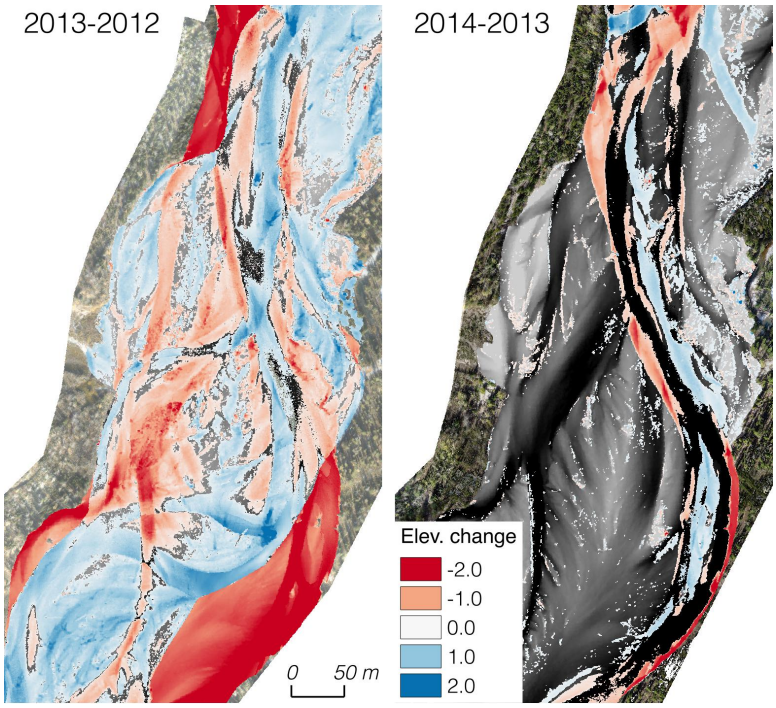

Figure 4.3: Thresholded DEMs of difference between survey years. Negative (red) elevation changes represent areas of erosion, positive (blue) values indicate deposition. DoDs are overlain on detrended DEMs within the active channel.

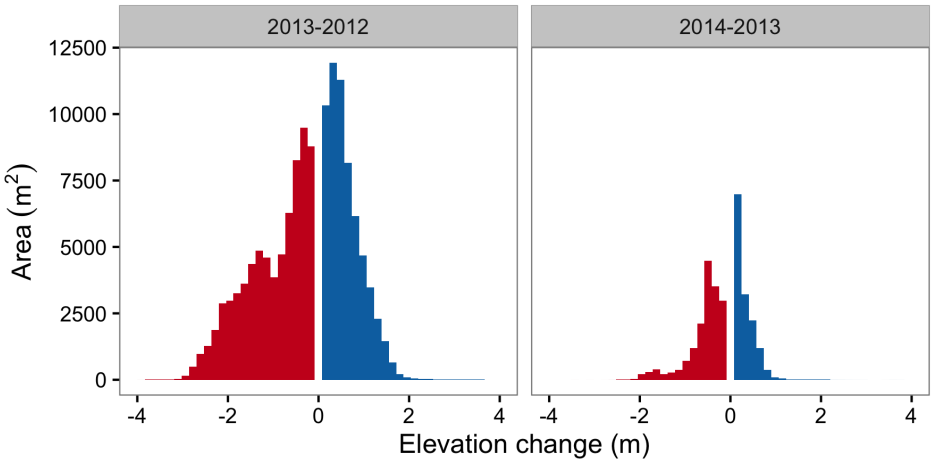

Figure 4.4: Histograms of thresholded elevation changes between surveys years. Negative (red) elevation changes represent erosion, positive (blue) values indicate deposition.

the entire active channel bed was affected and areas without discernible changes correspond to areas where scour and fill largely canceled out to a resultant elevation change below thresholds of detection. The adjustment was degradational overall due to bank erosion, but large volumes of sediment (from local bank erosion) were deposited within the channel as well. The magnitude of change during the 2014-2013 epoch was much smaller and impacts were less extensive. The DoD supports the fact that the 2014 freshet did not access (at least, in a geomorphically effective way) the higher elevation bartops and channels that remain from the 2013 flood; elevation changes are confined to the area around the low flow anabranch and reflect lateral adjustments through outer bank erosion. During this time period, 20% of the active channel experienced detectable turnover and the net change was also degradational.

4.3.2 Flow pattern changes

Results from the Nays2DH model runs give insights into the relationships between morphodynamics and flow patterns. Maps of specific discharge (Figure 4.5) reflect the rearrangement of low flow topography; 10 m^3/s flows in 2012 follow two

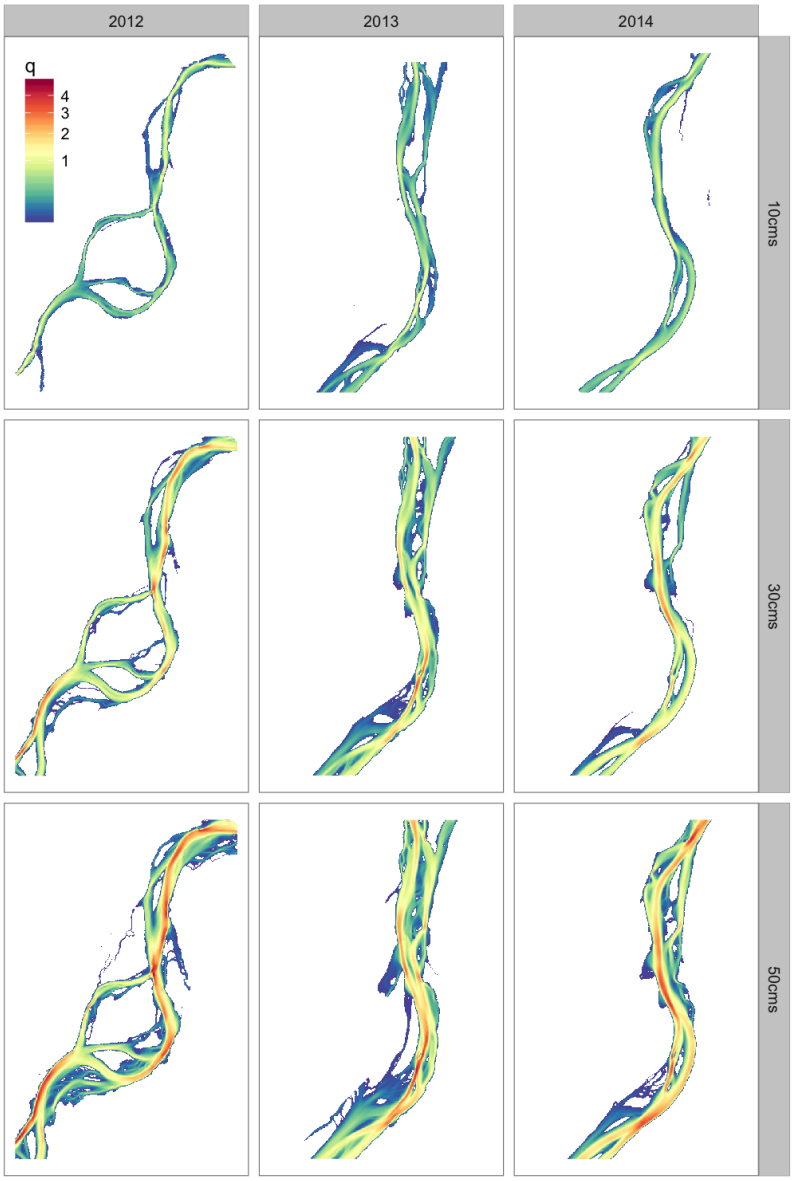

Figure 4.5: Steady flow hydrodynamic model results shown as maps of specific discharge (q, $m^2/s/m$) for each year (2012, 2013, 2014) and discharge (10, 30, 50 m^3/s) combination.

Table 4.3: Morphodynamic adjustments for each time period. % Area is the percentage of reach area experiencing detectable elevation change stratified by direction (aggradation vs. degradation), Σ Vol represents totals of volumetric change, Δ Z is average elevation change throughout the reach.

	% Area	Σ Vol (m^3)	Δ Z (m)
2013 - 2012			
Aggradation	40.1	37,223.8	0.61
Degradation	48.0	-73,899.6	-1.01
Net change		-36,675.8	-0.40
2014-2013			
Aggradation	9.3	4,496.6	0.32
Degradation	11.0	-9,676.8	-0.58
Net change		-5,180.1	-0.26

to three main anabranches splitting around large medial bars with associated flow convergence and scour pools where threads meet. In 2013, flow is more restricted to a wide primary channel produced by the flood but occasionally diverges as flows access other high-elevation secondary channels. The 2014 10 m^3/s flow is confined the to same general path as in 2013, but here fluvial reworking through the 2014 spring freshet appears to have entrenched flows even more into a single thread conveying the bulk of the discharge with less access to secondary channels. These patterns are accentuated as modeled discharges increase to 30 and 50 m^3/s; 2012 flows display a wider range of hydraulic conditions with deep scour and bend apex pools having locally high specific discharges but a significant portion of the flow is more spread through gradually sloping bar surfaces, secondary anabranches, and areas of slackwater. In 2013, these higher discharges also activate more anabranches and fill shallow areas, whereas the 2014 high discharges more strongly follow a main thalweg with high specific discharge values.

These changes in flow pattern can be further examined through reach average hydraulic parameters, joint depth-velocity frequency distributions, and individual univariate density distributions for depths and velocities. Overall, flows in 2012 are deeper and reach average hydraulic widths are less than 2013 for a given discharge

Table 4.4: Summary of reach average hydraulic parameters for each simulation. Y is depth, W is width, U is velocity, Fr is Froude number, τ is shear stress

Year	Q (m^3/s)	Y (m)	W (m)	U (m/s)	Fr (-)	τ (Pa)	W/Y (-)
2012	10	0.42	31.0	0.67	0.46	16.8	73.1
	30	0.51	45.1	1.03	0.49	32.6	87.5
	50	0.56	64.0	1.06	0.49	33.5	115.1
2013	10	0.30	38.4	0.69	0.42	16.6	128.4
	30	0.45	54.6	0.94	0.47	26.3	122.6
	50	0.52	68.8	1.06	0.49	31.5	132.4
2014	10	0.37	28.3	0.82	0.44	20.6	77.3
	30	0.51	42.5	1.07	0.49	31.9	82.5
	50	0.58	55.1	1.19	0.51	37.2	94.2

(Table 4.4). In 2014, widths are less than 2012 or 2013, corresponding to increased average velocities. This is reflected in a large change of width/depth (W/Y) ratio, which is much higher in the 2013 post-flood configuration than in 2012. By 2014, W/Y is once again reduced to values similar to before the flood.

Bivariate depth-velocity frequency distributions (Figure 4.6) confirm these general changes. The associations between depth and velocity (Figure 4.6) for the modeled flow data vary with discharge and by geomorphic configuration (year). In 2012, the positive association between depths and velocities is weak at 10 m^3/s, with a negative R^2 (-0.25) between the reach average slope-predicted curve and the actual flow distribution. In 2013 and 2014, the frequency distributions correspond more closely with the predicted curve (R^2 = 0.28, 0.23). All three years show evidence of a drowning out of topographic influence and roughness elements as discharge increases (more similar flow distributions despite different morphology; higher R^2), but the 2012 morphology remains distinct in its wide range of hydraulic conditions even at 50 m^3/s (for example, many high depth, low velocity points remain). 2013 and 2014, on the other hand, show a relatively low diversity of conditions by 30 and 50 m^3/s.

Examining the individual distributions of depth and velocity separately (Figure 4.7) is also valuable. All three years show a shift away from left-skewed velocity

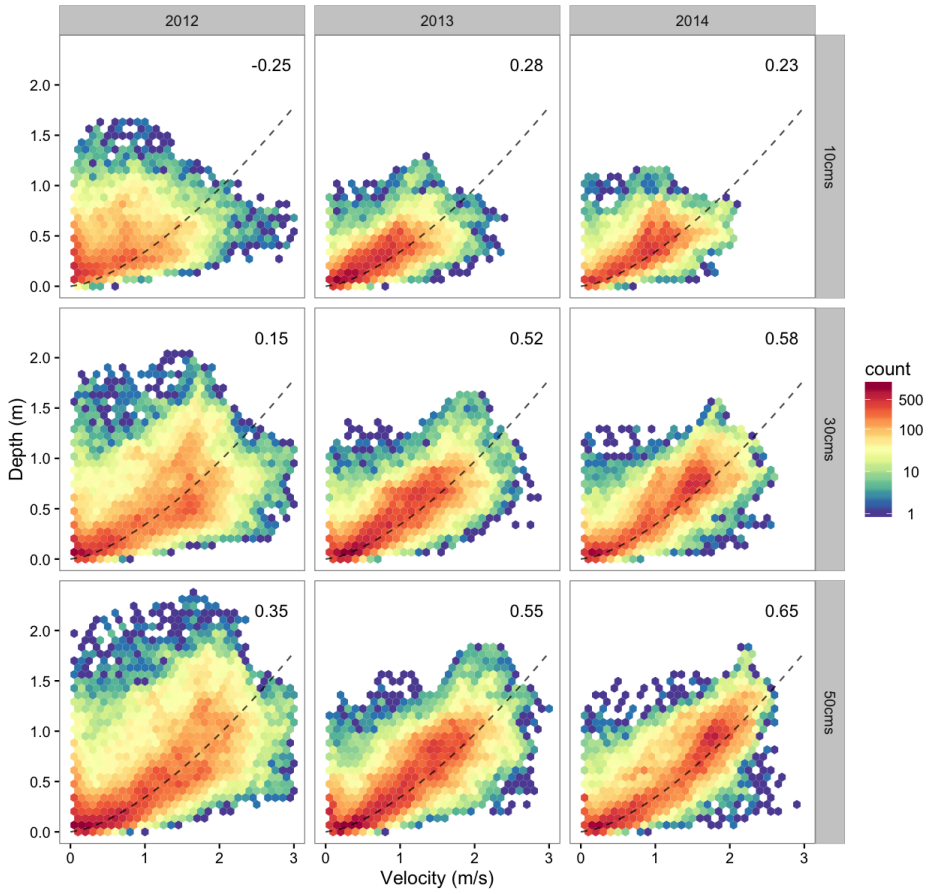

Figure 4.6: Joint depth-velocity frequency distributions. A simple flow resistance-predicted curve of depths and velocities is overlain (dashed line); R^2 between the curve and the modeled distributions is reported for each year-discharge combination.

and depth distributions as discharge increases. At higher discharges, velocity distributions begin to exhibit a more pronounced peak at velocities in the 1-2 m/s range, especially in the 2014 model runs. In the 2014 configuration, this high velocity peak is also evident at 10 m^3/s, indicating largely channelized flow patterns even at low discharges and corresponding to higher overall reach average velocities.

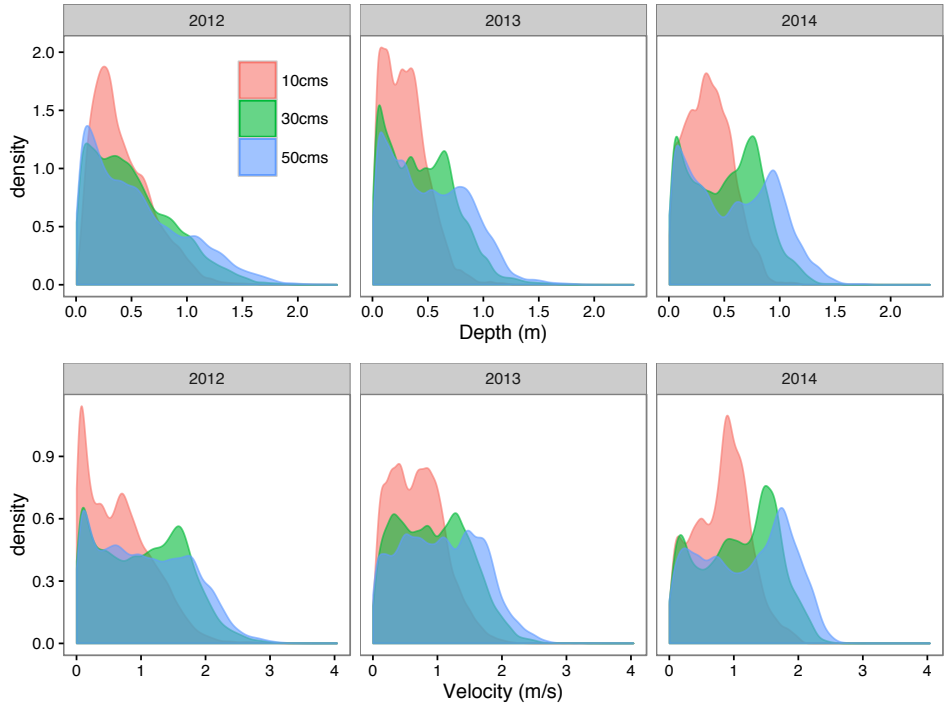

Figure 4.7: Individual depth and velocity density distributions

4.3.3 Cluster results

To further interpret the general changes in flow patterns in terms of reachscape composition and spatial structure, we classified the 2012 10 m^3/s flow data. Results of the fuzzy c-means clustering are shown in Figure 4.8. The four clusters stratify the depth-velocity flow field into groups of characteristic flow conditions (Table 4.5), and a detailed example view of the relationship between geomorphic setting, flow patterns, and clusters is shown in Figure 4.9. These clusters reflect specific hydraulic conditions associated with controls exerted by mesoscale bedforms and therefore largely correspond with the common descriptive geomorphic unit terms pool, riffle, and glide. Cluster 1 (low energy) represents low slope, low velocity environments with a shallow depths, typically found along stream margins, in shallow secondary channels, or in backwater areas of scarcely perceptible flow. Cluster 2 (pool) is deeper flow with a range of velocities below about 1 m/s and

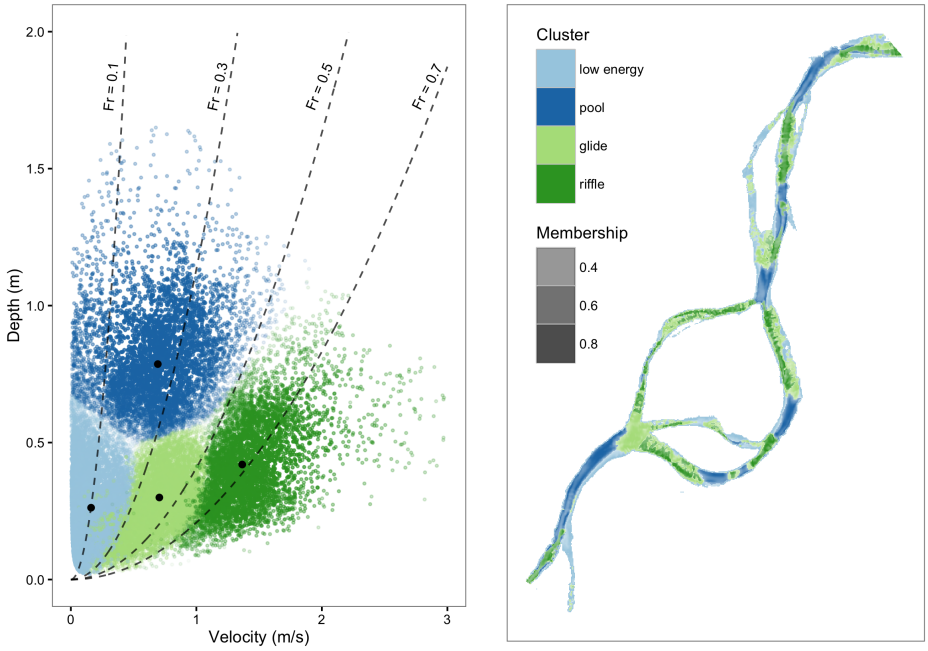

Figure 4.8: (a) Depth-velocity scatterplot for classified 2012 10 m^3/s data, with points stratified by color for each cluster. Point transparency is scaled by the membership of each point to its class. Lines of equal Froude number are overlain for reference. Black points indicate centers for each cluster. (b) Mapped patterns of 2012 10 m^3/s classification

low water surface slope. In the 2012 morphology, pool units are primarily found along outer bends or in areas of forced vertical or lateral expansion such as those associated with scour at anabranch confluences or around large wood jams. Cluster 3 (glide) is flow with moderate depths, velocities, and water surface slopes, generally found in areas of diverging flow or along lateral gradients flanking threads of higher intensity flow. Cluster 4 (riffle) is high velocity, high energy flow that often exhibits broken water surface texture. In general, riffle and pool clusters are thalweg flow conveying similar specific discharges, and the four clusters can be differentiated by Froude number, increasing from an average of 0.21 in low energy units, 0.33 in pools, 0.51 in glides, to 0.67 in riffles (Table 4.5). The paired blue/green color scheme also reflects the general conditions and locations of the clusters: blue for the low Froude number low energy and pool clusters, green for

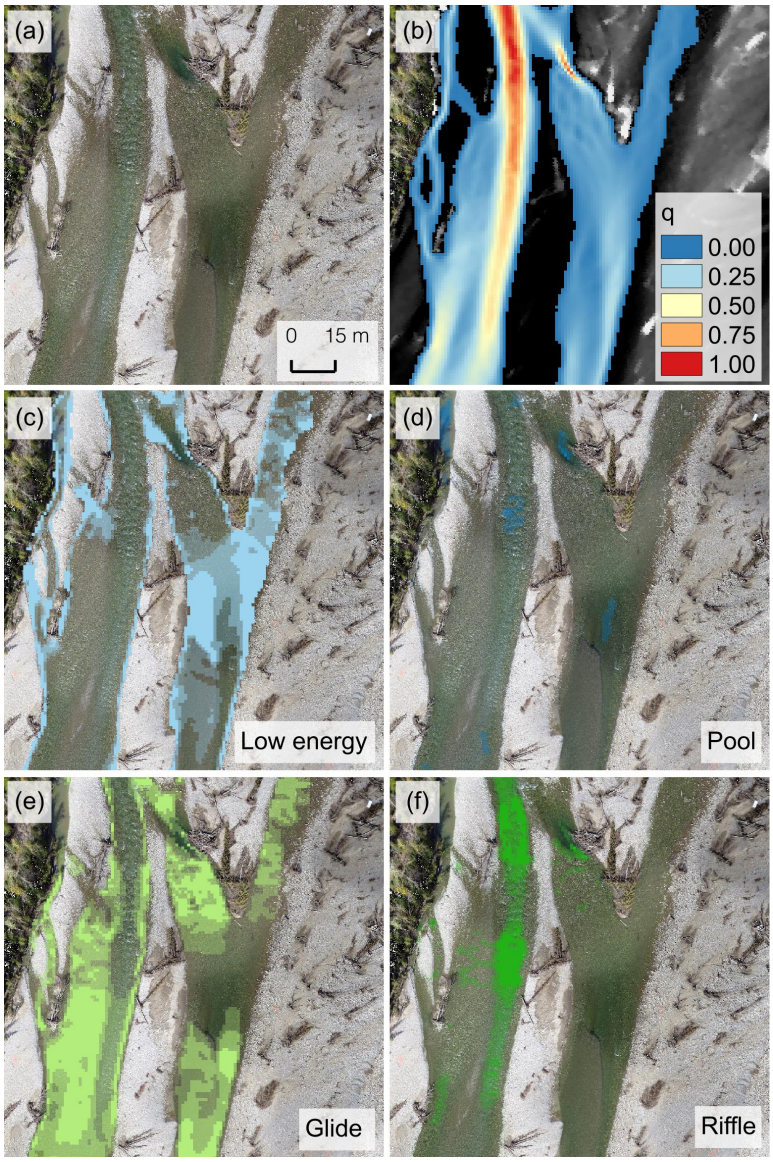

Figure 4.9: Detailed example view of (a) 2013 orthomosaic (b) specific discharge overlain on DEM (c-f) Low energy, pool, glide, riffle fuzzy unit patterns with transparency scaled by membership to each class

Table 4.5: Summary of clusters and representative average hydraulic characteristics

Cluster	Description	Depth (m)	Velocity (m)	Fr (-)	S_f (-)	q (m^2/s)
1	Low energy	0.20	0.23	0.21	0.0017	0.051
2	Pool	0.73	0.83	0.33	0.0021	0.58
3	Glide	0.29	0.76	0.51	0.0066	0.24
4	Riffle	0.45	1.39	0.67	0.012	0.64

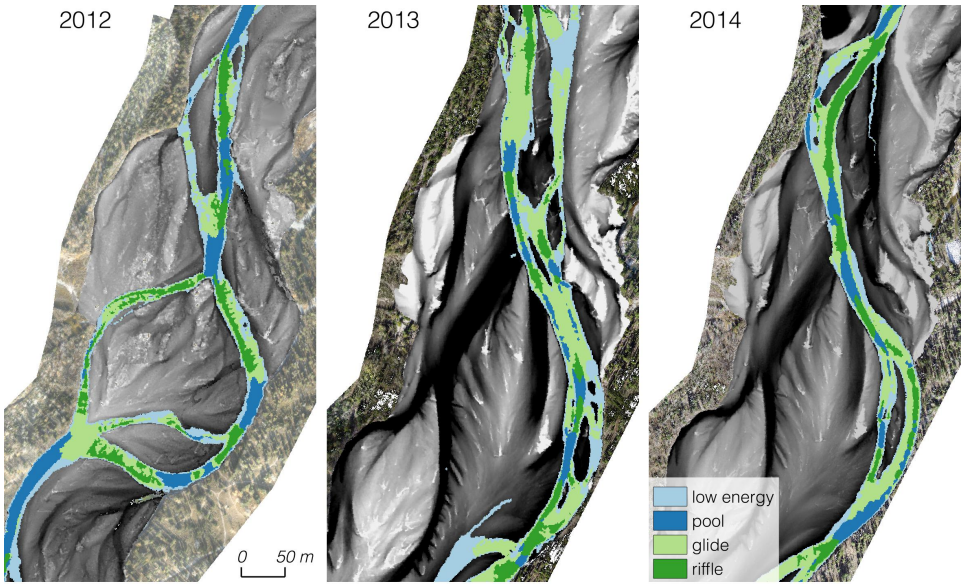

Figure 4.10: Spatial patterns of clusters at 10 m^3/s. Clusters are overlain on detrended DEMs within the active channel

higher Froude number glide and riffle clusters. The deeper mainstem pool and riffle clusters are then differentiated from their more marginal shallow low energy and glide counterparts as dark blue or green versus light blue or green.

Figure 4.10 shows the mapped patterns of these clusters for all three years at 10 m^3/s. At this discharge, geomorphic control on the flow patterns is most evident and the arrangement of clusters has the most relevance to fish that depend on specific low-flow hydraulic conditions throughout most of the year. For all three

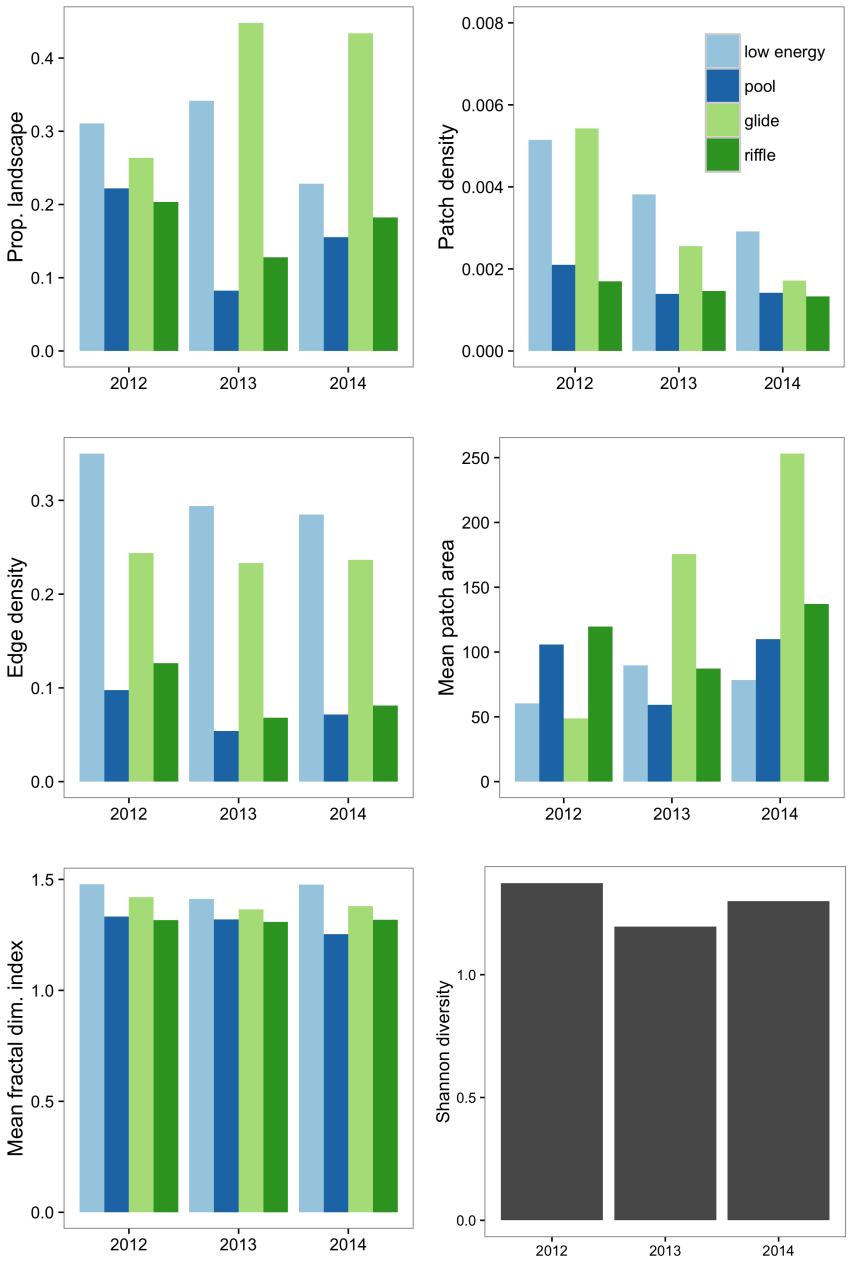

Figure 4.11: Measures of reach composition at 10 m^3/s

Table 4.6: Metrics of reachscape composition. Superscript *a* denotes class metrics (calculated for for each cluster class), superscript *b* indicates landscape metrics (calculated including all classes)

Spatial metric	Unit	Description
Proportion of landscape[a]	%	proportional abundance of each class
Edge density[a]	m/ha	standardized total edge length for each class
Mean fractal dimension index[a]	-	shape complexity from 1 (low) to 2 (high)
Patch density[a]	n/100ha	standardized number of patches of each class
Mean patch area[a]	m^2	average size of patches for each class
Shannon Diversity Index[b]	-	overall heterogeneity and diversity

geomorphic configurations, the clustering created spatially well-defined hydraulic units. Reachscape cluster composition is summed up as percentage of wetted area for each cluster in Figure 4.11a. In general, flow in 2012 morphology appears the most fluvially organized, with deep pools found at low gradient outer bends of the main anabranch transitioning into higher velocity riffle units in higher gradient sections. Areas where flow diverges into two or three anabranches are typically wider, shallower environments associated with glides. However, low energy patches are the most prevalent in this morphology (30% of wetted area), due to several prominent low gradient secondary channels and lateral transitions within the main channel driven by uneven cross sectional bed elevation distributions. In 2013, the geomorphic disruption from the large flood event and transition to high width/depth ratios manifests itself in reductions in pool and riffle clusters; more flow is carried through shallow, high energy slope stream areas corresponding to glide units (43% of area in 2013 vs. 24% in 2012). Pool and riffle units still exist, but they are more sporadic and less easily explained by planform configuration or bar-pool-riffle units. Low energy patches remain common given the shallow overall depths and several side channels. By 2014, hydraulic diversity increases slightly relative to 2013 as pool and riffle conditions reform in the main anabranch

thalweg, but the reach is still dominated by glide-type flow conditions and low energy environments are reduced in area.

Figure 11 also includes several metrics of landscape pattern chosen to interpret potentially ecologically relevant changes in spatial composition and shapes of the cluster patches. Descriptions of the metrics are shown in Table 4.6. Patch density, which reflects the number of patches present in a class, shows that at 10 m^3/s, low energy and glide units are much more frequent compared to pools or riffles in all three years. This generally corresponds to smaller mean patch areas for low energy and glide units, compared to the larger, more spatially contiguous pool and riffle units. However, the flood impacts appear to have resulted in a muting of this pattern; patch densities for low energy and glide classes are reduced in 2013 and even more in 2014 as glide units in particular become larger and more cohesive. These change are also reflected in edge density, a measure of edge length for each class, and fractal dimension index, a measure of shape complexity. For all three years, the elongate, linear shape of the more marginal glide and low energy units is quantified as higher edge density and fractal dimension index; pools and riffles are generally more rounded and simple-shaped with lower edge densities and fractal dimension index values. Between 2012 and 2013, a reduction in mean patch area, patch density, and edge density for pool and riffle clusters likely reflects the disorganized nature of post-flood morphology relative to the well-defined, elongate features in the pre-flood conditions. The final metric, Shannon Diversity index, is calculated at the landscape level (for all classes combined), and is highest in 2012, lower in 2013, and then recovers slightly in 2014. This is associated with a more even distribution of class areas in 2012 compared to the homogenization of conditions and dominance by glide units in 2013 and 2014.

Flow patterns change at higher discharges, resulting in different proportions and arrangements of patches throughout the reach. Figure 4.12 shows mapped cluster patterns for all three discharges, and Figure 4.13 shows changes in landscape metrics with discharge. Patterns of patch change with discharge are different between the three years, shown most simply by the proportion of landscape occupied by each class. In 2012, all four classes are relatively equal in proportion (20-30% of area) at all three discharges. In 2013, the low energy and glide units that dominate at 10 m^3/s become less common as discharge increases and more pool and

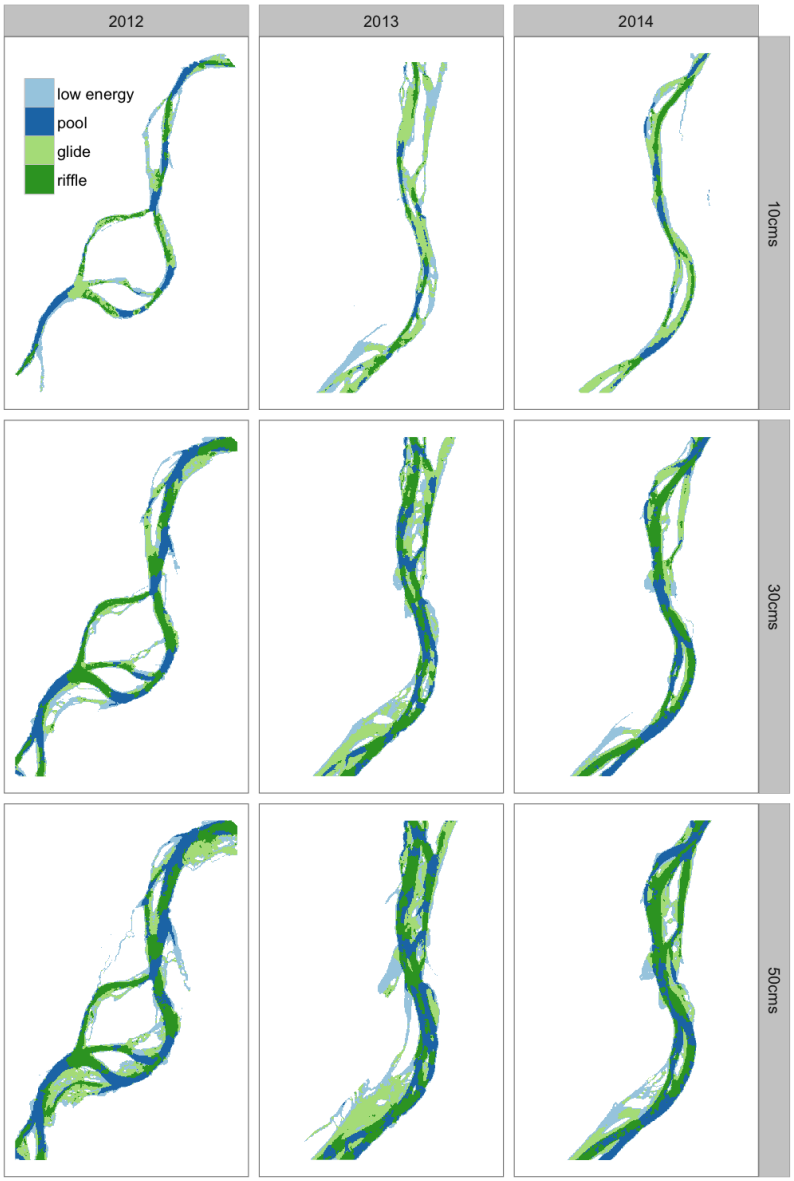

Figure 4.12: Spatial distributions of clusters for all three modeled discharges

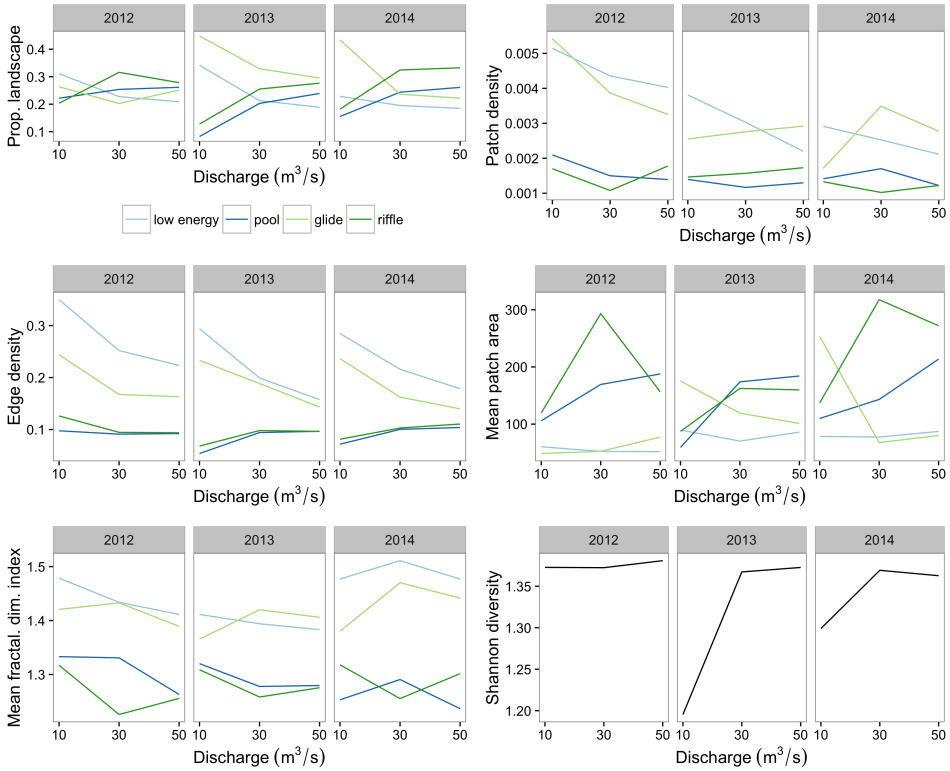

Figure 4.13: Measures of changes in reach composition with discharge

riffle-like conditions develop, with a more equal distribution of the four classes by 50 m^3/s. In 2014 the glide conditions that are most common at 10 m^3/s quickly give way to more pool and riffle areas, with riffle-like hydraulic conditions dominating by 50 m^3/s. Secondary anabranches that at 10 m^3/s are primarily low energy or glide units tend to transition to pool or riffle conditions with higher discharges as well, and the more marginal low energy or glide clusters are only found along shallow sloping bar edges, in backwater areas, or in smaller high elevation channels that had no flow at 10 m^3/s. Patch density and edge density display similar trends with discharge for the three years; pool and riffle units remain less frequent in number with low edge densities, whereas low energy and glide classes decline in patch and edge density as discharge increases. Pools and riffles also show increases in patch area with discharge as flow conditions coalesce into a quickly flowing main-

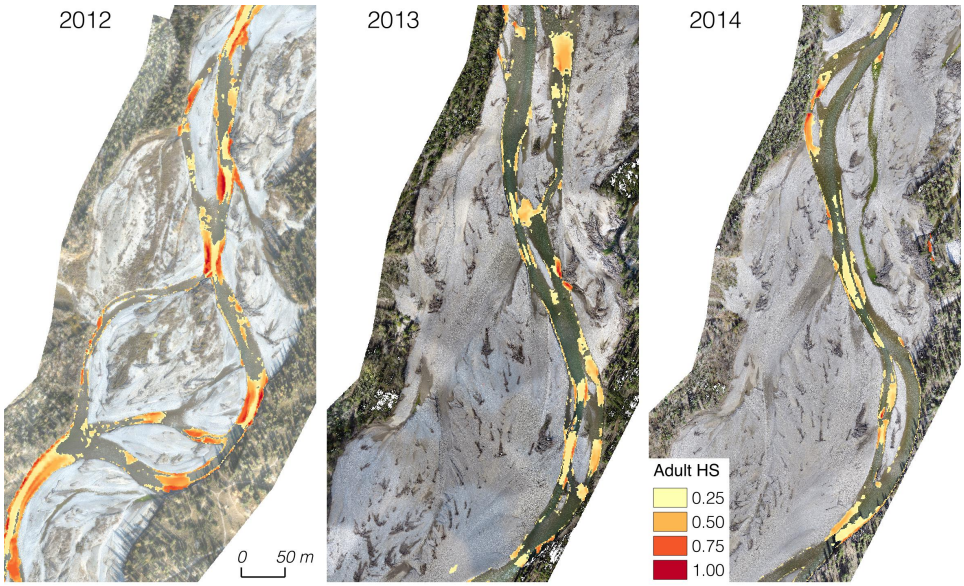

Figure 4.14: $Adult_{HS}$ patterns at 10 m^3/s. Only cells with HS>0.25 are shown.

stem that is less influenced by topographic highs or lows. These overall changes are reflected in the Shannon Diversity index, which is high for all discharges in 2012 and lowest in 2013 at 10 m^3/s but climbs with discharge as pool and riffle units become more common. 2014 has intermediate Shannon Diversity values for 10 m^3/s but reaches similar values to 2012 or 2013 by 30 m^3/s.

4.3.4 Brown trout habitat suitability

Calculated habitat suitability values for adult and juvenile brown trout put the documented hydrogeomorphic changes in a direct habitat impact context. Figure 4.14 shows mapped areas of habitat suitability for adult trout ($Adult_{HS}$) at 10 m^3/s. In this figure, only those areas with habitat suitability greater than 0.25 are displayed to emphasize potential habitat hotspots in relation to flow patterns. In 2012, highly suitable habitat is available along much of the reach; outer bends associated with desirable pool-like hydraulic conditions provide long linear stretches of good habitat, as do smaller-scale scour pools which are often associated with large wood jams. Lateral gradients also appear important; areas with sufficient depth and low

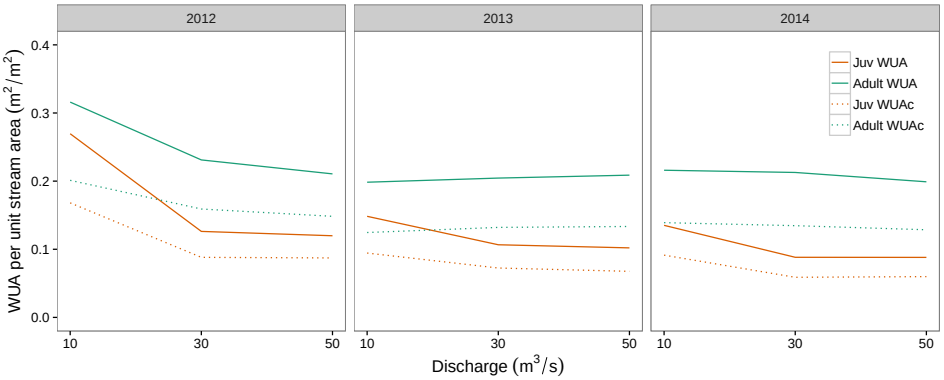

Figure 4.15: Changes in WUA and WUA_C per unit stream area for adult and juevenile brown trout.

enough velocities are found along either side of high velocity thalweg threads. In 2013, these high suitability areas are less widespread and few areas have the very high (i.e. HS>0.75) suitability values that were present in 2012. This is largely due to the wide, shallow nature of the post-flood flow and the lack of well defined pools, although small scour pools associated with LW accumulations still offer some habitat hotspots. By 2014, bank erosion and vertical scour once again provide access to more suitable flow conditions. However, although some small LW-associated scour pools still exist, sediment deposition and planform adjustment have cut off low flows from several large jams that previously provided good habitat. Spatial patterns of Juv_{HS} are largely the same as those for adults, but slightly more restricted due to lower velocity tolerances.

As a measure of total reach-scale suitability, habitat suitability changes can also be analyzed by calculating weighted usable area as the sum of each cell's habitat suitability multiplied by cell area (1 m^2) for each flow model. This also allows easy examination of overall changes in habitat suitability with discharge for the three years (Figure 4.15). Two measures of weighted usable area are calculated: one based only on depth and velocity preferences (WUA, from $Adult_{HS}$ and Juv_{HS}) to isolate purely hydraulic effects on habitat and one including the effect of overhead cover (WUA_C, from $Adult_{HSC}$, Juv_{HSC}). To account for the effect of increasing total wetted area as discharge increases, WUA is expressed on a per unit area basis

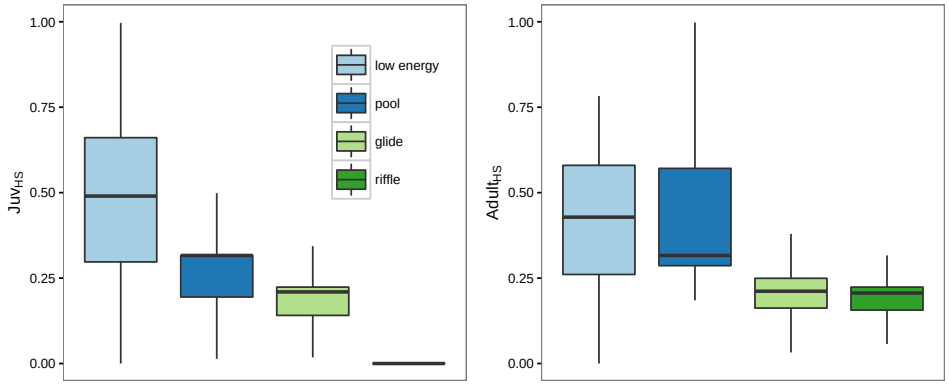

Figure 4.16: Distributions of (a) Juv_{HS} and (b) $Adult_{HS}$ for each 2012 10 m^3/s classified cluster

as a measure of intrinsic habitat quality. Summing up habitat suitability values this way confirms an overall reduction in habitat availability and quality as a result of the 2013 flood, especially at low flow; adult and juvenile WUA are highest in 2012 at 10 m^3/s and then low in 2013 and 2014. In 2012, WUA declines as discharge increases, especially for juveniles as velocity tolerances are quickly exceeded. Because 2013 and 2014 have less suitable 10 m^3/s conditions to begin with, this drop off with discharge is less strong; adult WUA is largely constant with discharge and juvenile WUA declines slightly between 30 and 50 m^3/s. Including the effect of cover preferences in the WUA calculations results in lower overall values because cover suitability declines quickly with distance from overhead cover, so much of the stream is less suitable by this more stringent measure. Although this effect is similar across the three years and discharges, cover availability is slightly higher in 2012 than 2013 and 2014, and always increases with discharge. Including C_{HS} in the WUA_C calculation therefore exacerbates the observed reduction in habitat suitability between 2012 and 2013-2014: flow depths and velocities are less suitable and access to overhead cover from LW and undercut banks is less widespread in the post-flood geomorphic configurations.

Figure 4.16 shows distributions of Juv_{HS} and $Adult_{HS}$ at 10 m^3/s associated with each fuzzy c-means cluster to evaluate whether the hydraulically defined clusters display distinct habitat suitability ranges. For juvenile trout, the low energy

cluster provides the most suitable conditions with low velocities; small bodied juveniles can also occupy the shallow depths in this cluster. These conditions are also highly suitable for adult trout but slightly less so due to a lower preference for very shallow depths. Pool habitats are the second most suitable for juveniles who can inhabit deep waters, but the range of velocities within this cluster means some pool areas are largely inhospitable due to low tolerance to velocities greater than about 0.5 m/s. Adult trout can use higher velocity conditions, so the pool cluster provides consistently high quality habitat. The higher Froude number glide and riffle clusters are generally less suitable for both juveniles and adults; juveniles in particular cannot tolerate high velocity riffle units at all.

4.4 Discussion

This study aimed to investigate the relationships between river morphodynamics, flow organization, and aquatic habitat. Through repeat surveys bracketing a large flood event, we characterized geomorphic change resulting from the flood and subsequent readjustment in the following year. Overall, we found that restructuring of morphology strongly impacted flow patterns in both a reach-average sense and in terms of the spatiotemporal arrangement of zones with distinct hydraulic characteristics. These changes resulted in a reduction in adult and juvenile brown trout habitat quality as measured through habitat suitability indices.

The geomorphic adjustments due to the 2013 flood were drastic. The detailed pre- and post-flood topographic datasets document spatial patterns of bank erosion, scour, and fill at a resolution that is rare for such high magnitude disturbance events. In general, the active channel widened by approximately 50 meters between 2012 and 2013. This is consistent with many other examples of large floods in the geomorphic literature [e.g. Magilligan, 1992, Kale, 2007, Hooke, 2008] and reflects an adjustment to forces far in excess of thresholds for entrainment of large grain sizes and bank erosion [Olsen et al., 1997, Eaton and Church, 2004]. Similar patterns of bank erosion were also observed along the rest of Elbow River and on rivers throughout the region. This primary effect of large floods reflects a channel form adjustment to a shallower, wider flow that reduces mean boundary shear stress until the flood pulse recedes or bank stability is reattained [Tamminga et al.,

2015, Eaton and Mackenzie, in review]. However, the more detailed geomorphic impacts and system responses of such widening are less understood and depend on valley and floodplain configuration, geomorphic history, and initial active channel geometry [Fuller, 2007]. At the Elbow study reach, bank erosion supplied large volumes of alluvium to the channel bed, resulting in substantial local aggradation despite the event being net degradational (Figure 4.3, Table 4.3). This sediment and the associated high flood transport rates erased the existing pre-flood morphology completely as large bars were constructed and dissected during the flood flows. These bar features have a long streamwise length scale that reflect a much longer sediment path length (the downstream displacement of particles over time) than the pre-flood channel forming flows would have exhibited [Pyrce and Ashmore, 2003]. These depositional features are also relatively tall due to the deep flows in which they formed [Church and Jones, 1982, Nicholas et al., 2016]. Similar effects have been reported by Wheaton et al. [2013], who documented a shift in braiding mechanisms to favor channel widening and transverse bar building as the magnitude and duration of flows above bankfull increased. They postulated that the large sediment loads and reduced topographic steering during large floods result in a reduction of braidplain heterogeneity, consistent with findings from Madej [1999] and Legleiter [2014b].

The 2013 flood therefore set the geomorphic constraints for the processes of readjustment during the following year (2013-2014). Because the channel configuration was set by such a high magnitude event that built high elevation barforms, the 2014 spring freshet (which peaked at approximately 100 m^3/s) was likely constricted to zones within the over-steepened low sinuosity path cut by the waning 2013 flood flows. Consequently, the 2014 geomorphic adjustment reflects a lower flow magnitude and shorter duration above sediment transport thresholds combined with topographic confinement, resulting in less areally extensive geomorphic turnover and smaller volumetric changes (Table 4.3). As opposed to the significant lateral instability evident in the 2012-2013 changes, the 2013-2014 morphodynamics appear to be progressing towards the reestablishment of lateral dynamic equilibrium through sedimentation in secondary channels, bank erosion, bar edge trimming, and unit bar accumulation that results in increases in sinuosity and

a more single thread channel pattern. This effect is net degradational, indicating that this readjustment process remains on-going.

These large, channel forming events (2013 flood and 2014 freshet) configure the geomorphic template within which the lower magnitude flows that are more ecohydraulically relevant operate. These smaller discharges are what we focused on through numerical flow modeling in this study, allowing for investigation of how flow patterns are conditioned by geomorphic change. Overall, we found that the 2013 flows were very wide and shallow compared to the same discharges in the 2012 geomorphic configuration (Figure 4.5, Table 4.4). This shows that the reach-scale widening and local deposition associated with the 2013 flood are reflected in smaller discharges as well. This wider shallower flow is also less hydraulically diverse (Figure 4.6), with a near complete loss of deep, slow areas at all three modeled discharges. Overall it appears the 2013 flow patterns are less fluvially organized; insufficient time of competent flows following the flood means there is a lack of sediment transport and sorting processes that lead to shear stress concentration and predictable patterns of pools scour and bar deposition or avulsion and new anabranch creation [e.g. Whiting and Dietrich, 1993, Burge, 2006, Harrison et al., 2011]. As a result, the topographic highs and lows or planform bifurcations that result in local differences in gradient and flow resistance are largely absent in the post-flood morphology. 2013 flows instead reflect the bar features and patterns created by a completely different scale of flow event than those that normally create hydraulic diversity in this system.

Although bed mobilization likely occurs somewhere between the 30 and 50 m^3/s discharges, patterns of elevated specific discharge at these discharges can hint at where geomorphic change will occur and explain observed changes. In 2012 at 50 m^3/s we see high specific discharges associated with outer bends and anabranch confluences (Figure 4.5). It is likely that these zones allow for compensating erosion and deposition while the channel's average dimensions remain generally constant and that this mode of adjustment was dominant during the previous years before the 2013 flood. In the 2013 50 m^3/s modeled discharge there is mainly one zone of elevated unit discharge in the upstream half of the reach; by 2014 this zone has shifted to the right outer bank as lateral migration progresses. This is associated with the reestablishment of shorter length-scale sediment transport processes and

the reorganization of coherent bar-pool-riffle units. However, the process is still on-going, as evidenced by the high shear stress in this configuration (Table 4.4) and the location of elevated forces at upstream end of outer bends. These more minor geomorphic adjustments between 2013 and 2014 result in slight changes in flow distributions and diversity. The 2014 10 m^3/s depth/velocity distribution has a slightly wider range of hydraulic conditions than 2013 (lower R^2, Figure 4.6). However, this effect is largely drowned out by 30 and 50 m^3/s, where the development of a cohesive deep, high velocity, thread is evident (Figure 4.7) and small scale elevation changes become less important.

Joint depth-velocity distributions provide a framework for interpreting the hydraulic conditions that control classified patch composition and distributions. In 2012, the diverse range of depth-velocity pairs (Figure 4.6a) at 10 m^3/s is reflected in the relatively even apportioning of flow points into the four clusters (Figure 4.11). The diverse class distribution remains relatively constant as discharge increases (Figure 4.13). 2012 flow conditions are therefore the most complex, as measured both on a continuous basis (low R^2, Figure 4.6) and when interpreted based on patterns of discrete classified units (high Shannon Diversity Index, Figure 4.13). This diversity can be explained by the geomorphic configuration in the pre-flood reach: alternating pool-riffle units in the main anabranch along with several substantial low gradient side channels create a wide range of flow conditions. In 2013, the lower hydraulic diversity and wide shallow flow conditions result in an unequal proportional assignment of cluster memberships; the reach is dominated by low energy and glide units at 10 m^3/s. By 2014 geomorphic adjustments result in a slight recovery of pool and riffle units relative to 2013, but diversity is still low. These differences in flow distributions and reachscape composition are most evident at 10 m^3/s; conditions tend to converge to more equal proportions of classes by 30 and 50 m^3/s as small-scale geomorphic forms become less important.

A benefit of classifying flow data is that it allows for explicit investigation of spatial flow patterns. With the fuzzy c-means approach used in this study and our analysis of the resulting clusters, we were able to address measures of patch shapes and sizes that may reflect underlying geomorphic features and have direct ecological relevance. We found some patterns that are relatively universal in our flow models; low energy and glide patches are generally smaller and more numerous,

with more complex shapes and higher edge densities than pool or riffle patches (Figure 4.13). This effect is likely a combination of the actual small scale of these hydromorphic units along with a classification artefact associated with fitting these slender, linear stream's edge features into 1 m^2 pixels [Wyrick and Pasternack, 2014]. Pool and riffle units, on the other hand, are generally more spatially contiguous and less fragmented due to the strong flow organization they are associated with, resulting in lower edge densities and fractal dimension index values. However, the geomorphic change throughout the study period appears to modify these patterns to some degree; pre-flood pool and riffle units are more elongate and linear at low flow than in 2013 or 2014. This is quantified by a decrease in edge density and mean patch area for these units as a result of the flood and reflects the disorganized nature of flow conditions in the post-flood morphologies.

Because each of the classified clusters has distinct hydraulic characteristics, the resulting hydromorphic unit maps can be linked with species' preferences for spatial investigation of habitat suitability. In the brown trout habitat context examined herein, applying preference curves to continuous depth and velocity data (Figure 4.14, Figure 4.15) gives a traditional appraisal of habitat suitability throughout the reach. By this metric, adult and juvenile habitat suitability declined as a result of the 2013 flood, especially at low flows. However, many fish species have been shown to have strong affinities for discrete habitat types [Schlosser, 1991, Nickelson et al., 1992, Rosenfeld and Boss, 2001] that may relate to more than just the hydraulic conditions in those habitat units. For example, availability of prey for drift-feeding salmonids is a primary driver of growth differences between slow and fast water habitat units [Nielsen, 1992, Reid and Thoms, 2008, Rosenfeld and Raeburn, 2009]. Spatial arrangements of habitats that generate benthic invertebrate drift that fish can feed on (riffles) versus energetically favorable feeding locations (pools), along with factors such as pool length that affect rates of depletion of prey through deposition or consumption by individual fish occupying that unit, are therefore important. Similarly, lateral velocity gradients such as fast currents close to velocity shelters are profitable in terms of energy gain [Fausch and White, 1981, Hughes and Dill, 1990], and the distribution of hydraulically sheltered sites and suitable sediment size patches can control spatial patterns of spawning suitability [Cienciala and Hassan, 2013]. For these reasons, predicting fish density

based on discrete habitat classes is often more accurate than based on continuous variables alone [Rosenfeld, 2003], especially when univariate habitat suitability criteria that ignore interactions between hydraulic variables are the basis for assessment of depth and velocity suitability [Ayllón et al., 2009]. In this context, the benefit of a bottom-up statistical classification approach is that the clustering based on depth, velocity, and Froude number integrates these factors and their interactions explicitly without a myopic focus on potentially species-specific suitability criteria [Poole et al., 1997, Schweizer et al., 2007]. This allows for an objective stratification of habitat units that relates to both underlying geomorphic processes and resulting habitat dynamics.

At the Elbow River study site, the overall picture of a decrease in habitat suitability as the result of the 2013 flood can be refined by accounting for the spatial characteristics of the classified habitat patches. For example, pool units declined in total areal proportion at 10 m^3/s between 2012 and 2013 (Figure 4.11), largely driving the observed decrease in WUA. However, riffle units also decreased in proportion. Although riffle units themselves are not highly suitable habitat when measured by hydraulic preference curves (Figure 4.16), their function as a zone of benthic invertebrate prey production makes them ecologically important to drift-feeding salmonids. The observed reductions in mean patch area and edge density for riffle units at 10 m^3/s could therefore be interpreted as further negative geomorphic consequences of the flood that result in less prey availability and fewer suitable riffle-adjacent holding and feeding zones for brown trout. However, territorial requirements and competition between individuals and different age classes are also mediated by spatial patterns of habitat zones; Ayllón et al. [2010] documented a positive scaling of territory size with brown trout body size, but salmonid territory area typically decreases as food abundance or habitat quality and complexity increase [Keeley, 2000, Imre et al., 2002, 2004, Venter et al., 2008]. The smaller, less numerous pool units and overall decrease in hydraulic diversity in the post-flood morphologies could therefore further stress salmonid populations due to increased competition for prime territories. Although unraveling these linkages and and the contrasting ecological requirements for different age classes and species requires more detailed direct information on spatiotemporal patterns of fish space use on Elbow River specifically, the classification procedure used in this study provides

a robust generic framework to address issues of the relationship between habitat dynamics for any lotic species and hydrogeomorphology.

The results of this study provide one way of quantifying the effects of a large flood disturbance event. Although the short time period (three years) covered in our UAV surveys makes prediction of future morphodynamic trajectories difficult, the primary immediate effect of the flood was a homogenization of sub-bankfull flow conditions and a decrease in hydraulic and habitat diversity. The readjustment during the one year following the flood event appears to be progressing towards a meandering laterally stable single thread channel, with the high elevation bar surfaces built during the 2013 flood acting as floodplain features largely disconnected from the low flow habitats. This reduction in geomorphic complexity is in contrast with many examples of ecological responses to large infrequent disturbance events in other systems, which are often cited as creating or maintaining heterogeneity [Romme and Knight, 1982, Foster et al., 1998]. In the case of Elbow River, the disturbance appears to be a clock-resetting event that returns the system to an initial state with complete geomorphic and habitat turnover [Phillips and Van Dyke, 2016]. This is different than examples of smaller magnitude flood disturbance dynamics, where shifting mosaic steady-state conditions are maintained [Arscott et al., 2002]. For Elbow River, smaller magnitude floods will be necessary to rework the geomorphic structure set by the 2013 flood, allowing for the recreation of heterogeneity through vertical and lateral erosion, meso-scale bedform construction, and avulsion mechanisms to create new secondary channels [Wheaton et al., 2013]. Judging by the rate of bank erosion and bar building observed between 2013 and 2014 and the historical record of large flows in the region, the time scale for such readjustment is likely on the scale of 50 years [Beechie et al., 2006]. However, potential changes in broader driving conditions such as shifts in flood frequency or rates of vegetation recolonization [Hervouet et al., 2011] with climate change may affect recovery trajectories. Continued careful monitoring of fluvial ecosystem conditions in an environmental change context will therefore be necessary to fully understand linked fluvial and ecological processes.

4.5 Conclusion

Stream morphodynamics, hydraulic organization, and aquatic habitat are intimately linked and sensitive to changes in governing conditions. In this contribution, we took advantage of detailed datasets characterizing river structural changes associated with a large flood event to examine these interrelationships in a disturbance context. By applying an objective stream habitat unit classification method to modeled distributions of hydraulic variables, we mapped patterns of hydgeomorphic features at a range of discharges for three unique geomorphic conditions bracketing the flood. We documented a general homogenization of flow conditions as a result of the flood associated with a loss of pool and riffle units. The effects of geomorphic change on flow patterns were most evident at low (10 m^3/s) discharges. These hydrogeomorphic changes resulted in a decline in habitat suitability for adult and juvenile brown trout when measured by conventional habitat suitability criteria; we also showed that a spatially explicit assessment of hydrogeomorphic conditions can complement and refine these traditional estimates of habitat impacts. Overall, this study provides an integrative assessment of the mechanisms driving fluvial ecosystem dynamics in an environmental change context.

Chapter 5

Conclusion

5.1 Overview

A thorough understanding of the complex interrelationships between geomorphology, hydrology, and aquatic ecology is necessary to support sustainable lotic ecosystem management in the face of natural and anthropogenic environmental change. Advancing this understanding requires short- and long-term investigation at a range of spatial scales and in different settings to develop and refine models of ecosystem evolution and predict potential responses to changes in driving conditions [Poff and Matthews, 2013]. To support this goal, focusing on pattern-process linkages, spatial structuring, scaling relationships and fluvial system dynamics is a priority to develop mechanistic understanding, as is the identification of proper model systems or species to use to answer research questions [Vaughan et al., 2009]. The development of new methodologies and conceptual frameworks for measuring and interpreting fluvial ecosystem complexities and dynamics will also facilitate research and development in this context [Fonstad and Marcus, 2010, Passalacqua et al., 2014, Tarolli, 2014].

The overall aim of the research in this dissertation was to use the case of an extreme flood event on a gravel bed river to study spatially explicit river morphodynamics and assess the impacts of geomorphic change on aquatic habitat structure and quality. This required the testing and application of new remote sensing methods using UAVs to efficiently and accurately measure ecosystem properties at tem-

poral and spatial scales appropriate to the research. Taken together, the three core research chapters present a novel approach to studying rivers: a comprehensive, multi-temporal, meter-scale-or-better model of submerged and subaerial topography and relevant ecological features produced efficiently through UAV-based photogrammetry and complemented by numerical hydrodynamic modeling to simulate hydraulic conditions and inform eco-hydrogeomorphic research questions.

5.2 Summary

In Chapter 2, the focus was on exploring UAV fluvial remote sensing applications and testing data quality. It was shown that UAV-based digital photogrammetry can produce high quality DEMs and orthomosaics that contain a wealth of information on previously hard to measure aspects of channel morphology and ecosystem structure. Vertical accuracy in the DEMs was high enough relative to the scale of most geomorphic features to allow for meaningful characterization of three dimensional morphology. Sediment sizes on exposed bars were also mapped empirically; however, the lack of information on submerged sediment sizes precludes detailed analysis of important factors such as sediment sorting in relation to flow patterns through different channel units or assessments of spatially variable hydraulic roughness. Similarly, neither the DEM nor empirical measures of grain size can resolve features such as stone cells or other stabilizing micro-scale bedforms that can have important hydrogeomorphic consequences [Church et al., 1998, Lawless and Robert, 2001, Hassan et al., 2008, Hardy et al., 2010]. Although methods aimed at estimating submerged grain sizes and characterizing their spatial variability exist [e.g., Carbonneau et al., 2005, Nelson et al., 2014], such applications are most suitable to shallow, optically clear parts of the stream and accurate submerged grain size determination remains a challenge.

Another focus of Chapter 2 was to test methods of bathymetric correction that are required to account for overpredictions of submerged elevations in the optical photogrammetry. Although both the tested methods improved vertical accuracy, they introduce further uncertainty into the process and submerged vertical errors remained about twice as large as those from exposed areas. Application and testing of other methods such as theoretical approaches or active remote sensing

techniques [e.g., Fonstad and Marcus, 2005, Feurer et al., 2008, Legleiter, 2015] could provide alternative ways to quantify bathymetry and correct underwater elevations, but this gap between submerged and exposed topographic accuracy needs to be addressed further [Flener, 2015]. Similarly, the reliance on estimation of a water surface elevation for the depth correction process necessitates accurate water's edge elevations along the entire stream. While this was not a problem in the wide, shallow, non-forested Elbow River active channel, it could prove difficult in other fluvial settings. Chapter 2 also showed that the high resolution orthomosaic can be used to map features that contribute to aquatic habitat for fish species such as LW distributions, cutbank locations, water surface roughness, and offstream or instream vegetation. While manually digitizing these features is simple and accurate, broader application and more efficient workflows could be developed through the application of automated image classification techniques [e.g., Fernandez-Diaz et al., 2014, Overstreet and Legleiter, 2014, James and Robson, 2014, Casado et al., 2015]. The final important aspect of Chapter 2 was the demonstration that the photogrammetry derived, corrected DEM was of sufficient accuracy and resolution to initialize and run a 2D numerical hydrodynamic model. This opens up the overall method to a much wider range of investigations that explicitly consider the importance of spatial flow properties; for the purposes of the chapter the model results were combined with mapped habitat features to produce refined estimates of habitat suitability and availability for brown trout.

Chapter 3 built on the methodological framework developed in Chapter 2 to focus on the purely geomorphic impacts of an extreme flood event in June 2013. Many studies of flood morphodynamics exist, and field-based examples are common in the geomorphic literature as a way of examining process-form relationships. However, the accuracy and resolution of the pre- and post-flood UAV-collected data used to characterize the geomorphic effects of the Elbow River flood are unprecedented. When combined with numerical flow modeling, such an approach allowed for detailed investigation of reach-scale spatial patterns of erosion and deposition and potential hydraulic controls on observed geomorphic change. It was shown that significant bank erosion and channel widening occurred, resulting in a net depositional event despite large local volumes of sediment being supplied to the channel bed. Reorganization of channel pattern to reflect the large flows resulted

in an increase in streamwise and across-stream variability measured through semi-variograms as tall, long bar feature were constructed and dissected. To test the predictability of geomorphic changes from pre-flood data, spatially continuous grain size maps were combined with flow model estimated shear stress to assess thresholds for sediment entrainment and mobility and see if these explained observed patterns of erosion and deposition. Although such an approach may provide valuable insight into controls on morphodynamics in near-threshold conditions, the geomorphic changes during the 2013 flood event were of such high magnitude that mechanisms of sediment flux become much more important than just entrainment. Prediction of potential flood effects in a management context is therefore best treated in a probabilistic manner to set bounds on potential vertical and lateral limits of geomorphic impacts [e.g., Krapesch et al., 2011, Clifford, 2012, Blanton and Marcus, 2013, Buffin-Bélanger et al., 2015]. To explain and predict more detailed geomorphic changes, better inclusion of the spatial distribution of bed load transport is needed. Progress is being made in this direction through physical modeling, coupled hydrodynamic/morphodyamic numerical models and field measures of sediment transport in relation to local hydraulic controls [e.g., Rennie and Church, 2010, Asahi et al., 2013, Nicholas et al., 2013, Wheaton et al., 2013, Church and Ferguson, 2015, Williams et al., 2015, Eaton and Mackenzie, in review], but this avenue of research remains largely unexplored.

Chapter 4 took the general geomorphic changes documented in Chapter 3 and extended them to include fluvial readjustment in the year following the flood event. These changes to the physical river structure were then combined with 2D hydrodynamic models to assess how changes to reach-scale morphology affect the organization of flow at the sub-bankfull discharges that define aquatic habitat throughout most of the year. Although the temporal resolution of the UAV surveys (1 survey/year) means smaller event-scale geomorphic changes may be subsumed into the overall yearly perspective, the relatively simple, nival flow regime on Elbow River means the majority of geomorphic work is confined to one large event each year. The three topographic configurations (2012, 2013, 2014) therefore provide a meaningful characterization of morphodynamics over the study period. Treating the three geomorphic configurations as static and then 'pouring' water through them with the 2D hydrodynamic model is then an efficient way to document hy-

drogeomorphic relationships. Although 2D flow modeling remains an uncertain process that is heavily influenced by data quality and model calibration and verification [e.g., Oreskes et al., 1994, Kondolf et al., 2000, Beven, 2001, Lane and Richards, 2001, Legleiter et al., 2011, Cienciala and Hassan, 2016], the errors in predicted hydraulic properties are generally within 20 to 30% and are comparable to those based on field data [Pasternack et al., 2006]. Given the enhanced spatial coverage and resolution of such methods, they provide a valuable means of assessing spatial and temporal hydraulic dynamism, particularly when combined with ecological perspectives [Bergen et al., 2001, Reynolds, 2002, Clifford et al., 2005, Pasternack et al., 2006].

The results of Chapter 4 indicated that flood-induced changes to the physical form of the reach had profound impacts on flow patterns. Interestingly, the overall increase in streamwise and across-stream variability within the entire active channel documented in Chapter 3 was not reflected directly in the sub-bankfull flow conditions; post-flood hydraulics were instead less diverse than pre-flood conditions. This was associated with a loss of the pool and riffle-like conditions that give rise to diverse depth-velocity pairs. In terms of aquatic habitat, these hydromorphic changes were shown to be deleterious for adult and juvenile brown trout, with a general loss of suitable hydraulic conditions and a reorganization of the spatial characteristics of high quality patches. The fuzzy c-means clustering method provided an objective fluvial landform classification procedure with which to assess spatiotemporal changes; a secondary benefit of this approach is that it forces an explicit heuristic examination of hydraulic properties and depth-velocity distributions. Although this requires some subjective decisions about the most appropriate number of classes and clustering parameters, the end result is a deeper understanding of the underlying data in relation to the study setting.

5.3 Conclusions

Overall, this dissertation provides a thorough, integrative analysis of fluvial hydrogeomorphology and aquatic habitat in the context of an extreme flood event on a gravel-bed river. The research contributes to the fields of fluvial remote sensing, hydrology, geomorphology, and aquatic ecology and embraces the multi-

directional linkages between them. Viewing rivers in a spatially continuous, high resolution manner such as that provided by UAV-based remote sensing facilitates the inclusion of all aspects of fluvial heterogeneity. This scale of analysis also meshes easily with reach-scale numerical and physical models, further allowing for the comparison of landscape patterns and ecological structure with experimental investigations and hypothesis testing of underlying mechanisms. These approaches are also relatively new in the fluvial sciences; as technologies and methodologies advance and mature, eco-hydrogeomorphic investigations will become more common and sophisticated. When combined with new frameworks for extracting and assimilating data and information at different scales, approaches similar to those used in this dissertation will provide a valuable contribution to the understanding and management of rivers as interconnected, human-influenced complex systems in an ever-changing environment.

Bibliography

T. B. Abbe and D. R. Montgomery. Large woody debris jams, channel hydraulics and habitat formation in large rivers. *Regulated Rivers Research & Management*, 12(23):201–221, 1996. → pages 6

J. D. Armstrong, P. S. Kemp, G. Kennedy, M. Ladle, and N. J. Milner. Habitat requirements of Atlantic salmon and brown trout in rivers and streams. *Fisheries Research*, 62(2):143–170, 2003. → pages 19, 64

D. B. Arscott, K. Tockner, D. van der Nat, and J. V. Ward. Aquatic habitat dynamics along a braided alpine river ecosystem (Tagliamento River, northeast Italy). *Ecosystems*, 5(8):0802–0814, 2002. → pages 101

K. Asahi, Y. Shimizu, J. Nelson, and G. Parker. Numerical simulation of river meandering with self-evolving banks. *Journal of Geophysical Research: Earth Surface*, 118(4):2208–2229, 2013. → pages 106

D. Ayllón, A. Almodóvar, G. G. Nicola, and B. Elvira. Interactive effects of cover and hydraulics on brown trout habitat selection patterns. *River Research and Applications*, 25(8):1051–1065, 2009. → pages 19, 100

D. Ayllón, A. Almodóvar, G. G. Nicola, and B. Elvira. Modelling brown trout spatial requirements through physical habitat simulations. *River Research and Applications*, 26(9):1090–1102, 2010. → pages 100

D. Ayllón, A. Almodóvar, G. G. Nicola, and B. Elvira. The influence of variable habitat suitability criteria on PHABSIM habitat index results. *River Research and Applications*, 28(8):1179–1188, 2012. → pages 13, 22

R. Bagnold. An approach to the sediment transport problem from general physics. *US Geological Survey Professional Paper*, pages 231–291, 1966. → pages 60

R. Bagnold. An empirical correlation of bedload transport rates in flumes and natural rivers. *Proceedings of the Royal Society of London. A. Mathematical and Physical Sciences*, 372(1751):453–473, 1980. → pages 60

J.-S. Bailly, Y. Le Coarer, P. Languille, C.-J. Stigermark, and T. Allouis. Geostatistical estimations of bathymetric lidar errors on rivers. *Earth Surface Processes and Landforms*, 35(10):1199–1210, 2010. → pages 28

V. Baker. Paleoflood hydrology and extraordinary flood events. *Journal of Hydrology*, 96(1):79–99, 1987. → pages 48

V. Baker. Geological fluvial geomorphology. *Bulletin of the Geological Society of America*, 100:1157–1167, 1988. → pages 3

T. J. Beechie, M. Liermann, M. M. Pollock, S. Baker, and J. Davies. Channel pattern and river-floodplain dynamics in forested mountain river systems. *Geomorphology*, 78(1-2):124–141, 2006. → pages 101

L. Benda. Effects of post-wildfire erosion on channel environments, Boise River, Idaho. *Forest Ecology and Management*, 178(1-2):105–119, 2003. → pages 6

R. Benjankar, D. Tonina, and J. McKean. One-dimensional and two-dimensional hydrodynamic modeling derived flow properties: impacts on aquatic habitat quality predictions. *Earth Surface Processes and Landforms*, 40(3):340–356, 2014. → pages 67

S. D. Bergen, S. M. Bolton, and J. L. Fridley. Design principles for ecological engineering. *Ecological Engineering*, 18(2):201–210, 2001. → pages 107

K. Beven. On modelling as collective intelligence. *Hydrological Processes*, 15 (11):2205–2207, 2001. → pages 107

J. C. Bezdek, R. Ehrlich, and W. Full. Fcm: The fuzzy c-means clustering algorithm. *Computers & Geosciences*, 10(2):191–203, 1984. → pages 73

S. Bird, D. Hogan, and J. Schwab. Photogrammetric monitoring of small streams under a riparian forest canopy. *Earth Surface Processes and Landforms*, 35(8): 952–970, 2010. → pages 12, 18, 41

P. M. Biron, G. Choné, T. Buffin-Bélanger, S. Demers, and T. Olsen. Improvement of streams hydro-geomorphological assessment using LiDAR DEMs. *Earth Surface Processes and Landforms*, 38(15):1808–1821, 2013. → pages 13

P. Blanton and W. A. Marcus. Transportation infrastructure, river confinement, and impacts on floodplain and channel habitat, Yakima and Chehalis rivers, Washington, U.S.A. *Geomorphology*, 189(C):55–65, May 2013. → pages 106

I. Boavida, J. M. Santos, C. Katopodis, M. T. Ferreira, and A. Pinheiro. Uncertainty in predicting the fish-response to two-dimensional habitat modeling using field data. *River Research and Applications*, 29:1164–1174, 2012. → pages 13, 31

D. T. Booth, S. E. Cox, and G. Simonds. Riparian monitoring using 2-cm GSD aerial photography. *Ecological Indicators*, 7(3):636–648, 2007. → pages 14

K. Bovee. Instream flow methodology. *US Fish and Wildlife Service. FWS/OBS*, 82:26, 1982. → pages 7

K. Bovee, B. L. Lamb, J. M. Bartholow, C. B. Stalnaker, and J. Taylor. Stream habitat analysis using the instream flow incremental methodology. Technical report, DTIC Document, 1998. → pages 7

Z. Bowen and R. Waltermire. Evaluation Of Light Detection And Ranging (LIDAR) For Measuring River Corridor Topography1. *JAWRA Journal of the American Water Resources Association*, 38(1):33–41, 2002. → pages 30

J. Brasington, B. Rumsby, and R. McVey. Monitoring and modelling morphological change in a braided gravel bed river using high resolution GPS based survey. *Earth Surface Processes and Landforms*, 25(9):973–990, 2000. → pages 36

J. Brasington, J. Langham, and B. Rumsby. Methodological sensitivity of morphometric estimates of coarse fluvial sediment transport. *Geomorphology*, 53(3):299–316, 2003. → pages 31, 70

G. Brierley, K. Fryirs, and V. Jain. Landscape connectivity: the geographic basis of geomorphic applications. *Area*, 38(2):165–174, 2006. → pages 65

T. Buffin-Bélanger, P. M. Biron, M. Larocque, S. Demers, T. Olsen, G. Choné, M.-A. Ouellet, C.-A. Cloutier, C. Desjarlais, and J. Eyquem. Freedom space for rivers: An economically viable river management concept in a changing climate. *Geomorphology*, pages 1–12, May 2015. → pages 106

J. Buffington and D. Montgomery. Geomorphic classification of rivers. In E. Wohl and J. Shroder, editors, *Treatise on Geomorphology; Fluvial Geomorphology*, volume 9, pages 730–767. Academic Press, 2013. → pages 66

C. M. Bunt, S. J. Cooke, C. Katopodis, and S. McKinley. Movement and summer habitat of brown trout (Salmo trutta) below a pulsed discharge hydroelectric generating station. *Regulated Rivers: Research & Management*, 15:395–403, 1999. → pages 22

L. M. Burge. Stability, morphology and surface grain size patterns of channel bifurcation in gravel–cobble bedded anabranching rivers. *Earth Surface Processes and Landforms*, 31(10):1211–1226, 2006. → pages 97

J. Butler, S. Lane, J. Chandler, and E. Porfiri. Through-water close range digital photogrammetry in flume and field environments. *The Photogrammetric Record*, 17(99):419–439, 2002. → pages 12

P. Carbonneau. Catchment-scale mapping of surface grain size in gravel bed rivers using airborne digital imagery. *Water Resources Research*, 40(7), 2004. → pages 19, 45

P. Carbonneau, M. A. Fonstad, W. A. Marcus, and S. J. Dugdale. Making riverscapes real. *Geomorphology*, 137(1):74–86, 2012. → pages 1, 12, 61, 65

P. E. Carbonneau, S. N. Lane, and N. E. Bergeron. Cost-effective non-metric close-range digital photogrammetry and its application to a study of coarse gravel river beds. *International Journal of Remote Sensing*, 24(14):2837–2854, 2003. → pages 13

P. E. Carbonneau, N. Bergeron, and S. N. Lane. Automated grain size measurements from airborne remote sensing for long profile measurements of fluvial grain sizes. *Water Resources Research*, 41(11), 2005. → pages 104

P. E. Carbonneau, S. N. Lane, and N. Bergeron. Feature based image processing methods applied to bathymetric measurements from airborne remote sensing in fluvial environments. *Earth Surface Processes and Landforms*, 31(11): 1413–1423, 2006. → pages 9

M. Casado, R. Gonzalez, T. Kriechbaumer, and A. Veal. Automated Identification of River Hydromorphological Features Using UAV High Resolution Aerial Imagery. *Sensors*, 15(11):27969–27989, Nov. 2015. → pages 105

J. Chandler, P. Ashmore, C. Paola, M. Gooch, and F. Varkaris. Monitoring river-channel change using terrestrial oblique digital imagery and automated digital photogrammetry. *Annals of the Association of American Geographers*, 92(4):631–644, 2002. → pages 30

D. Chapman. Food and space as regulators of salmonid populations in streams. *American Naturalist*, 100(913):345–357, 1966. → pages 64

A. Chappell, G. Heritage, I. Fuller, A. Large, and D. Milan. Geostatistical analysis of ground-survey elevation data to elucidate spatial and temporal river

channel change. *Earth Surface Processes and Landforms*, 28(4):349–370, 2003. → pages 44, 45

M. Charlton, A. Large, and I. Fuller. Application of airborne LiDAR in river environments: the River Coquet, Northumberland, UK. *Earth Surface Processes and Landforms*, 28(3):299–306, 2003. → pages 36

T. Cheng, M. Molenaar, and H. Lin. Formalizing fuzzy objects from uncertain classification results. *International Journal of Geographical Information Science*, 15(1):27–42, 2001. → pages 73

K. A. Cherkauer, S. J. Burges, R. N. Handcock, J. E. Kay, S. K. Kampf, and A. R. Gillespie. Assessing satellite-based and aircraft-based thermal infrared remote sensing for monitoring Pacific Northwest river temperature. *JAWRA Journal of the American Water Resources Association*, 41(5):1149–1159, 2005. → pages 12

M. Church. Records of recent geomorphological events. In R. Cullingford, D. Davidson, and J. Lewin, editors, *Timescales in Geomorphology*, pages 13–28. Wiley and Sons, 1980. → pages 66

M. Church. Bed material transport and the morphology of alluvial river channels. *Annu Rev Earth Planet Sci*, 34:325–354, 2006. → pages 5, 49

M. Church. Mountains and montane channels. In T. Burt and R. Allison, editors, *Sediment Cascades: An Integrated Approach*, pages 17–53. John Wiley and Sons, 2010. → pages 6

M. Church and R. I. Ferguson. Morphodynamics: Rivers beyond steady state. *Water Resources Research*, 51(4):1883–1897, Apr. 2015. → pages 106

M. Church and D. Jones. Channel bars in gravel bed rivers. In R. D. Hey, J. C. Bathurst, and C. Thorne, editors, *Gravel Bed Rivers*, pages 1–26. Wiley, Chichester, UK, 1982. → pages 96

M. Church, M. Hassan, and J. Wolcott. Stabilizing self-organized structures in gravel-bed stream channels: field and experimental observations. *Water Resources Research*, 34(11):3169–3179, 1998. → pages 14, 104

P. Cienciala and M. A. Hassan. Linking spatial patterns of bed surface texture, bed mobility, and channel hydraulics in a mountain stream to potential spawning substrate for small resident trout. *Geomorphology*, 197:96–107, 2013. → pages 99

P. Cienciala and M. A. Hassan. Sampling variability in estimates of flow characteristics in coarse-bed channels: Effects of sample size. *Water Resources Research*, 2016. → pages 107

S. J. Clarke, L. Bruce-Burgess, and G. Wharton. Linking form and function: towards an eco-hydromorphic approach to sustainable river restoration. *Aquatic Conservation: Marine and Freshwater Ecosystems*, 13(5):439–450, 2003. → pages 64

N. Clifford, M. Acreman, and D. Booker. Hydrological and hydraulic aspects of river restoration uncertainty for ecological purposes. *River restoration: managing the uncertainty in restoring physical habitat*, pages 105–138, 2008. → pages 64

N. Clifford, N. G. Wright, G. Harvey, A. M. Gurnell, O. P. Harmar, and P. J. Soar. Numerical modeling of river flow for ecohydraulic applications: Some experiences with velocity characterization in field and simulated data. *Journal of Hydraulic Engineering*, 136(12):1033–1041, 2009. → pages 67

N. J. Clifford. River restoration: Widening perspectives. *Gravel-Bed Rivers: Processes, Tools, Environments*, pages 150–159, 2012. → pages 106

N. J. Clifford, P. J. Soar, O. P. Harmar, A. M. Gurnell, G. E. Petts, and J. C. Emery. Assessment of hydrodynamic simulation results for eco-hydraulic and eco-hydrological applications: A spatial semivariance approach. *Hydrological processes*, 19(18):3631–3648, 2005. → pages 107

J. Costa. Response and recovery of a Piedmont watershed from tropical storm Agnes, June 1972. *Water Resources Research*, 10(1):106–112, 1974. → pages 36

R. F. Courtney, G. L. Walder, and R. L. Vadas. Instream flow requirements for fish in the Kananaskis River. Technical report, Calgary, AB, 1998. → pages 20, 22, 75

J. Croke, P. Todd, C. Thompson, F. Watson, R. Denham, and G. Khanal. The use of multi temporal LiDAR to assess basin-scale erosion and deposition following the catastrophic January 2011 Lockyer flood, SE Queensland, Australia. *Geomorphology*, 184:111–126, 2013. → pages 36

D. W. Crowder and P. Diplas. Assessing changes in watershed flow regimes with spatially explicit hydraulic models. *JAWRA Journal of the American Water Resources Association*, 38(2):397–408, 2002. → pages 66

W. Davis. Biological assessment and criteria: Building on the past ws davis tp simon biological assessment and criteria: Tools for water resource planning and decision making lewis publishers boca raton. *Florida*, 15:29, 1995. → pages 7

C. L. Dent, G. S. Cumming, and S. R. Carpenter. Multiple states in river and lake ecosystems. *Philosophical Transactions of the Royal Society B: Biological Sciences*, 357(1421):635–645, 2002. → pages 66

J. R. Desloges and M. Church. Geomorphic implications of glacier outburst flooding: Noeick River valley, British Columbia. *Canadian Journal of Earth Sciences*, 29(3):551–564, 1992. → pages 36, 59, 61, 66

W. Dietrich, J. Kirchner, H. Ikeda, and F. Iseya. Sediment supply and the development of the coarse surface layer in gravel-bedded rivers. *Nature*, 340 (6230):215–217, 1989. → pages 61

P. W. Downs and G. M. Kondolf. Post-project appraisals in adaptive management of river channel restoration. *Environmental Management*, 29(4):477–496, 2002. → pages 14

J. Duan. Simulation of streambank erosion processes with a two-dimensional numerical model. In R. Harmon and W. Doe, editors, *Landscape Erosion and Evolution Modeling*, pages 389–428. Springer US, 2001. → pages 37

S. Dugdale, P. Carbonneau, and D. Campbell. Aerial photosieving of exposed gravel bars for the rapid calibration of airborne grain size maps. *Earth Surface Processes and Landforms*, 35(6):627–639, 2010. → pages 65

M. J. Dunbar, K. Alfredsen, and A. Harby. Hydraulic-habitat modelling for setting environmental river flow needs for salmonids. *Fisheries Management and Ecology*, 19(6):500–517, 2011. → pages 66

B. Eaton and M. Church. A rational sediment transport scaling relation based on dimensionless stream power. *Earth Surface Processes and Landforms*, 36(7): 901–910, 2010. → pages 60

B. Eaton and M. Lapointe. Effects of large floods on sediment transport and reach morphology in the cobble-bed Sainte Marguerite River. *Geomorphology*, 40 (3):291–309, 2001. → pages 37

B. Eaton and L. Mackenzie. Morphodynamics of steep gravel-cobble streams: 2. effects of extreme floods on steady-state channels. *Journal of Geophysical Research: Earth Surface*, in review. → pages 96, 106

B. Eaton, M. Church, and R. Millar. Rational regime model of alluvial channel morphology and response. *Earth Surface Processes and Landforms*, 29(4): 511–529, 2004. → pages 5

B. Eaton, R. Millar, and S. Davidson. Channel patterns: Braided, anabranching, and single-thread. *Geomorphology*, 120(3-4):353–364, 2010. → pages 6

B. C. Eaton and M. Church. A graded stream response relation for bed load–dominated streams. *Journal of Geophysical Research: Earth Surface*, 109 (F3), 2004. → pages 95

H. A. Einstein. *The bed-load function for sediment transportation in open channel flows*. Number 1026. US Department of Agriculture, 1950. → pages 6

F. Engelund and J. Fredsøe. A sediment transport model for straight alluvial channels. *Hydrology Research*, 7(5):293–306, 1976. → pages 6

K. Fausch, C. Torgersen, C. Baxter, and H. Li. Landscapes to riverscapes: Bridging the gap between research and conservation of stream fishes. *BioScience*, 52(6):483, 2002. → pages 1, 7, 12, 13, 61, 65

K. D. Fausch and R. J. White. Competition between brook trout (salvelinus fontinalis) and brown trout (salmo trutta) for positions in a michigan stream. *Canadian Journal of Fisheries and Aquatic Sciences*, 38(10):1220–1227, 1981. → pages 99

R. Ferguson. Flow resistance equations for gravel- and boulder-bed streams. *Water Resources Research*, 43(5), 2007. → pages 4, 49

R. Ferguson. Time to abandon the manning equation? *Earth Surface Processes and Landforms*, 35(15):1873–1876, 2010. → pages 71

J. C. Fernandez-Diaz, C. L. Glennie, W. E. Carter, R. L. Shrestha, M. P. Sartori, A. Singhania, C. J. Legleiter, and B. T. Overstreet. Early results of simultaneous terrain and shallow water bathymetry mapping using a single-wavelength airborne lidar sensor. *Selected Topics in Applied Earth Observations and Remote Sensing, IEEE Journal of*, 7(2):623–635, 2014. → pages 105

D. Feurer, J. Bailly, C. Puech, Y. Le Coarer, and A. Viau. Very-high-resolution mapping of river-immersed topography by remote sensing. *Progress in Physical Geography*, 32(4):403–419, 2008. → pages 105

P. F. Fisher. Is gis hidebound by the legacy of cartography? *The Cartographic Journal*, 35(1):5–9, 1998. → pages 73

F. A. Fitzpatrick. A comparison of multi-disciplinary methods for measuring physical conditions of streams. In J. Dorava, D. R. Montgomery, B. Palcsak, and F. A. Fitzpatrick, editors, *Geomorphic Processes and Riverine Habitat*, pages 7–18. Wiley Online Library, 2001. → pages 8

C. Flener. *Remote sensing for three-dimensional modelling of hydromorphology*. PhD thesis, University of Turku, 2015. → pages 10, 105

C. Flener, M. Vaaja, A. Jaakkola, A. Krooks, H. Kaartinen, A. Kukko, E. Kasvi, H. Hyyppä, J. Hyyppä, and P. Alho. Seamless mapping of river channels at high resolution using mobile LiDAR and UAV-photography. *Remote Sensing*, 5 (12):6382–6407, 2013. → pages 18, 38

M. Fonstad and W. Marcus. High resolution, basin extent observations and implications for understanding river form and process. *Earth Surface Processes and Landforms*, 35(6):680–698, 2010. → pages 38, 103

M. Fonstad, J. Dietrich, B. Courville, J. Jensen, and P. Carbonneau. Topographic structure from motion: a new development in photogrammetric measurement. *Earth Surface Processes and Landforms*, 38(4):421–430, 2013. → pages 9, 13, 14, 36

M. A. Fonstad and W. A. Marcus. Remote sensing of stream depths with hydraulically assisted bathymetry (HAB) models. *Geomorphology*, 72(1-4): 320–339, 2005. → pages 105

D. R. Foster, D. H. Knight, and J. F. Franklin. Landscape patterns and legacies resulting from large, infrequent forest disturbances. *Ecosystems*, 1(6):497–510, 1998. → pages 101

P. Friend and R. Sinha. Braiding and meandering parameters. *Geological Society, London, Special Publications*, 75(1):105–111, 1993. → pages 76

C. A. Frissell, W. J. Liss, C. E. Warren, and M. D. Hurley. A hierarchical framework for stream habitat classification: viewing streams in a watershed context. *Environmental management*, 10(2):199–214, 1986. → pages 7

J. G. Fryer. A simple system for photogrammetric mapping in shallow water. *The Photogrammetric Record*, 11(62):203–208, 1983. → pages 8, 18

J. G. Fryer and H. T. Kniest. Errors in depth determination caused by waves in through-water photogrammetry. *The Photogrammetric Record*, 11(66): 745–753, 1985. → pages 18

I. C. Fuller. Geomorphic work during a "150-year" storm: contrasting behaviors of river channels in a New Zealand catchment. *Annals of the Association of American Geographers*, 97(4):665–676, 2007. → pages 96

J. Gardner. Some geomorphic effects of a catastrophic flood on the Grand River, Ontario. *Canadian Journal of Earth Sciences*, 14(10):2294–2300, 1977. → pages 36, 61

K. J. Gaston and T. M. Blackburn. A critique for macroecology. *Oikos*, pages 353–368, 1999. → pages 65

S. M. Gende, R. T. Edwards, M. F. Willson, and M. S. Wipfli. Pacific salmon in aquatic and terrestrial ecosystems: Pacific salmon subsidize freshwater and terrestrial ecosystems through several pathways, which generates unique management and conservation issues but also provides valuable research opportunities. *BioScience*, 52(10):917–928, 2002. → pages 64

S. V. Gregory, F. J. Swanson, W. A. McKee, and K. W. Cummins. An ecosystem perspective of riparian zones. *BioScience*, 41(8):540–551, 1991. → pages 6

J. Grove, J. Croke, and C. Thompson. Quantifying different riverbank erosion processes during an extreme flood event. *Earth Surface Processes and Landforms*, 38(12):1393–1406, 2013. → pages 36, 66

A. Gupta and H. Fox. Effects of high magnitude floods on channel form: A case study in Maryland Piedmont. *Water Resources Research*, 10(3):499–509, 1974. → pages 36, 66

A. Gurnell, W. Bertoldi, and D. Corenblit. Changing river channels: The roles of hydrological processes, plants and pioneer fluvial landforms in humid temperate, mixed load, gravel bed rivers. *Earth-Science Reviews*, 111(1-2): 129–141, 2012. → pages 36

K. L. Halwas and M. Church. Channel units in small, high gradient streams on Vancouver Island, British Columbia. *Geomorphology*, 43(3):243–256, 2002. → pages 65

R. J. Hardy, J. L. Best, S. N. Lane, and P. E. Carbonneau. Coherent flow structures in a depth-limited flow over a gravel surface: The influence of surface roughness. *J Geophys Res*, 115(F3), July 2010. → pages 104

T. B. Hardy and R. C. Addley. Vertical integration of spatial and hydraulic data for improved habitat modelling using geographic information systems. *IAHS publication*, (266):65–76, 2001. → pages 13

R. E. Hari, D. M. Livingstone, R. Siber, P. Burkholdt-Holm, and H. Guettinger. Consequences of climatic change for water temperature and brown trout populations in alpine rivers and streams. *Global Change Biology*, 12(1):10–26, 2006. → pages 6

L. Harrison, C. Legleiter, M. Wydzga, and T. Dunne. Channel dynamics and habitat development in a meandering, gravel bed river. *Water Resources Research*, 47(4), 2011. → pages 36, 97

M. Hassan, B. J. Smith, D. Hogan, D. S. Luzi, A. E. Zimmermann, and B. C. Eaton. Sediment storage and transport in coarse bed streams: scale considerations. In H. Habersack, H. Piegay, and M. Rinaldi, editors, *Gravel-Bed Rivers VI: From Process Understanding to River Restoration*, pages 473–496. Elsevier, 2008. → pages 65, 104

C. Hauer and H. Habersack. Morphodynamics of a 1000-year flood in the kamp river, austria, and impacts on floodplain morphology. *Earth Surface Processes and Landforms*, 34(5):654–682, 2009. → pages 72

C. Hauer, G. Mandlburger, and H. Habersack. Hydraulically related hydro-morphological units: description based on a new conceptual mesohabitat evaluation model (MEM) using LiDAR data as geometric input. *River Research and Applications*, 25(1):29–47, 2009. → pages 13

C. Hauer, G. Mandlburger, B. Schober, and H. Habersack. Morphologically related integrative management concept for reconnecting abandonded channels based on airborne LiDAR data and habitat modeling. *River Research and Applications*, 30(5):537–556, 2012. → pages 66

J. Heggenes and S. J. Saltveit. Seasonal and spatial microhabitat selection and segregation in young Atlantic Salmon, Salmo-Salar L, and Brown Trout, Salmo-Trutta L, in a Norwegian River. *Journal of Fish Biology*, 36(5): 707–720, 1990. → pages 64

A. Hervouet, R. Dunford, H. Piégay, B. Belletti, and M.-L. Trémélo. Analysis of Post-flood Recruitment Patterns in Braided-Channel Rivers at Multiple Scales Based on an Image Series Collected by Unmanned Aerial Vehicles, Ultra-light Aerial Vehicles, and Satellites. *GIScience & Remote Sensing*, 48(1):50–73, Mar. 2011. → pages 101

E. Hickin and H. Sichingabula. The geomorphic impact of the catastrophic October 1984 flood on the planform of Squamish River, southwestern British

Columbia. *Canadian Journal of Earth Sciences*, 25(7):1078–1087, 1988. → pages 61

D. L. Hogan and M. Church. Hydraulic geometry in small, coastal streams: progress toward quantification of salmonid habitat. *Canadian Journal of Fisheries and Aquatic Sciences*, 46(5):844–852, 1989. → pages 6

J. Hooke. Temporal variations in fluvial processes on an active meandering river over a 20-year period. *Geomorphology*, 100(1):3–13, 2008. → pages 95

M. Horritt and P. Bates. Evaluation of 1D and 2D numerical models for predicting river flood inundation. *Journal of Hydrology*, 268(1):87–99, 2002. → pages 37

C. Hugenholtz, B. Moorman, K. Riddell, and K. Whitehead. Small unmanned aircraft systems for remote sensing and earth science research. *Eos, Transactions American Geophysical Union*, 93(25):236–236, 2012. → pages 14, 33, 38

C. Hugenholtz, K. Whitehead, O. Brown, T. Barchyn, A. LeClair, K. Riddel, and H. T. Geomorphological mapping with a small unmanned aircraft system (sUAS): Feature detection and accuracy assessment of a photogrammetrically-derived digital terrain model. *Geomorphology*, 2013. → pages 14, 30, 38

N. F. Hughes and L. M. Dill. Position choice by drift-feeding salmonids - model and test for Arctic Grayling (Thymallus-Arcticus) in sub-arctic mountain streams, Interior Alaska. *Journal of the Fisheries Board of Canada*, 47(10): 2039–2048, 1990. → pages 64, 99

F. Hugue, M. Lapointe, B. Eaton, and A. Lepoutre. Satellite-based remote sensing of running water habitats at large riverscape scales: Tools to analyze habitat heterogeneity for river ecosystem management. *Geomorphology*, 253:353–369, 2016. → pages 8, 65

G. Hutchinson. Concluding remarks. In *Cold Spring Harbour Symposia on quantitative biology: population studies: animal ecology and demography. Cold Spring Harbor Laboratory, Cold Spring Harbor, New York, USA*, pages 415–427, 1957. → pages 64

I. Imre, J. W. Grant, and E. R. Keeley. The effect of visual isolation on territory size and population density of juvenile rainbow trout (oncorhynchus mykiss). *Canadian Journal of Fisheries and Aquatic Sciences*, 59(2):303–309, 2002. → pages 100

I. Imre, J. Grant, and E. Keeley. The effect of food abundance on territory size and population density of juvenile steelhead trout (oncorhynchus mykiss). *Oecologia*, 138(3):371–378, 2004. → pages 100

R. B. Jackson, S. R. Carpenter, C. N. Dahm, D. M. McKnight, R. J. Naiman, S. L. Postel, and S. W. Running. Water in a changing world. *Ecological applications*, 11(4):1027–1045, 2001. → pages 64

M. James and S. Robson. Mitigating systematic error in topographic models derived from UAV and ground-based image networks. *Earth Surface Processes and Landforms*, 39(10):1413–1420, 2014. → pages 38, 105

L. Javernick, J. Brasington, and B. Caruso. Modeling the topography of shallow braided rivers using Structure-from-Motion photogrammetry. *Geomorphology*, 213:166–182, 2014. → pages 9, 36

L. Javernick, D. Hicks, R. Measures, B. Caruso, and J. Brasington. Numerical modelling of braided rivers with Structure-from-Motion-derived terrain models. *River Research and Applications*, 2015. → pages 9, 65

A. J. Jensen and B. O. Johnsen. The functional relationship between peak spring floods and survival and growth of juvenile Atlantic salmon (Salmo salar) and brown trout (Salmo trutta). *Functional Ecology*, 13(6):778–785, 1999. → pages 63

V. S. Kale. Geomorphic effectiveness of extraordinary floods on three large rivers of the indian peninsula. *Geomorphology*, 85(3):306–316, 2007. → pages 95

C. r. Katopodis. Case studies of instream flow modelling for fish habitat in Canadian Prairie Rivers. *Canadian Water Resources Journal*, 28(2):199–216, 2003. → pages 20

E. R. Keeley. An experimental analysis of territory size in juvenile steelhead trout. *Animal Behaviour*, 59(3):477–490, 2000. → pages 100

E. A. Keller. Areal sorting of bed-load material: the hypothesis of velocity reversal. *Geological Society of America Bulletin*, 82(3):753–756, 1971. → pages 67

J. L. Kemp, D. M. Harper, and G. A. Crosa. Use of 'functional habitats' to link ecology with morphology and hydrology in river rehabilitation. *Aquatic conservation: marine and freshwater ecosystems*, 9(1):159–178, 1999. → pages 74

P. Komar. Selective gravel entrainment and the empirical evaluation of flow competence. *Sedimentology*, 34(6):1165–1176, 1987. → pages 49

G. M. Kondolf. Assessing salmonid spawning gravel quality. *Transactions of the American Fisheries Society*, 129(1):262–281, 2000. → pages 6

G. M. Kondolf, E. W. Larsen, and J. G. Williams. Measuring and modeling the hydraulic environment for assessing instream flows. *North American Journal of Fisheries Management*, 20(4):1016–1028, 2000. → pages 107

J. Korman, M. Kaplinski, and T. S. Melis. Effects of fluctuating flows and a controlled flood on incubation success and early survival rates and growth of age-0 rainbow trout in a large regulated river. *Transactions of the American fisheries Society*, 140(2):487–505, 2011. → pages 63

G. Krapesch, C. Hauer, and H. Habersack. Scale orientated analysis of river width changes due to extreme flood hazards. *Natural Hazards and Earth System Science*, 11(8):2137–2147, 2011. → pages 36, 37, 59, 72, 106

R. W. Lacey and R. G. Millar. Reach scale hydraulic assessment of instream salmonid habitat restoration. *JAWRA Journal of the American Water Resources Association*, 40(6):1631–1644, 2004. → pages 20

R. T. Lackey. Salmon policy: science, society, restoration, and reality. *Environmental Science & Policy*, 2(4):369–379, 1999. → pages 1

J. Lancaster and B. J. Downes. Linking the hydraulic world of individual organisms to ecological processes: putting ecology into ecohydraulics. *River Research and Applications*, 26(4):385–403, 2010. → pages 7

E. Lane. The importance of fluvial morphology in hydraulic engineering. *Proceedings of the American Society of Civil Engineers*, 81:1–17, 1955. → pages 3, 6

E. Lane. *A study of the shape of channels formed by natural streams flowing in erodible material*. US Army Engineer Division, Missouri River, 1957. → pages 35

S. Lane. The measurement of river channel morphology using digital photogrammetry. *The Photogrammetric Record*, 16(96):937–961, 2000. → pages 9, 13, 18, 23, 30, 36, 41

S. Lane and K. Richards. Linking river channel form and process: time, space and causality revisited. *Earth Surface Processes and . . .* , 22:249–260, 1997. → pages 66, 67

S. N. Lane and K. S. Richards. The 'validation'of hydrodynamic models: some critical perspectives. *Model validation: perspectives in hydrological science*, 413:439, 2001. → pages 107

S. N. Lane, R. M. Westaway, and D. Murray Hicks. Estimation of erosion and deposition volumes in a large, gravel-bed, braided river using synoptic remote sensing. *Earth Surface Processes and Landforms*, 28(3):249–271, 2003. → pages 36, 70

M. Lapointe, Y. Secretan, S. Driscoll, N. Bergeron, and M. Leclerc. Response of the Ha! Ha! River to the flood of July 1996 in the Saguenay region of Quebec: Large scale avulsion in a glaciated valley. *Water Resources Research*, 34(9): 2383–2392, 1998. → pages 12, 36

J. Laronne and M. Carson. Interrelationships between bed morphology and bed-material transport for a small, gravel-bed channel. *Sedimentology*, 23(1): 67–85, 1976. → pages 60

M. Lawless and A. Robert. Scales of boundary resistance in coarse-grained channels: turbulent velocity profiles and implications. *Geomorphology*, 39(3): 221–238, 2001. → pages 104

M. Leclerc. Ecohydraulics: a new interdisciplinary frontier for cfd. *Computational Fluid Dynamics: Applications in Environmental Hydraulics*, pages 429–460, 2005. → pages 64

M. Leclerc, A. Boudreault, T. A. Bechara, and G. Corfa. Two-dimensional hydrodynamic modeling: a neglected tool in the instream flow incremental methodology. *Transactions of the American Fisheries Society*, 124(5):645–662, 1995. → pages 75

R. F. Leclerc and E. J. Hickin. The internal structure of scrolled floodplain deposits based on ground-penetrating radar, north thompson river, british columbia. *Geomorphology*, 21(1):17–38, 1997. → pages 8

C. Legleiter. A geostatistical framework for quantifying the reach-scale spatial structure of river morphology: 1. Variogram models, related metrics, and relation to channel form. *Geomorphology*, 205:65–84, 2014a. → pages 44

C. Legleiter and P. Kyriakidis. Spatial prediction of river channel topography by kriging. *Earth Surface Processes and Landforms*, 33(6):841–867, 2008. → pages 44

C. Legleiter, W. Marcus, and R. Lawrence. Effects of sensor resolution on mapping instream habitats. *Photogrammetric Engineering and Remote Sensing*, 68(8):801–807, 2002. → pages 65

C. Legleiter, D. Roberts, and R. Lawrence. Spectrally based remote sensing of river bathymetry. *Earth Surface Processes and Landforms*, 34(8):1039–1059, 2009. → pages 18, 33, 42

C. J. Legleiter. Remote measurement of river morphology via fusion of LiDAR topography and spectrally based bathymetry. *Earth Surface Processes and Landforms*, 37(5):499–518, 2012. → pages 18, 30, 41

C. J. Legleiter. A geostatistical framework for quantifying the reach-scale spatial structure of river morphology: 2. Application to restored and natural channels. *Geomorphology*, 205:85–101, 2014b. → pages 37, 44, 45, 96

C. J. Legleiter. Calibrating remotely sensed river bathymetry in the absence of field measurements: Flow resistance equation-based imaging of river depths (freebird). *Water Resources Research*, 51(4):2865–2884, 2015. → pages 105

C. J. Legleiter and M. F. Goodchild. Alternative representations of in-stream habitat: classification using remote sensing, hydraulic modeling, and fuzzy logic. *International Journal of Geographical Information Science*, 19(1): 29–50, 2005. → pages 68, 73

C. J. Legleiter, D. A. Roberts, W. A. Marcus, and M. A. Fonstad. Passive optical remote sensing of river channel morphology and in-stream habitat: Physical basis and feasibility. *Remote Sensing of Environment*, 93(4):493–510, 2004. → pages 9, 18, 65

C. J. Legleiter, P. C. Kyriakidis, R. R. McDonald, and J. M. Nelson. Effects of uncertain topographic input data on two-dimensional flow modeling in a gravel-bed river. *Water Resources Research*, 47(3), 2011. → pages 27, 107

J. Lejot, C. Delacourt, H. Piegay, T. Fournier, M.-L. Trémélo, and P. Allemand. Very high spatial resolution imagery for channel bathymetry and topography from an unmanned mapping controlled platform. *Earth Surface Processes and Landforms*, 32(11):1705–1725, 2007. → pages 14, 30, 38

L. Leopold and T. Maddock. The hydraulic geometry of stream channels and some physiographic implications. *US Geological Survey Professional Paper*, 252, 1953. → pages 3

L. Leopold and M. Wolman. River channel patterns: braided, meandering, and straight. *US Geological Survey Professional Paper*, 282-B, 1957. → pages 3, 6, 35

Z. Li. Variation of the accuracy of digital terrain models with sampling interval. *The Photogrammetric Record*, 14(79):113–128, 1992. → pages 23

E. Lindley. Regime channels. *Punjab Engineering Conference, Institute of British Geography*, 1919. → pages 3

T. Lisle, J. Nelson, J. Pitlick, M. Madej, and B. Barkett. Variability of bed mobility in natural, gravel-bed channels and adjustments to sediment load at local and reach scales. *Water Resources Research*, 36(12):3743–3755, 2000. → pages 38, 60, 65

T. E. Lisle. Effects of aggradation and degradation on riffle-pool morphology in natural gravel channels, northwestern California. *Water Resources Research*, 18(6):1643–1651, 1982. → pages 65

M. E. Litvan, T. W. Stewart, C. L. Pierce, and C. J. Larson. Effects of grade control structures on the macroinvertebrate assemblage of an agriculturally impacted stream. *River research and applications*, 24(2):218–233, 2008. → pages 7

M. Lorang, D. Whited, F. Hauer, J. Kimball, and J. Stanford. Using airborne multispectral imagery to evaluate geomorphic work across floodplains of gravel-bed rivers. *Ecological Applications*, 15(4):1209–1222, 2005. → pages 8

D. Lowe. Distinctive image features from scale-invariant keypoints. *International Journal of Computer Vision*, 60(2):91–110, 2004. → pages 41

D. Lyzenga. Remote sensing of bottom reflectance and water attenuation parameters in shallow water using aircraft and landsat data. *International Journal of Remote Sensing*, 2(1):71–82, 1981. → pages 9, 42

M. L. MacWilliams, J. M. Wheaton, G. B. Pasternack, R. L. Street, and P. K. Kitanidis. Flow convergence routing hypothesis for pool-riffle maintenance in alluvial rivers. *Water Resources Research*, 42(10), 2006. → pages 65

I. Maddock. The importance of physical habitat assessment for evaluating river health. *Freshwater biology*, 41(2):373–391, 1999. → pages 66

M. A. Madej. Temporal and spatial variability in thalweg profiles of a gravel-bed river. *Earth Surface Processes and Landforms*, 24(12):1153–1169, 1999. → pages 96

T. Madsen, H. Enevoldsen, and T. Jørgensen. Effects of water velocity on photosynthesis and dark respiration in submerged stream macrophytes. *Plant, Cell & Environment*, 16(3):317–322, 1993. → pages 64

F. Magilligan. Thresholds and the spatial variability of flood power during extreme floods. *Geomorphology*, 5(3):373–390, 1992. → pages 36, 59, 66, 95

W. A. Marcus, C. J. Legleiter, R. J. Aspinall, J. W. Boardman, and R. L. Crabtree. High spatial resolution hyperspectral mapping of in-stream habitats, depths, and woody debris in mountain streams. *Geomorphology*, 55(1-4):363–380, 2003. → pages 65

C. May, B. Pryor, T. Lisle, and M. Lang. Coupling hydrodynamic modeling and empirical measures of bed mobility to predict the risk of scour and fill of salmon redds in a large regulated river. *Water Resources Research*, 45(5), 2009. → pages 38, 60

L. A. Mertes. Remote sensing of riverine landscapes. *Freshwater biology*, 47(4): 799–816, 2002. → pages 65

N. Micheletti, J. H. Chandler, and S. N. Lane. Investigating the geomorphological potential of freely available and accessible structure-from-motion photogrammetry using a smartphone. *Earth Surface Processes and Landforms*, 40(4):473–486, 2015. → pages 9, 36

R. Millar. Theoretical regime equations for mobile gravel-bed rivers with stable banks. *Geomorphology*, 64(3-4):207–220, 2005. → pages 6, 36

R. Millar and M. Quick. Effect of bank stability on geometry of gravel rivers. *Journal of Hydraulic Engineering*, 119(2):1343–1363, 1993. → pages 5

R. G. Millar. Grain and form resistance in gravel-bed rivers. *Journal of Hydraulic Research*, 37(3):303–312, 1999. → pages 21

A. Miller. Flood hydrology and geomorphic effectiveness in the central Appalachians. *Earth Surface Processes and Landforms*, 15(2):119–134, 1990. → pages 36

N. Milner, J. Elliott, J. Armstrong, R. Gardiner, J. Welton, and M. Ladle. The natural control of salmon and trout populations in streams. *Fisheries Research*, 62(2):111–125, 2003. → pages 64

D. Montgomery and J. Buffington. Channel Processes, Classification, and Response. In R. Naiman and R. Bilby, editors, *River Ecology and Management*, pages 13–42. Springer-Verlag New York, Inc., New York, 2004. → pages 5

D. L. Morantz, R. K. Sweeny, C. S. Shirvell, and D. A. Longard. Selection of microhabitat in summer by juvenile Atlantic salmon (Salmo-Salar). *Journal of the Fisheries Board of Canada*, 44(1):120–129, 1987. → pages 64

S. Nakano and M. Murakami. Reciprocal subsidies: dynamic interdependence between terrestrial and aquatic food webs. *Proceedings of the National Academy of Sciences of the United States of America*, 98(1):166–170, 2001. → pages 64

L. Nardi and M. Rinaldi. Spatio-temporal patterns of channel changes in response to a major flood event: the case of the Magra River (central- northern Italy). *Earth Surface Processes and Landforms*, 2014. → pages 37

J. Nelson and R. McDonald. Mechanics and modeling of flow and bed evolution in lateral separation eddies, report, grand canyon environmental studies. *Stud., Flagstaff, Ariz*, 1996. → pages 71

J. S. Nelson and M. J. Paetz. *The fishes of Alberta*. University of Alberta, 1992. → pages 68

P. A. Nelson, D. Bellugi, and W. E. Dietrich. Delineation of river bed-surface patches by clustering high-resolution spatial grain size data. *Geomorphology*, 205(C):102–119, Jan. 2014. → pages 104

M. Newson. The geomorphological effectiveness of floods – a contribution stimulated by two recent events in mid Wales. *Earth Surface Processes*, 5(1): 1–16, 1980. → pages 36

M. Newson and C. Newson. Geomorphology, ecology and river channel habitat: mesoscale approaches to basin-scale challenges. *Progress in Physical Geography*, 24(2):195–217, 2000. → pages 66

A. Nicholas, P. Ashworth, G. Sambrook Smith, and S. Sandbach. Numerical simulation of bar and island morphodynamics in anabranching megarivers. *Journal of Geophysical Research: Earth Surface*, 118(4):2019–2044, 2013. → pages 106

A. P. Nicholas, G. H. S. Smith, M. L. Amsler, P. J. Ashworth, J. L. Best, R. J. Hardy, S. N. Lane, O. Orfeo, D. R. Parsons, A. J. Reesink, et al. The role of discharge variability in determining alluvial stratigraphy. *Geology*, 44(1):3–6, 2016. → pages 96

T. E. Nickelson, J. D. Rodgers, S. L. Johnson, and M. F. Solazzi. Seasonal changes in habitat use by juvenile coho salmon (oncorhynchus kisutch) in oregon coastal streams. *Canadian Journal of Fisheries and Aquatic Sciences*, 49(4):783–789, 1992. → pages 99

J. L. Nielsen. Microhabitat-specific foraging behavior, diet, and growth of juvenile coho salmon. *Transactions of the American Fisheries Society*, 121(5): 617–634, 1992. → pages 99

N. Noffke. Geobiology–a holistic scientific discipline. *Palaeogeography, Palaeoclimatology, Palaeoecology*, 219(1):1–3, 2005. → pages 64

B. Notebaert, G. Verstraeten, G. Govers, and J. Poesen. Qualitative and quantitative applications of LiDAR imagery in fluvial geomorphology. *Earth Surface Processes and Landforms*, 34(2):217–231, 2009. → pages 30

D. Olsen, A. Whitaker, and D. F. Potts. Assessing stream channel stability thresholds using flow competence estimates at bankful stage. *JAWRA Journal of the American Water Resources Association*, 33(6):1197–1207, 1997. → pages 95

N. Oreskes, K. Shrader-Frechette, K. Belitz, et al. Verification, validation, and confirmation of numerical models in the earth sciences. *Science*, 263(5147): 641–646, 1994. → pages 107

B. Overstreet and C. Legleiter. Mapping water surface roughness in a shallow, gravel-bed river using hyperspectral imagery. In *AGU Fall Meeting Abstracts*, volume 1, page 1057, 2014. → pages 105

A. Papanicolaou, M. Elhakeem, and B. Wardman. Calibration and verification of a 2d hydrodynamic model for simulating flow around emergent bendway weir structures. *Journal of Hydraulic Engineering*, 137(1):75–89, 2010. → pages 71

P. Parasiewicz. MesoHABSIM: A concept for application of instream flow models in river restoration planning. *Fisheries*, 26(9):6–13, 2001. → pages 66

G. Parker. Selective sorting and abrasion of river gravel. ii: Applications. *Journal of Hydraulic Engineering*, 117(2):150–171, 1991. → pages 49

H. Parker and P. Klingeman. On why gravel bed streams are paved. *Water Resources Research*, 18(5):1409–1423, 1982. → pages 61

M. Parsons, M. C. Thoms, and R. H. Norris. Scales of macroinvertebrate distribution in relation to the hierarchical organization of river systems. *Journal*

of the North American Benthological Society, 22(1):105–122, 2003. → pages 64

M. Parsons, C. A. McLoughlin, M. W. Rountree, and K. H. Rogers. The biotic and abiotic legacy of a large infrequent flood disturbance in the Sabie River, South Africa. *River Research and Applications*, 22(2):187–201, 2006. → pages 66

P. Passalacqua, J. Hillier, and P. Tarolli. Innovative analysis and use of high-resolution DTMs for quantitative interrogation of Earth-surface processes. *Earth Surface Processes and Landforms*, 39(10):1400–1403, 2014. → pages 38, 62, 103

G. B. Pasternack, C. L. Wang, and J. E. Merz. Application of a 2d hydrodynamic model to design of reach-scale spawning gravel replenishment on the mokelumne river, california. *River Research and Applications*, 20(2):205–225, 2004. → pages 75

G. B. Pasternack, A. T. Gilbert, J. M. Wheaton, and E. M. Buckland. Error propagation for velocity and shear stress prediction using 2D models for environmental management. *Journal of Hydrology*, 328(1-2):227–241, 2006. → pages 67, 107

M. Perignon, G. Tucker, E. Griffin, and J. Friedman. Effects of riparian vegetation on topographic change during a large flood event, Rio Puerco, New Mexico, USA. *Journal of Geophysical Research: Earth Surface*, 118(3):1193–1209, 2013. → pages 31, 37

J. D. Phillips and C. Van Dyke. Principles of geomorphic disturbance and recovery in response to storms. *Earth Surface Processes and Landforms*, 2016. → pages 101

H. Piegay, S. Darby, E. Mosselman, and N. Surian. A review of techniques available for delimiting the erodible river corridor: a sustainable approach to managing bank erosion. *River Research and Applications*, 21(7):773–789, 2005. → pages 37

J. Pitlick. Response and recovery of a subalpine stream following a catastrophic flood. *Geological Society of America Bulletin*, 105(5):657–670, 1993. → pages 36

N. L. Poff and J. H. Matthews. Environmental flows in the anthropocence: past progress and future prospects. *Current Opinion in Environmental Sustainability*, 5(6):667–675, 2013. → pages 103

J. W. Pomeroy. The 2013 flood event in the South Saskatchewan and Elk River basins: Causes, assessment and damages. *Canadian Water Resources Journal*, pages 1–13, 2015. → pages 69

G. C. Poole, C. A. Frissell, and S. C. Ralph. In-stream habitat unit classification: Inadequacies for monitoring and some consequences for management. *JAWRA Journal of the American Water Resources Association*, 33(4):879–896, 1997. → pages 8, 73, 100

J. R. Post and F. D. Johnston. *Status of the bull trout (Salvelinus confluentus) in Alberta*. Alberta Sustainable Resource Development Edmonton, 2002. → pages 68

C. J. Pyle, K. S. Richards, and J. H. Chandler. Digital photogrammetric monitoring of river bank erosion. *The Photogrammetric Record*, 15(89): 753–764, 1997. → pages 13

R. Pyrce and P. Ashmore. The relation between particle path length distributions and channel morphology in gravel-bed streams: A synthesis. *Geomorphology*, 56(1-2):167–187, 2003. → pages 96

A. Rango and A. S. Laliberte. Impact of flight regulations on effective use of unmanned aircraft systems for natural resources applications. *Journal of Applied Remote Sensing*, 4(1):043539–043539–12, 2010. → pages 33

M. Reid and M. Thoms. Surface flow types, near-bed hydraulics and the distribution of stream macroinvertebrates. *Biogeosciences Discussions*, 5(2): 1175–1204, 2008. → pages 99

C. D. Rennie and M. Church. Mapping spatial distributions and uncertainty of water and sediment flux in a large gravel bed river reach using an acoustic doppler current profiler. *Journal of Geophysical Research: Earth Surface*, 115 (F3), 2010. → pages 106

C. Reynolds. Ecological pattern and ecosystem theory. *Ecological modelling*, 158 (3):181–200, 2002. → pages 107

K. S. Richards. The morphology of riffle-pool sequences. *Earth Surface Processes*, 1(1):71–88, 1976. → pages 65

K. S. Richards. Channel geometry in the riffle-pool sequence. *Geografiska Annaler: Series A, Physical Geography*, pages 23–27, 1978. → pages 65

W. H. Romme and D. H. Knight. Landscape diversity: the concept applied to yellowstone park. *BioScience*, 32(8):664–670, 1982. → pages 101

J. Rosenfeld. Assessing the habitat requirements of stream fishes: an overview and evaluation of different approaches. *Transactions of the American fisheries Society*, 132(5):953–968, 2003. → pages 64, 100

J. S. Rosenfeld and S. Boss. Fitness consequences of habitat use for juvenile cutthroat trout: energetic costs and benefits in pools and riffles. *Canadian Journal of Fisheries and Aquatic Sciences*, 58(3):585–593, 2001. → pages 99

J. S. Rosenfeld and E. Raeburn. Effects of habitat and internal prey subsidies on juvenile coho salmon growth: implications for stream productive capacity. *Ecology of Freshwater Fish*, 18(4):572–584, 2009. → pages 99

J. S. Rosenfeld, K. Campbell, E. S. Leung, J. Bernhardt, and J. Post. Habitat effects on depth and velocity frequency distributions: Implications for modeling hydraulic variation and fish habitat suitability in streams. *Geomorphology*, 130(3-4):127–135, 2011. → pages 7, 13, 67

D. C. Rowe, C. L. Pierce, and T. F. Wilton. Fish assemblage relationships with physical habitat in wadeable iowa streams. *North American Journal of Fisheries Management*, 29(5):1314–1332, 2009. → pages 7

A. H. Roy, C. L. Faust, M. C. Freeman, and J. L. Meyer. Reach-scale effects of riparian forest cover on urban stream ecosystems. *Canadian Journal of Fisheries and Aquatic Sciences*, 62(10):2312–2329, 2005. → pages 6

I. J. Schlosser. Stream fish ecology: a landscape perspective. *BioScience*, 41(10): 704–712, 1991. → pages 1, 99

S. Schumm and H. Khan. Experimental study of channel patterns. *Geological Society of America Bulletin*, 83:1755–1770, 1972. → pages 4

P. Schürch, A. L. Densmore, N. J. Rosser, M. Lim, and B. W. McArdell. Detection of surface change in complex topography using terrestrial laser scanning: application to the Illgraben debris-flow channel. *Earth Surface Processes and Landforms*, 36(14):1847–1859, 2011. → pages 30

S. Schweizer, M. E. Borsuk, I. Jowett, and P. Reichert. Predicting joint frequency distributions of depth and velocity for instream habitat assessment. *River Research and Applications*, 23(3):287–302, 2007. → pages 67, 72, 100

D. R. O. Silva, R. Ligeiro, R. M. Hughes, and M. Callisto. Visually determined stream mesohabitats influence benthic macroinvertebrate assessments in headwater streams. *Environmental monitoring and assessment*, 186(9): 5479–5488, 2014. → pages 64, 66

M. J. Smith, J. Chandler, and J. Rose. High spatial resolution data acquisition for the geosciences: kite aerial photography. *Earth Surface Processes and Landforms*, 34(1):155–161, 2009. → pages 14

K. Smokorowski and T. Pratt. Effect of a change in physical structure and cover on fish and fish habitat in freshwater ecosystems-a review and meta-analysis. *Environmental Reviews*, 15(NA):15–41, 2007. → pages 7

J. A. Stallins. Geomorphology and ecology: unifying themes for complex systems in biogeomorphology. *Geomorphology*, 77(3):207–216, 2006. → pages 6, 66

B. Statzner, J. A. Gore, and V. H. Resh. Hydraulic stream ecology - Observed patterns and potential applications. *Journal of the North American Benthological Society*, 7(4):307–360, 1988. → pages 64, 74

M. Stevens and C. Nordin. Critique of the regime theory for alluvial channels. *Journal of Hydraulic Engineering*, 113(11):1359–1380, 1987. → pages 4

M. J. Stewardson and T. A. McMahon. A stochastic model of hydraulic variations within stream channels. *Water Resources Research*, 38(1):8–1–8–, Jan. 2002. → pages 67, 72

A. D. Tamminga, B. C. Eaton, and C. H. Hugenholtz. Uas-based remote sensing of fluvial change following an extreme flood event. *Earth Surface Processes and Landforms*, 40(11):1464–1476, 2015. → pages 95

P. Tarolli. High-resolution topography for understanding Earth surface processes: Opportunities and challenges. *Geomorphology*, 216:295–312, 2014. → pages 62, 103

C. A. Taylor, M. L. Warren Jr, J. Fitzpatrick Jr, H. H. Hobbs III, R. F. Jezerinac, W. L. Pflieger, and H. W. Robison. Conservation status of crayfishes of the united states and canada. *Fisheries*, 21(4):25–38, 1996. → pages 1

C. Thompson and J. Croke. Geomorphic effects, flood power, and channel competence of a catastrophic flood in confined and unconfined reaches of the upper lockyer valley, southeast queensland, australia. *Geomorphology*, 197: 156–169, 2013. → pages 66

C. Thompson, J. Croke, J. Grove, and G. Khanal. Spatio-temporal changes in river bank mass failures in the Lockyer Valley, Queensland, Australia. *Geomorphology*, 191(C):129–141, 2013. → pages 36

M. C. Thoms. Variability in riverine ecosystems. *River Research and Applications*, 22(2):115–121, 2006. → pages 66

M. C. Thoms and M. Parsons. Eco-geomorphology: an interdisciplinary approach to river science. *International Association of Hydrological Sciences, Publication*, (276):113–119, 2002. → pages 8

T. Toutin. Comparison of stereo-extracted DTM from different high-resolution sensors: SPOT-5, EROS-a, IKONOS-II, and QuickBird. *IEEE Transactions on Geoscience and Remote Sensing*, 42(10):2121–2129, 2004. → pages 32

M. Turner and V. H. Dale. Comparing large, infrequent disturbances: What have we learned? *Ecosystems*, 1(6):493–496, 1998. → pages 66

M. G. Turner, W. L. Baker, C. J. Peterson, and R. K. Peet. Factors influencing succession: lessons from large, infrequent natural disturbances. *Ecosystems*, 1 (6):511–523, 1998. → pages 66

B. Van Horne. Density as a misleading indicator of habitat quality. *The Journal of Wildlife Management*, pages 893–901, 1983. → pages 7, 64

I. P. Vaughan, M. Diamond, A. M. Gurnell, K. A. Hall, A. Jenkins, N. J. Milner, L. A. Naylor, D. A. Sear, G. Woodward, and S. J. Ormerod. Integrating ecology with hydromorphology: a priority for river science and management. *Aquatic Conservation: Marine and Freshwater Ecosystems*, 19(1):113–125, 2009. → pages 2, 64, 65, 103

O. Venter, J. W. Grant, M. V. Noel, and J.-w. Kim. Mechanisms underlying the increase in young-of-the-year Atlantic salmon (Salmo salar) density with habitat complexity. *Canadian Journal of Fisheries and Aquatic Sciences*, 65 (9):1956–1964, 2008. → pages 100

D. Vericat, J. Brasington, J. Wheaton, and M. Cowie. Accuracy assessment of aerial photographs acquired using lighter-than-air blimps: low-cost tools for mapping river corridors. *River Research and Applications*, 25(8):985–1000, 2008. → pages 14

T. Waddle. Field evaluation of a two-dimensional hydrodynamic model near boulders for habitat calculation. *River Research and Applications*, 26(6): 730–741, 2009. → pages 20

C. Wallis, I. Maddock, F. Visser, and M. Acreman. A framework for evaluating the spatial configuration and temporal dynamics of hydraulic patches. *River Research and Applications*, 28(5):585–593, 2010. → pages 67

J. Warburton. Channel change in relation to meltwater flooding, Bas Glacier d'Arolla, Switzerland. *Geomorphology*, 11(2):141–149, 1994. → pages 36

J. Ward. Riverine landscapes: biodiversity patterns, disturbance regimes, and aquatic conservation. *Biological conservation*, 83(3):269–278, 1998. → pages 1, 8

M. L. Warren Jr and B. M. Burr. Status of freshwater fishes of the united states: overview of an imperiled fauna. *Fisheries*, 19(1):6–18, 1994. → pages 1

M. J. Wassen and A. P. Grootjans. Ecohydrology: an interdisciplinary approach for wetland management and restoration. *Plant Ecology*, 126(1):1–4, 1996. → pages 64

A. Watts, V. Ambrosia, and E. Hinkley. Unmanned aircraft systems in remote sensing and scientific research: Classification and considerations of use. *Remote Sensing*, 4(12):1671–1692, 2012. → pages 14, 38

R. Westaway, S. Lane, and D. Hicks. The development of an automated correction procedure for digital photogrammetry for the study of wide, shallow, gravel bed rivers. *Earth Surface Processes and Landforms*, 25(2):209–226, 2000. → pages 18, 23, 41

R. Westaway, S. Lane, and D. Hicks. Remote sensing of clear-water, shallow, gravel-bed rivers using digital photogrammetry. *Photogrammetric Engineering and Remote Sensing*, 67(11):1271–1282, 2001. → pages 13, 18, 41

R. Westaway, S. Lane, and D. Hicks. Remote survey of large-scale braided, gravel-bed rivers using digital photogrammetry and image analysis. *International Journal of Remote Sensing*, 24(4):795–815, 2003. → pages 41, 65

J. Wheaton, J. Brasington, S. Darby, J. Merz, G. Pasternack, D. Sear, and D. Vericat. Linking geomorphic changes to salmonid habitat at a scale relevant to fish. *River Research and Applications*, 26(4):469–486, 2010a. → pages 13, 31, 36

J. Wheaton, J. Brasington, S. Darby, and D. Sear. Accounting for uncertainty in DEMs from repeat topographic surveys: improved sediment budgets. *Earth Surface Processes and Landforms*, 35(2):136–156, 2010b. → pages 43, 70

J. Wheaton, J. Brasington, S. Darby, A. Kasprak, D. Sear, and D. Vericat. Morphodynamic signatures of braiding mechanisms as expressed through change in sediment storage in a gravel-bed river. *Journal of Geophysical Research: Earth Surface*, 118(2):759–779, 2013. → pages 36, 96, 101, 106

J. M. Wheaton, K. A. Fryirs, G. Brierley, S. G. Bangen, N. Bouwes, and G. O'Brien. Geomorphic mapping and taxonomy of fluvial landforms. *Geomorphology*, 248(C):273–295, 2015. → pages 66

K. Whitehead and C. Hugenholtz. Remote sensing of the environment with small unmanned aircraft systems (UASs), part 1: A review of progress and challenges. *Journal of Unmanned Vehicle Systems*, 2(3):69–85, 2014. → pages 38

K. Whitehead, C. Hugenholtz, S. Myshak, O. Brown, A. LeClair, A. Tamminga, T. Barchyn, B. Moorman, and B. Eaton. Remote sensing of the environment with small unmanned aircraft systems (UASs), part 2: Scientific and commercial applications. *Journal of Unmanned Vehicle Systems*, 2(3):86–102, 2014. → pages 38

P. J. Whiting and W. E. Dietrich. Experimental constraints on bar migration through bends: Implications for meander wavelength selection. *Water Resources Research*, 29(4):1091–1102, 1993. → pages 97

J. A. Wiens. Riverine landscapes: taking landscape ecology into the water. *Freshwater Biology*, 47(4):501–515, 2002. → pages 1, 65

R. L. Wilby, H. Orr, G. Watts, R. W. Battarbee, P. M. Berry, R. Chadd, S. J. Dugdale, M. J. Dunbar, J. A. Elliott, C. Extence, D. M. Hannah, N. Holmes, A. C. Johnson, B. Knights, N. J. Milner, S. J. Ormerod, D. Solomon, R. Timlett, P. J. Whitehead, and P. J. Wood. Evidence needed to manage freshwater ecosystems in a changing climate: Turning adaptation principles into practice. *Science of the Total Environment, The*, 408(19):4150–4164, 2010. → pages 65

P. Wilcock and J. Crowe. Surface-based transport model for mixed-size sediment. *Journal of Hydraulic Engineering*, 129(2):120–128, 2003. → pages 49

P. Wilcock and B. McArdell. Surface-based fractional transport rates: Mobilization thresholds and partial transport of a sand-gravel sediment. *Water Resources Research*, 29(4):1297–1312, 1993. → pages 37, 38

P. Wilcock and B. McArdell. Partial transport of a sand/gravel sediment. *Water Resources Research*, 33(1):235–245, 1997. → pages 37

J. D. Williams, M. L. Warren Jr, K. S. Cummings, J. L. Harris, and R. J. Neves. Conservation status of freshwater mussels of the united states and canada. *Fisheries*, 18(9):6–22, 1993. → pages 1

R. Williams, J. Brasington, D. Vericat, D. Hicks, F. Labrosse, and M. Neal. Monitoring braided river change using terrestrial laser scanning and optical bathymetric mapping. In M. Smith, P. Paron, and J. Griffiths, editors, *Geomorphological mapping: Methods and Applications*, pages 507–532. Elsevier, 2011. → pages 8, 36

R. Williams, J. Brasington, M. Hicks, R. Measures, C. Rennie, and D. Vericat. Hydraulic validation of two-dimensional simulations of braided river flow with spatially continuous aDcp data. *Water Resources Research*, 49(9):5183–5205, 2013a. → pages 28, 37, 72

R. Williams, J. Brasington, D. Vericat, and D. Hicks. Hyperscale terrain modelling of braided rivers: fusing mobile terrestrial laser scanning and optical bathymetric mapping. *Earth Surface Processes and Landforms*, 39(2):167–183, 2013b. → pages 18, 30, 42, 65

R. Williams, C. Rennie, J. Brasington, D. Hicks, and D. Vericat. Linking the spatial distribution of bed load transport to morphological change during high-flow events in a shallow braided river. *Journal of Geophysical Research: Earth Surface*, 120(3):604–622, 2015. → pages 106

S. J. Winterbottom and D. J. Gilvear. Quantification of channel bed morphology in gravel-bed rivers using airborne multispectral imagery and aerial photography. *Regulated Rivers: Research & Management*, 13(6):489–499, 1997. → pages 9, 18, 65

E. Wohl. The complexity of the real world in the context of the field tradition in geomorphology. *Geomorphology*, 200:50–58, 2013. → pages 65

M. Wolman and J. Miller. Magnitude and frequency of forces in geomorphic processes. *The Journal of Geology*, pages 54–74, 1960. → pages 10, 35

A. Woodget, P. Carbonneau, F. Visser, and I. Maddock. Quantifying submerged fluvial topography using hyperspatial resolution UAS imagery and structure from motion photogrammetry. *Earth Surface Processes and Landforms*, 2014. → pages 9, 38

J. R. Wyrick and G. Pasternack. Geospatial organization of fluvial landforms in a gravel–cobble river: Beyond the riffle–pool couplet. *Geomorphology*, 213: 48–65, May 2014. → pages 66, 72, 99